Does Low-Magnitude High-Frequency Vibration Enhance Bone Remodeling in Fracture Healing?

CHOW, Dick Ho Kiu

A Thesis Submitted in Partial Fulfilment
of the Requirements for the Degree of
Master of Philosophy
in
Orthopaedics and Traumatology

The Chinese University of Hong Kong

August 2010


香港中文大學
圖書館系統
29 AUG 2012
UNIVERSITY
LIBRARY SYSTEM
THE CHINESE UNIVERSITY OF HONG KONG

Thesis/Assessment Committee

Professor Wing-hoi CHEUNG (Thesis Supervisor)

Professor Kwok-sui LEUNG (Thesis Co-supervisor)

Professor Ling QIN (Internal Examiner)

Professor Kwok-pui FUNG (Internal Examiner)

Abstract of thesis entitled:

Does Low-Magnitude High-Frequency Vibration Enhance Bone Remodeling in Fracture Healing?

Submitted by CHOW Dick Ho Kiu

for the degree of Master of Philosophy

at The Chinese University of Hong Kong in July 2010

Abstract

Low-magnitude high-frequency vibration (LMHFV), a noninvasive and systemic biophysical intervention, improved bone healing, accelerated callus formation and mineralization of the closed femoral fracture in young female rats, and adult osteoporotic or nonosteoporotic female rats. LMHFV treated rats showed larger callus size in the middle of treatment period. At the end of treatment, faster remodeling was observed and the callus size was comparable to sham. However, the influence of LMHFV on bone remodeling was not full understood due to insufficient information. Therefore, the effect of LMHFV on fracture healing of osteoporotic rats during bone remodeling was investigated in the presence of ibandronate, which functioned as an antagonist to bone remodeling. Bisphosphonate suppresses bone resorption and lead to uncoupling of bone formation and resorption in bone remodeling. This causes inhibition of bone remodeling. Our hypothesis was that LMHFV enhances callus remodeling during fracture healing.

Closed femoral fracture was created in nine-month old ovariectomy-induced osteoporotic Sprague-Dawley rats. The rats were randomly assigned into one of four treatment groups (Sham (CG), LMHFV only (VG), ibandronate only (BG), or both LMHFV and ibandronate (VBG)). Each treatment group had four different treatment durations (2, 4, 6, or 8 weeks). The changes of bone remodeling in fracture healing was investigated with respect to radiological, microarchitectural, histomorphometrical, and biochemical analyses. In addition, the differences among treatment groups and the interactions of the two treatments were investigated by one-way ANOVA with bonferonni post-hoc test and two-way ANOVA respectively.

VG had the fastest drop in callus area and width, and bone volume to tissue volume ratio (BV/TV); whereas, a plateaued trend in BG and VBG was observed. With respect to callus mineralization, VG had the highest mineral apposition rate (MAR) at week 6. Biochemical analyses of bone markers found that the serum concentration of bone formation marker (osteocalcin) and bone resorption marker (Tartrate-resistant acid phosphatase (TRAP5b)) were higher compared to other

groups at week 8.

The fastest callus reduction indicated that LMHFV enhanced bone remodeling. The highest mineral apposition rate suggested that LMHFV enhanced callus mineralization, an important process in callus remodeling. The increased serum concentration of osteocalcin and TRAP5b in VG implied increased osteoblast and osteoclast activity. This increase in cellular activity is associated with enhanced remodeling. Furthermore, LMHFV partially reversed the inhibition of bone remodeling by ibandronate suggested LMHFV had an opposite effect on bone remodeling to ibandronate.

In conclusion, the hypothesis that LMHFV accelerated fracture healing by enhancing callus remodeling is confirmed. This study helped to understand the mechanism of fracture healing enhancement by LMHFV and the effect of LMHFV on bone remodeling. The enhanced remodeling by LMHFV might have great potential in clinical application by allowing faster patient recovery.

摘 要

當前研究表明，作為一項非侵入性、系統性生物物理幹預手段，低振幅高頻率振動（LMHFV）可加速年輕雌性大鼠閉合性股骨骨折的骨痂形成與礦化，進而促進癒合。進一步研究顯示，LMHFV對骨質疏鬆性與非骨質疏鬆性成年雌性大鼠的骨折癒合亦均具有促進作用。在骨折癒合中期，相對於對照組，行LMHFV治療的大鼠骨痂形態較大。後期，治療組的骨重塑過程較快，最終可達到與對照組類似的骨痂形態。然而，迄今關於LMHFV對骨重塑階段影響的研究較少，其作用機理尚未明了。因此，我們運用骨重塑拮抗劑——伊班膦酸鹽來探究LMHFV在骨質疏鬆性大鼠骨折癒合之骨重塑階段中的作用。雙膦酸鹽（伊班膦酸鹽之一）可抑制骨吸收，解離骨重塑期骨形成與骨吸收的自然過程，進而抑制骨重塑。我們預期LMHFV可促進骨折癒合中的骨痂改建過程。

本實驗首先採用雌性SD大鼠行卵巢切除術以誘導骨質疏鬆模型，至9月齡創建閉合性股骨骨折，然後將其隨機分成4組[對照組（CG）、LMHFV組（VG）、伊班膦酸鈉組（BG）及LMHFV+伊班膦酸鈉組（VBG）]，每組設有四個治療時間段（2,4,6,8週），其間通過放射影像學、微觀結構計量學、組織形態計量學以及生化檢驗等方法，觀察骨折癒合過程中骨重塑的演變情況。另外，分別運用單因素方差分析之bonferonni post-hoc檢驗與雙因素方差分析對各治療組之間的差異以及兩種治療方法間的相互作用進行統計學分析。

X線影像學與顯微CT微觀測量均顯示在骨重塑期LMHFV治療組骨痂吸收最為顯著，表現為骨痂面積與寬度下降最快，骨折段骨性組織體積對總組織體積比率（BV/TV）亦然。然而在BG組與VBG組，上述指標變化卻趨向平緩。骨礦化評測顯示，VG組在第6週礦化沉積率（MAR）最高。骨代謝指標的生化分析發現，第8週時，VG組骨生成標記物（骨鈣素）與骨吸收標記物（抗酒石酸酸性磷酸）的血清濃度均高於其他各組。

VG組具有最快的骨痂吸收率，表明LMHFV促進了骨重塑。礦化沉積率最高說明LMHFV可加速骨痂礦化，此過程對於骨痂改建極為重要。骨代謝指標血清濃度的上升提示成骨細胞與破骨細胞的活性增强，此正性作用與促進重塑有很大相關。此外，LMHFV部分扭轉了伊班膦酸鈉抑制骨重塑的作用，表明LMHFV在骨重塑階段具有與伊班膦酸鈉相反的效能。

綜上所述，該實驗證實了之前關於LMHFV可通過促進骨痂改建來加速骨折癒合的假設。本研究有助於闡明LMHFV促進骨折癒合的機制，以及其在骨重塑階段的作用。鑒於LMHFV可增强骨重塑的作用，其在加速病患康復方面具備巨大的臨床應用潛能。

Publications

Papers

1. Chow DH, Leung KS, Qin L, Leung AH, Cheung WH. Low-Magnitude High-Frequency Vibration (LMHFV) Enhances Bone Remodeling in Osteoporotic Rat Femoral Fracture Healing, J Orthop Res (Submitted May 2010, Conditionally Accepted July 2010)

Conference Abstracts

1. Chow DH, Leung KS, Qin L, Cheung WH. Enhanced Bone Remodeling Mechanism in Fracture Healing by Low-Magnitude High-Frequency Vibration Treatment, the 56th Annual Meeting of the Orthopaedic Research Society, 2010, New Orleans, Louisiana

2. Chow DH, Leung KS, Qin L, Cheung WH. Enhanced Bone Remodeling in Fracture Healing by Low-Magnitude High-Frequency Vibration Treatment, International Conference on Osteoporosis and Bone Research 2010, Shenzhen, China

3. Chow DH, Leung KS, Qin L, Cheung WH. Low-Magnitude High-Frequency Vibration Accelerated Callus Remodeling in Osteoporotic Rat Femoral Fracture, the International Society for Fracture Repair 12th Biennial Conference, 2010, London, United Kingdom

4. Chow DH, Cheung WH, Qin L, Leung KS. A Mechanistic Study on the Enhanced Bone Remodeling in Fracture Healing by Vibration Treatment, the 4th Internation Congress of Chinese Orthopedics Association, 2009, Xiamen, China

5. Chow DH, Cheung WH, Qin L, Leung KS. Investigation of the Enhanced Bone Remodeling Mechanism in Fracture Healing by Vibration Treatment, the 29th Annual Congress of the Hong Kong Orthopedics Association, 2009, Hong Kong SAR, China

Acknowledgement

I would like to express my gratitude to my supervisor, Professor WH Cheung, for his guidance and supervision my project. I would also like to thank Professor KS Leung for giving me valuable advices and taught me that explaining the results precisely is more important than just presenting them. Without the guidance of my supervisors, this manuscript would be be possible.

I want to also thank Professor L Qin for his helpful advice on the project. I have to thank Dr. CW Chan for teaching me the undecalcified histomorphometry techniques. In addition, I have to thank Professor. HY Yeung for his help and thorough discussion on the microarchitectural analysis using the μCT. I would like to give special thanks to Dr. KF Tam, Ms. WY Hung, Ms. WS Lee, Mr. WC Chin, Mr. CH Fung, and Mr. MH Sun.

I am grateful to my parents and my girlfriend for their love, support, and understanding.

This project is supported the the Osteosynthesis and Trauma Care (OTC) Research Grant (131006-KSWH).

This thesis is dedicated to my parents. Without their unconditional love and support, I would not have completed this thesis.

Contents

List of Figures

List of Tables

List of Abbreviations

3D	Three dimensional
$CaCl_2$	Calcium chloride
ANOVA	Analysis of Variance
AP	Anterior-posterior
BG	Bisphosphonate group
BMD	Bone Mineral Density
BV	Total bone volume
BV_h	Volume of high-density bone
BV_l	Volume of low-density bone
CA	Callus area
CG	Control group
Cg.Ar/Cl.Ar	Ratio of cartilage area to callus area
CUHK	The Chinese University of Hong Kong
CW	Callus width
DXA	Dual X-Ray Absorptiometry
EC_{50}	Effective concentration that produces a 50% of therapeutic response
ED_{50}	Effective dose that produces a therapeutic response in 50% of the people taking it
ELISA	Enzyme-Linked Immunosorbent Assay
FPP	Farnesyl Diphosphonate
g	Gravitation acceleration
GGPP	Geranylgeranyl Diphosphoate
GI tract	Gastrointestinal Tract

i.p.	Intraperitoneal injection
K-wire	Kirschner wire
LASEC	Laboratory Animal Services Center
LIPUS	Low-intensity ultrasound stimulation
LMHFV	Low-Magnitude High-Frequency Vibration
MAR	Mineral apposition rate
MMA	Methylmethacrylate
MST	Mechanostat Theory
N-BP	Nitrogen-containing bisphosphonate
OPG	Osteoprotegerin
OVX	Ovariectomy
PI	Propidium iodide
PTH	Parathyroid Hormone
PUFA	Polyunsaturated Fatty Acid
r_e	Endosteal radius
r_p	Periosteal radius
RANKL	Receptor Activator of NFκB Ligand
ROI	Region of Interest
sc	Subcutaneous injection
SD	Standard deviation
SD rat	Sprague-Dawley rat
TRAP5b	Tartrate-resistant acid phosphatase
TV	Total tissue volume
VBG	Both bisphosphonate and LMHFV treated group
VEGF	Vascular endothelial growth factor
VG	LMFHV group
WHO	World Health Organization

Chapter 1

Introduction

1.1 Bone and its Cellular Components

Bone is a dynamic and well-organized structure in the body. At a microscope level, bone is made up of cells which are housed in bone matrix. The bone matrix includes organic and inorganic components. At a cellular level, bone cells, which contribute to the maintains of bone, includes osteoblast, osteoclast, and osteocytes. At a macroscopic level, there are two types of bone, woven bone and lamellar bone. Woven bone is considered as immature bone while lamellar bone is mature bone. Lamellar bone has better mechanical strength compared to woven bone. In addition, lamellar bone and woven bone form two marco bone structure: cortical bone and trabecular bone. These two type of organization of bone have different mechanical strength. All these different levels of organization are the contributing factors to the overall mechanical of the bone.

1.1.1 Cellular Components of Bone

Bone is one of the hardest substances in the body. Bone is the primary structure framework that supports and protects the organs, such as the brain, lungs and heart, in the body[49]. The bones also act as a levers for the muscles attached to them and also serve as a reservoir for several minerals such as calcium[49].

Bone is a specialized connective tissue with a calcified extracellular matrix. This extracellular matrix is composed of fibers (primarily collagen type I) and ground substance (rich in proteoglycans and glycoproteins such as osteocalcin). The bone matrix has inorganic (composed of mostly calcium and phosphorus, known as calcium hydroxyapatite) and organic constituents (90% collagen type I). The glycoproteins such as osteocalcin bind to hydroxyapatite. The hardness and strength of bone are due to this association of the calcium hydroxyapatite and collagen[49].

The external surface of bone, except the synovial articulations, is covered with periosteum, an outer layer of dense fibrous connective tissue and an inner cellular layer of osteoprogenitor cells[49]. The endosteum, a thin layer of connective tissue which consists of osteoprogenitor cells and osteoblast, lines the central cavity of bone[49].

Osteoblast

The bone cells are lying within the extracellular matrix. These cells include osteoblast, osteoclast, and osteocytes. Osteoblasts are differentiated from osteoprogenitor cells. Osteoblast is defined as a cell that produces osteoid or bone matrix. These bone forming cells are responsible for synthesis of the organic constituents of bone matrix. When osteoblasts are surrounded by the calcified matrix, they become osteocytes. Osteoblasts are responsive to parathyroid hormone (PTH) and produce osteocalcin.

Osteocytes

Osteocytes are the most abundant bone cells. After osteoblasts secreted matrix and the bone matrix calcifed, osteoblast differentiated into osteocytes. Osteocytes are matured osteoblasts that are trapped in the calcified matrix called lacunae. Osteocytes have extensive cell processes that establish contact with adjacent osteocytes[33]. Osteocytes secret substances for bone maintenance and cellular regulation of calcium exchange[33]. Osteocytes also have also been implicated in

mechanotransduction and serve as mechanosensors[20, 49, 65].

Osteoclast

Osteoclasts are multinucleated giant cells ($20-100\mu m$) and are responsible for bone resorption[49]. Osteoclasts are differentiated from hematopoietic stem cells from bone marrow, which can also differentiated into monocytes and macrophages[15, 33]. Osteoclast is located in regions of bone resorption called Howships lacunae (Figure 1.1)[15, 33]. Another major apparent feature of osteoclast is the extensive foldings of cell membrane at region of bone resorption. These cell membrane foldings are known as ruffled border[15, 33]. During bone resorption, osteoclast secrets hydrogen ion by carbonic anhydrase system to lower the pH of the resorption region. This would increase the solubility of apatite crystals. After the mineral is removed, the organic components of the matrix is broken down by proteolytic digestion[15, 33].

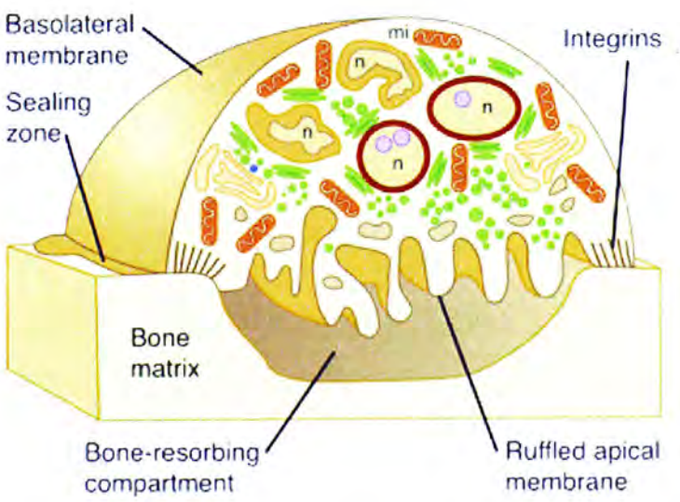

Figure 1.1: Bone resorption by osteoclast[48]. The cell membrane of osteoclast is folded into ruffled border. The resorption region is known as Howships lacunae. (Reprinted from Ganong *et al.* 2009)[48]

The bone resorption activity is regulated by two hormones, PTH and calcitonin[15, 49]. PTH is produced by parathyroid gland and it stimulates bone resorption which leads to increase of serum calcium concentration. On the other hand, calcitonin is produced by thyroid gland and it suppresses bone resorption which decreases

calcium concentration[15].

1.1.2 Macroscopic Structure

Cortical bone has four times the mass of trabecular bone but the metabolic turnover of trabecular bone is eight time higher than cortical bone. Since bone turnover happens on the bone surface, the trabecular bone has a faster bone turnover rate than cortical bone is because trabecular bone has larger bone surface compared to cortical bone[33].

Cortical Bone

Cortical bone composes the diaphysis of long bone and envelopes the cuboid bones[33]. Mechanical stress that cortical bone is subjected to is bending and torsional forces, and compression forces. In small animals, the cortical bone does not have special arrangement for the vascular network. However, in larger animals, the cortical bone is made up of layers of lamellar bone and woven bone while the vascular channels are located in the woven bone[33].

Trabecular Bone

Trabecular bone is found at the metaphysis and epiphysis of long bone and cuboid bones[15, 33]. Trabecular bone forms three-dimensional branching lattice in area of mechanical stress. The predominate mechanical stress that trabecular bone is subjected seems to be compression.

1.1.3 Microscopic Structure

As mentioned previously, there are two different organization of both structure, which is cortical bone and trabecular bone. Woven bone and lamellar bone can be found in both cortical bone and trabecular bone.

Woven Bone

At the microscopic level, there are two forms of bone: woven bone and lamellar bone. Woven bone is normally found in the embryo and the newborn, metaphyseal region of growing bone, and fracture callus[15, 33]. Also, it is found in tumors, osteogenesis imperfecta, and pagetic bone. Woven bone is considered as primitive and immature bone. It contains no uniform orientation of the collagen fibers. The mineral content and cells in woven bone are randomly arranged[15, 33]. Woven bone has an isotropic mechanical characteristic because the random orientation of collagen fibers. Therefore, mechanical characteristics of woven bone would be similar regardless the orientation of forces applied[33].

Lamellar Bone

Lamellar bone is relatively more mature than woven bone[33]. Lamellar bone is formed from remodeling of woven bone. Lamellar bone begins to form one month after birth and would eventually replace most of the woven bone by four years old. Lamellar bone is found in mature skeleton in both trabecular and cortical bone[15, 33]. The collagen fiber in lamellar bone is highly organized and oriented with the direction of stress. Therefore, lamellar bone has an isotropic mechanical characteristic and the greatest strength would be parallel to the longitudinal axis of the collagen fibers[33].

1.2 Fracture Healing

Fracture healing is a complex and ordered process that involves coordination of many different processes[33, 126]. These processes resemble those that are found in skeletal development and growth[33, 126].This repairing process is different from repair of other tissue because a fracture is repaired by bone instead of a scar tissue[33]. Therefore, after a fracture is healed, the preexisting properties of the bone are restored[33]. Fracture healing involves a series of regenerative processes which begin

at the moment of fractures[33]. This complex process is conventionally divided into four stages as a result of histological observations. Each stage is characterized by a specific cellular and molecular event (Figure 1.3)[33, 126]. The four stages are inflammation, soft callus formation, hard callus formation, and bone remodeling (Figure 1.2[33, 126].

1.2.1 Inflammation

A fracture caused the disruption of the integrity of soft tissue, vascular function and marrow architecture. The local bleeding at the fracture site develop into a hematoma. This hematoma signals the infiltration of degranulating platelets, macrophages, and other inflammatory cells such as granulocytes, lymphocytes, and monocytes[33, 126]. The inflammatory cells would secret cytokines that are important in regulating the early stages of fracture healing. These cells would also secret growth factors which would recruit additional inflammatory cells in a positive feedback loop. These growth factors and cytokines would lead to invasion of multipotent mesenchymal stem cells which orginated from the periosteum, bone marrow, circulation, and surrounding soft tissues (Figure 1.2a)[126].

1.2.2 Soft Callus Formation

Soft callus formed by chondrocytes and fibroblasts[126]. The chondrocytes are differentiated from mesenchymal progenitors and they replace the hematoma at the fracture site with cartilage[126]. Fibroblasts replace the deficient cartilage production region with fibrous tissue. This produces a central fibrocartilaginous bridge between the fractured bone (Figure 1.2b). This semi-rigid cartilaginous callus provides some mechanical support to the fracture. Under the stimulation of vascular endothelial growth factor (VEGF), vascular endothelial cells would invade the soft callus and ingrowth of blood vessels[126]. This infiltration of blood vessel is important for the mineralization of the callus[24, 56]

1.2.3 Hard Callus Formation

The soft callus is removed gradually by chondroclasts and the hard callus is formed by osteoblast (Figure 1.2c)[126]. The hard callus initially contains woven bone, which is nearly identical to the secondary spongiosa of the growth plate[33]. This process of formation of bone from a cartilage template is known as endochondral bone formation[33, 126]. Hard callus can form in the absence of soft callus. This process is known as intramembranous bone formation and often occur in fracture with high mechanical stability or adjacent to fracture site and an existing bone surface[33, 126]. Hard callus formation involves responses in the periosteum and external soft tissues. Delay of healing can be caused by damaged periosteum because the periostem is rich in stem cells[33, 126].

1.2.4 Bone Remodeling

Bone remodeling, the last stage of a traditional four stages fracture healing, is a coupled process of bone resorption and formation which replaces woven bone with lamellar bone and restores the standard cortical structure (Figure 1.2d)[126, 130, 88, 85, 125]. The key cell type for bone remodeling and resorption of mineralized bone is osteoclasts. Osteoclast replaces the less mechanical support woven bone with high mechanical strength laminar bone in bone remodeling[125].

1.3 Low Magnitude High Frequency Vibration (LMHFV) Stimulation

Vibration is a form of oscillation. The magnitude of a sinusoidal vibration can be expressed as the displacement from the neutral point with the equation

$$M(t) = A \times sin(2\pi ft + \theta)$$

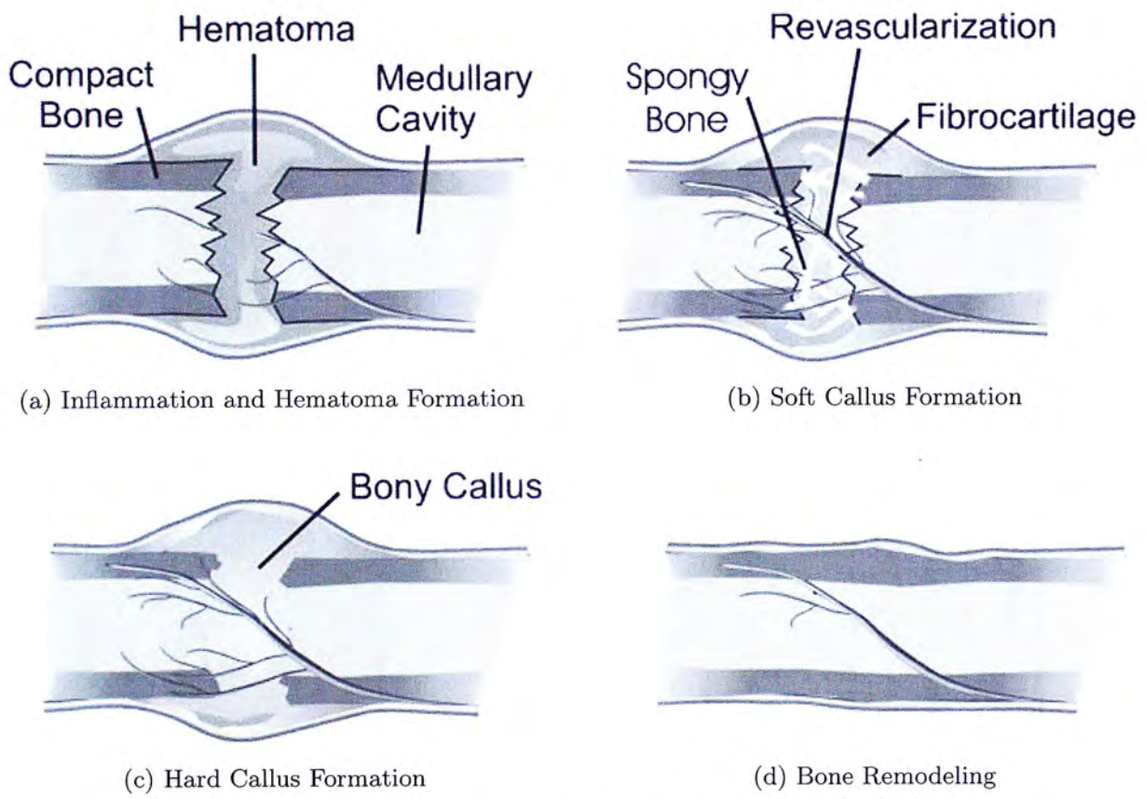

(a) Inflammation and Hematoma Formation

(b) Soft Callus Formation

(c) Hard Callus Formation

(d) Bone Remodeling

Figure 1.2: Four stages of fracture healing. a: Inflammation and hematoma formation. b: Soft callus formation. c: Hard callus formation. d: Bone remodeling. (Reprinted from Lieberman *et al.* 2005)[79]

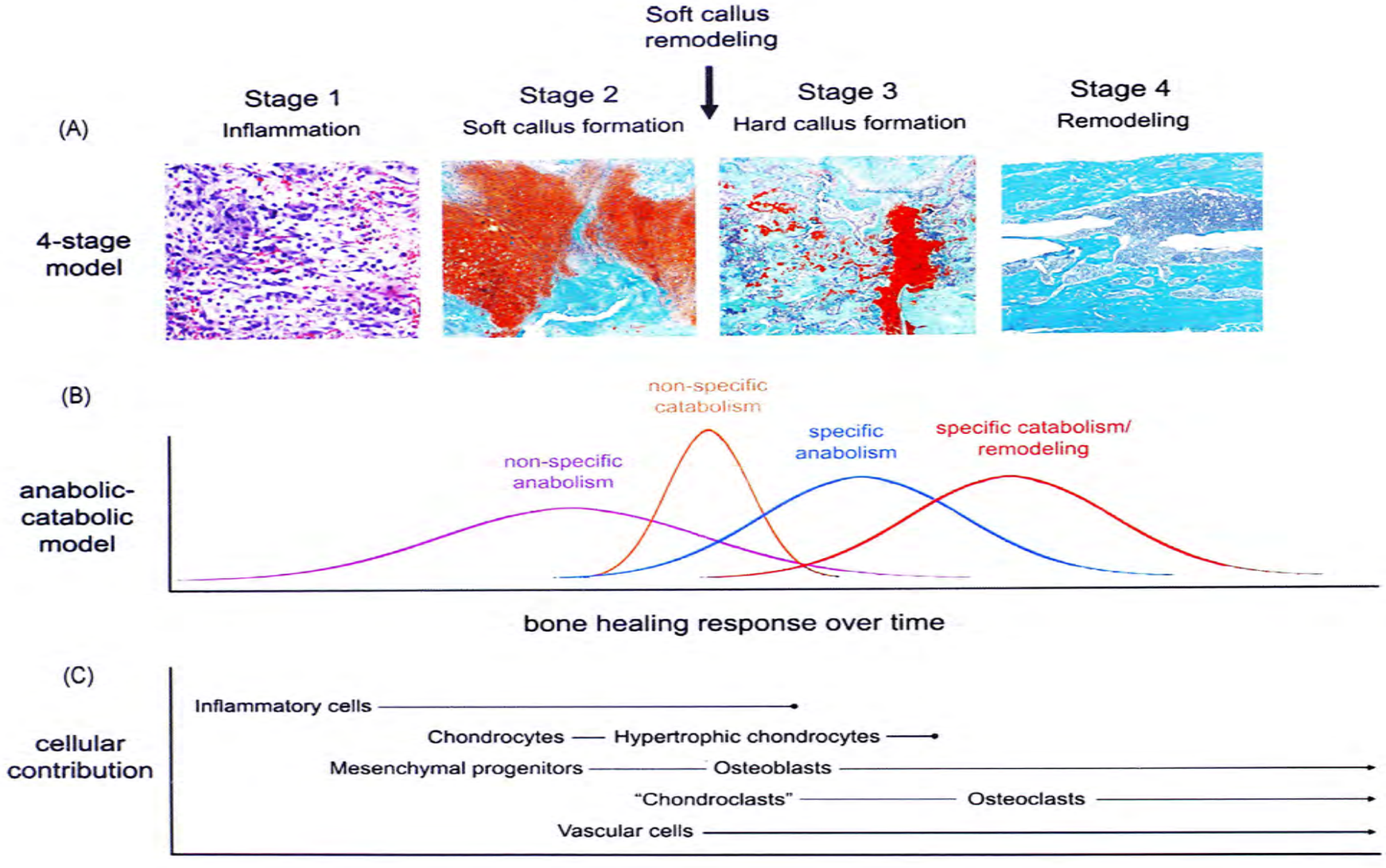

Figure 1.3: Different involvements of cells during different stages of fracture healing. a: Histological representation of four stages of fracture healing. b: Anabolic and catabolic process during different stage of fracture healing. c: The cells that participates in different stages of fracture healing. (Reprinted from Schindeler *et al.* 2008)[126]

The maximal displacement from the neutral point is defined as the amplitude (A). The number of cycles of the wave in a unit of time is called the frequency (f). From this equation, the acceleration from the vibration, in terms of the gravitational force of the earth, can be calculated by the equation

$$g = \frac{A(2\pi f)^2}{9.81}$$

From the frequency of the wave (f) and the duration of the treatment, the number of loading cycles can be calculated as Loading Cycle = Frequency × Duration of Treatment.

Furthermore, the frequency or strain rate is important to determine the response of bone to the mechanical stimulation. This is because the strain threshold required to maintain bone mass follows a nonlinear function of loading cycle number (Figure 1.4)[108]. This suggested that the total amount of strain required to maintain bone mass depends on the total number of loading cycle. As mentioned previously, number of loading cycle is the product of frequency of the waveform and the duration of treatment.

1.3.1 Mechanical Stimulation

Wolff's Law

In 1892, Wolff stated that mechanics can change the architecture of bone[45]. The Wolff's law states that

> Every change in the form and function of bone or of their function alone is followed by certain definite changes in their internal architecture, and equally definite alteration in their external conformation, in accordance with mathematical laws.

Even though the Wolff's law predicts that there is changes in bone architecture after mechanical loading, however it does not state the mechanism on how this change occurs[45].

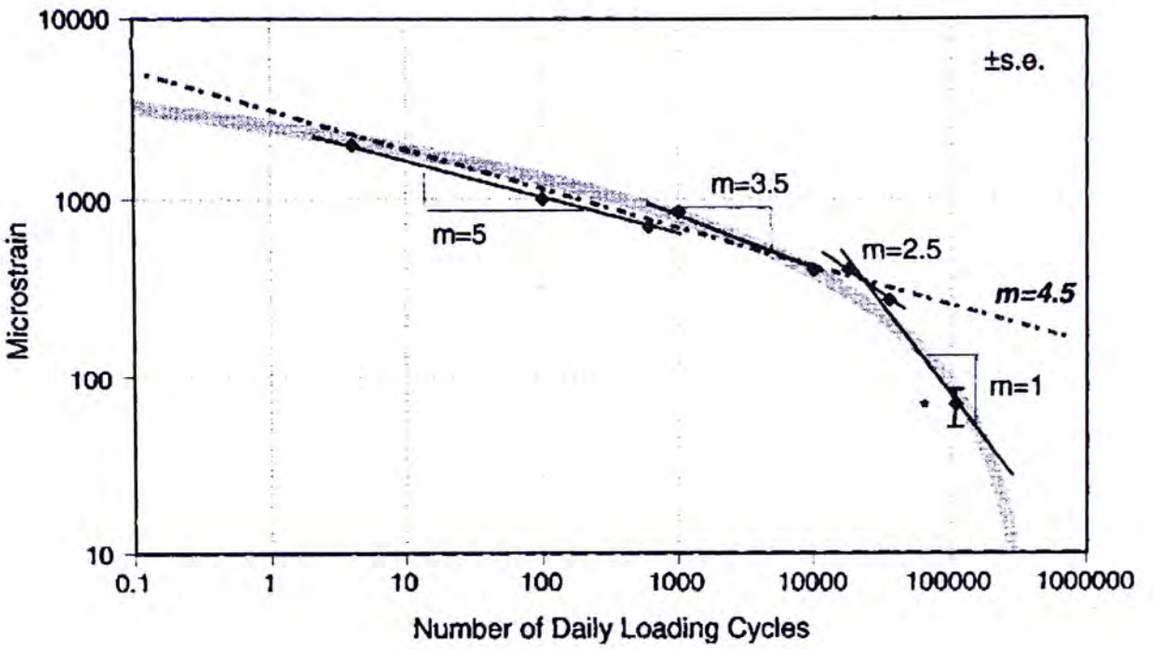

Figure 1.4: There is a nonlinear relationship between stain threshold and number of loading cycle. As the number of cycles increases, the strain required to maintain bone mass decreases. However, the changes are not proportional to each other. (Reprinted from Qin *et al.* 1998)[108]

Mechanostat Theory

The mechaostat theory (MST) is proposed by Frost[47, 46, 136]. MST states that weight-bearing bones are genetically equipped with physiological signal threshold for maximal and minimal strains. Mechanical strain is a function of load-bearing[117]. During passive activities such as standing, muscle would generate less than 5 microstrain in amplitude with a frequency of 10 – 50 Hz[44]. The bone mass is regulated by bone strains via feedback mechanism which is analogous to the temperature regulation by a thermostat[136]. Therefore, when the upper limit of bone stain is reached, there would be a net bone synthesis. However, when bone stain reaches the lower threshold, there would be a net bone resorption (Figure 1.5)[136]. The mechanical loading between these two thresholds would have no net change of net bone mass.

Under different physiological conditions, the threshold values might change in order to stimulate bone formation or bone resorption[136]. In osteoporosis, calcium and estrogen depletion might shift the thresholds to the right. Therefore,

higher mechanical load would be needed to stimulate bone formation. Microfractures might lower the thresholds so less mechanical loading is needed to stimulate bone formation[136].

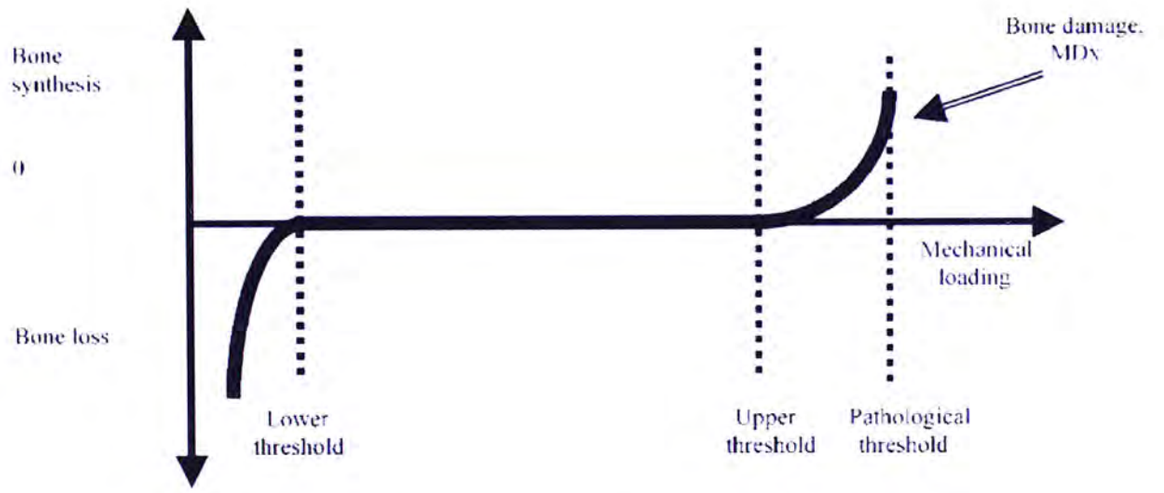

Figure 1.5: The mechanostat theory proposed by Frost[45, 136]. When mechanical loading of the bone reaches the upper threshold, there would be a net bone synthesis. On the other hand, when bone is disused and mechanical loading reaches the lower threshold, there would be a net bone resorption. However, when there is excessive loading and bone stain reaches the pathological threshold, the bone would be damaged. (Reprined from Frost 1994)[45]

1.3.2 Effect of LMHFV on Bone

Low-magnitude High-Frequency Vibration (LMHFV) is a form of systemic, noninvasive, and cyclic biophysical stimulation. Vibration has potential effects on physiological systems and the potential interplay among systems. Vibration modulates skeletal, muscular, endocrine, nervous, and vascular systems. Rubin *et al.* reported that adult sheep that stand on a vibration platform for 20 min/day for 5 days a week over one year had increased femoral trabecular bone density by 32%[117]. Gusi *et al.* reported that postmenopausal women treated with vibration had increased bone mineral density by 4.3% compared to walking[54]. Xie *et al.* reported that vibration can inhibit trabecular bone resorption in growing skeleton which might

increase peak bone mass non-pharmacologically[142].

LMHFV effect on Fracture Healing

LMHFV not only have an effect on intact bone, it also have an effect on fractured bone. In our previous study, LMHFV (0.3 g, 35 Hz) enhanced fracture healing in three month old non-osteoporotic Sprague-Dawley rats (SD rats), and nine month old ovariectomy (OVX)-induced osteoporotic and nomral adult rats[76, 129]. The three month old SD rats that were treated with LMHFV for four week and the rate of fracture healing was improved by 25 – 30%[76]. The rats under LMHFV stimulation had larger callus than sham rats (Figure 1.6)[76]. The healed fracture after 4 weeks of LMHFV had better mechanical strength (50.1% stronger than sham) with respect to ultimate load and stiffness[76]. This suggested acceleration of fracture healing. Furthermore, similar results were found in the nine month old rats. These rats were treated with LMHFV for eight weeks. LMHFV promoted fracture healing in OVX group in all callus measurements especially in the early phases of healing[129]. Callus formation, mineralization and remodeling were enhanced by 25 – 30% compared to the OVX control. In addition, the energy to failure was enhanced by 70%[129].

In young, adult nonosteoporotic, and adult OVX-induced osteoporotic rats, the LMHFV treated rats had larger callus measurement in the middle of treatment period (Week 2 and week 4 for young and adult rats respectively) (Figure 1.6 and 1.7). Moreover, at the end of treatment period (week 4 and week 8 for young and adult rats respectively), the LMHFV stimulated rats had comparable callus measurement to their respective control rats. From this observation in LMHFV rats, LMHFV might not only enhance the early phases of fracture healing but also the later bone remodeling phase. The rate of disappearance of callus seems to be faster in LMHFV treated rats than sham. This effect suggested that the later phase of fracture healing might be influenced by LMHFV.

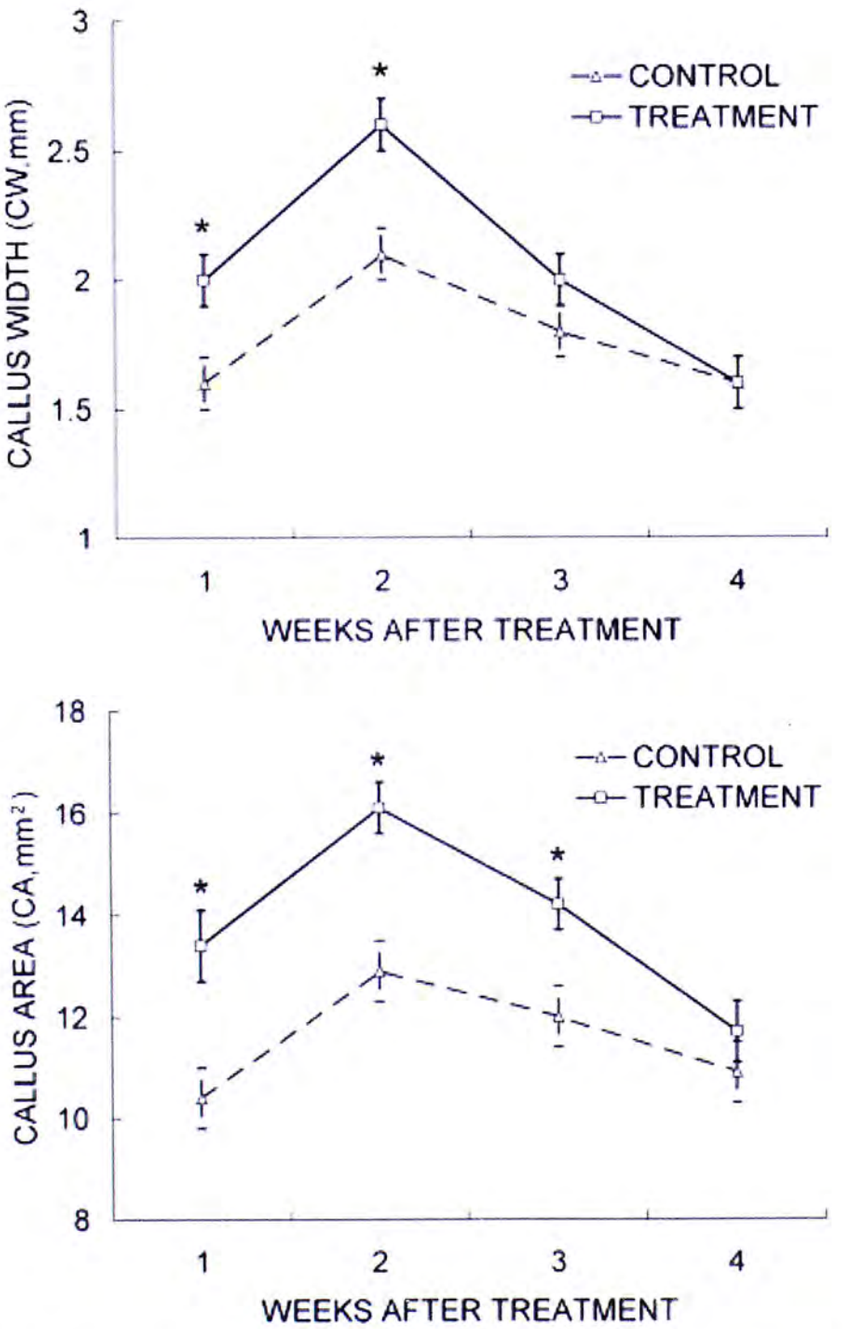

Figure 1.6: Callus area and width in three month old rats. (Reprinted from Leung *et al.* 2009)[76]

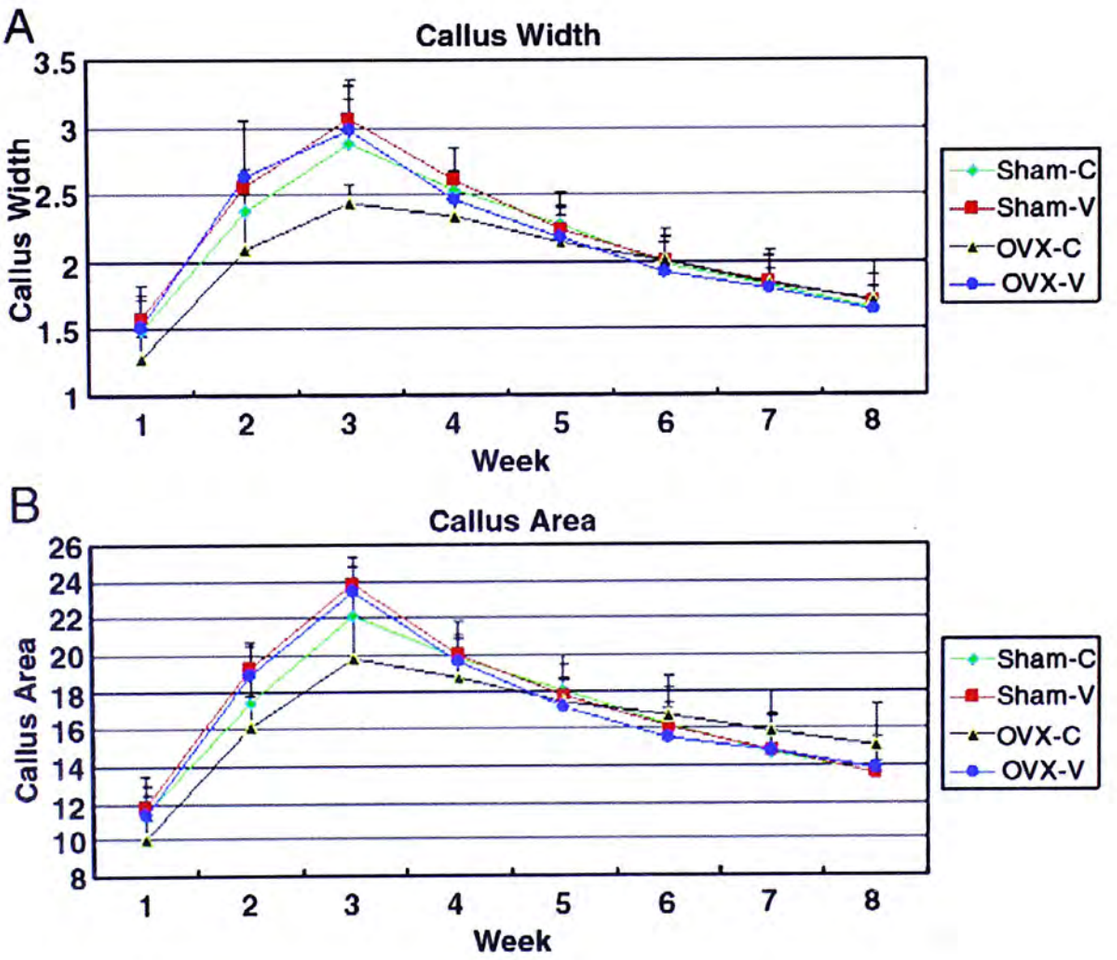

Figure 1.7: Callus area and width in nine-month old OVX-induced osteoporotic and nonosteoporotic rats. (Reprinted from Shi *et al.* 2010)[129]

1.4 Osteoporosis and Osteoporotic Fractures

Osteoporosis

Osteoporosis means porous bone. According to the World Health Organization (WHO), osteoporosis is defined as:

> a systemic skeletal disorder characterized by low bone mass and microarchitectural deterioration of bone tissue, with a subsequent increase in bone fragility and susceptibility to fracture[7].

The first Consensus Conference on Osteoporosis of the new millennium proposal a new definition of osteoporosis as:

> a skeletal disorder characterized by compromised bone strength predisposing to an increased risk of fracture[7].

Osteoporosis is diagnosed by measuring the bone mineral density (BMD) using dual X-ray absorptiometry (DXA). When BMD is more than 2.5 standard deviation below the sex-matched young adult mean, this would be classified as "established osteoporosis"[7, 57]. On the other hand, osteopenia, which defined as low bone mass, was set at BMD is between $1.0 - 2.5$ standard deviation lower than average[7].

Osteoporotic Fracture

Osteoporotic fractures affect women more than heart attacks, strokes, and cancers that occur in female only combined[7]. Vertebral, distal forearm, and hip fracture incidence increases exponentially with age (Figure 1.8)[57]. Therefore, osteoporotic fractures at these locations are regarded as typical[124]. In addition, risk of fracture increases in patients who had any type of fragility fracture previously[116]. A vertebral fracture would increase the risk of a subsequent vertebral fractures by 10-folds[124].

1.4.1 Epidemiology of Osteoporotic Fracture

Osteoporosis is a major health problem. Osteoporosis is identified as one of the most important diseases, along with hypertension and diabetes mellitus, that is affecting the human[7]. Each year, approximately 200 million people are at risk of an osteoporotic fracture and 40% of women and 14% of men over 50 years of age will experience fractures related to osteoporosis[30]. In 2000, it was estimated that there was 424,000 and 1,098,000 hip fractures in men and women respectively[50]. As life expectancy increases, there would be 800,000 and 1.8 million hip fractures by the year of 2025 in men and women respectively[50]. In 1990, the direct and indirect cost of hip fracture costed about $34.8 billion USD annually[57]. In 1997, the annual cost reached $131.5 billion USD[124]. The cost is expected to increase substantially and globally over the next 50 years with the aging population[57].

In Hong Kong, a cross-section study found women over 60 and women over 70 years old had lower mean bone mass than young healthy women by 30% and 50% respectively[59]. Therefore, prevalence of osteoporosis in Hong Kong would also increase substantially with aging population. The current trend suggested that in 2015, 5293 women and 2349 men would have a hip fracture[61].

1.4.2 Pathophysiology

Bone strength is contributed by many skeletal characteristics and bone qualities[124, 135]. These include macroarchitecture of bone (shape and geometry), microarchitecture of both cortical and trabecular bone, matrix and mineral composition, degree of mineralization, microdamage accumulation, and the rate of bone remodeling and turnover[124, 135]. As mentioned in section 1.4, osteoporosis is a skeletal disorder characterized by low bone mass and microarchitectural deterioration of bone tissue. These morphological changes lead to increase in bone fragility and increase incidence of fracture.

In postmenopausal women, bone mass decreases due to decrease in estrogen production and other age-related mechanisms such as secondary hyperparathyroidism

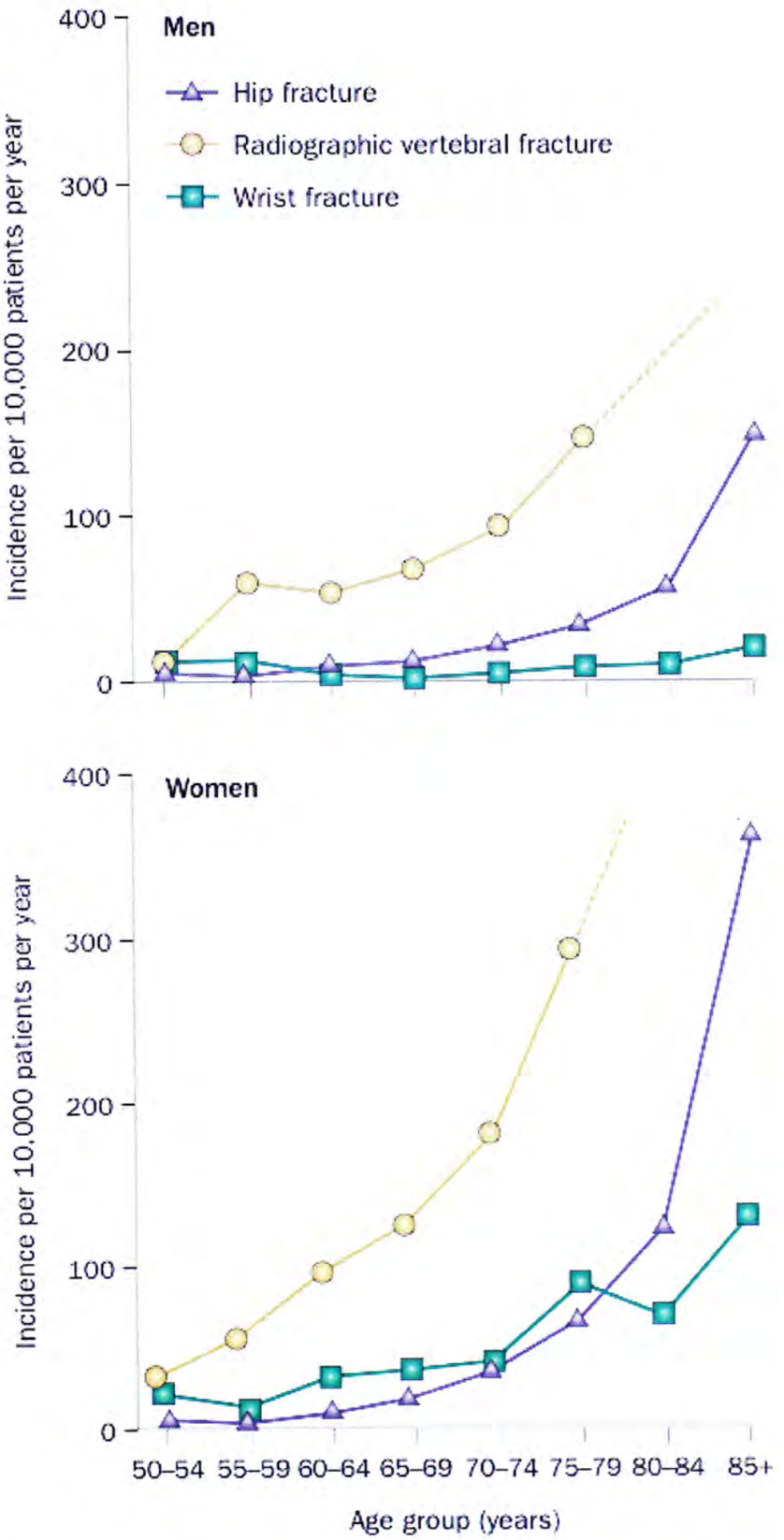

Figure 1.8: Exponential increase of fracture incidence at hip, wrist and vertebra with age in males and females. (Reprinted from Sambrook *et al.* 2006)[124]

and reduced mechanical loading[124]. Skeleton is continually remodeled by a coupled activity of bone formation and bone resorption. This coupled activity is not balance in postmenopausal osteoporosis. Due to aging, osteoblasts become dysfunction[37]. Therefore, the activity of osteoblast and osteoclast is not balanced. In addition, the rate of bone remodeling is increased. This would magnify the decrease in bone mass caused by the imbalance of bone remodeling[124]. This would also lead to a progressive loss of trabecular bone due to increased osteoclastogenesis[124].

Estrogen exerts anti-resorptive effects on bone at a cellular level. The receptor activator of NFκB ligand (RANKL) is a signaling molecule for osteoclast differentiation and increased bone resorption. Normally, RANKL binding on osteoclast is blocked by osteoprotegerin protein (OPG). Estrogen stimulates the production of OPG in osteoblast. Estrogen deficiency in postmenopausal women caused an up regulation of RANKL and down regulation of OPG. Therefore, this would enhance the osteoclast activity and survival would leads to increase bone resorption.

Menopause is associated with decrease calcium absorption and increase calcium excretion which would lead to calcium imbalance[98]. Calcium absorption falls with age due to decline in gastrointestinal sensitivity to calcitriol, also known as 1,25-dihydroxycholecalciferol. This molecule is responsible for dietary calcium absorption (Figure 1.9)[48, 98]. The increased calcium excretion is probably due to increase in bone resorption in menopause and reduction of calcium reabsorption in the tubular of the kidney[98]. Therefore, the serum calcium concentration and bone calcium content would decrease even further. Estrogen enhances intestinal absorption efficiency and improves renal calcium conservation[58]. Therefore, postmenopausal women might have lower serum calcium concentration due to estrogen deficiency.

Under low calcium condition, the body would secret parathyroid hormone (PTH)(Figure 1.9)[131]. PTH is a hormone that is secreted by the parathyroid glands[48]. PTH increases bone resorption and mobilize Ca^{2+}. This is a compensatory mechanism by the body to increase calcium concentration. This increase in secretion of PTH would cause secondary hyperparathyroidism. In addition, estrogen seems to have a

direct depressive action on the parathyroid gland while estrogen deficiency increases the sensitivity of bone to PTH[131]. Therefore, the increased sensitivity of bone to PTH and increased secretion of PTH would further decrease the mineral content in bone in people with postmenopausal osteoporosis.

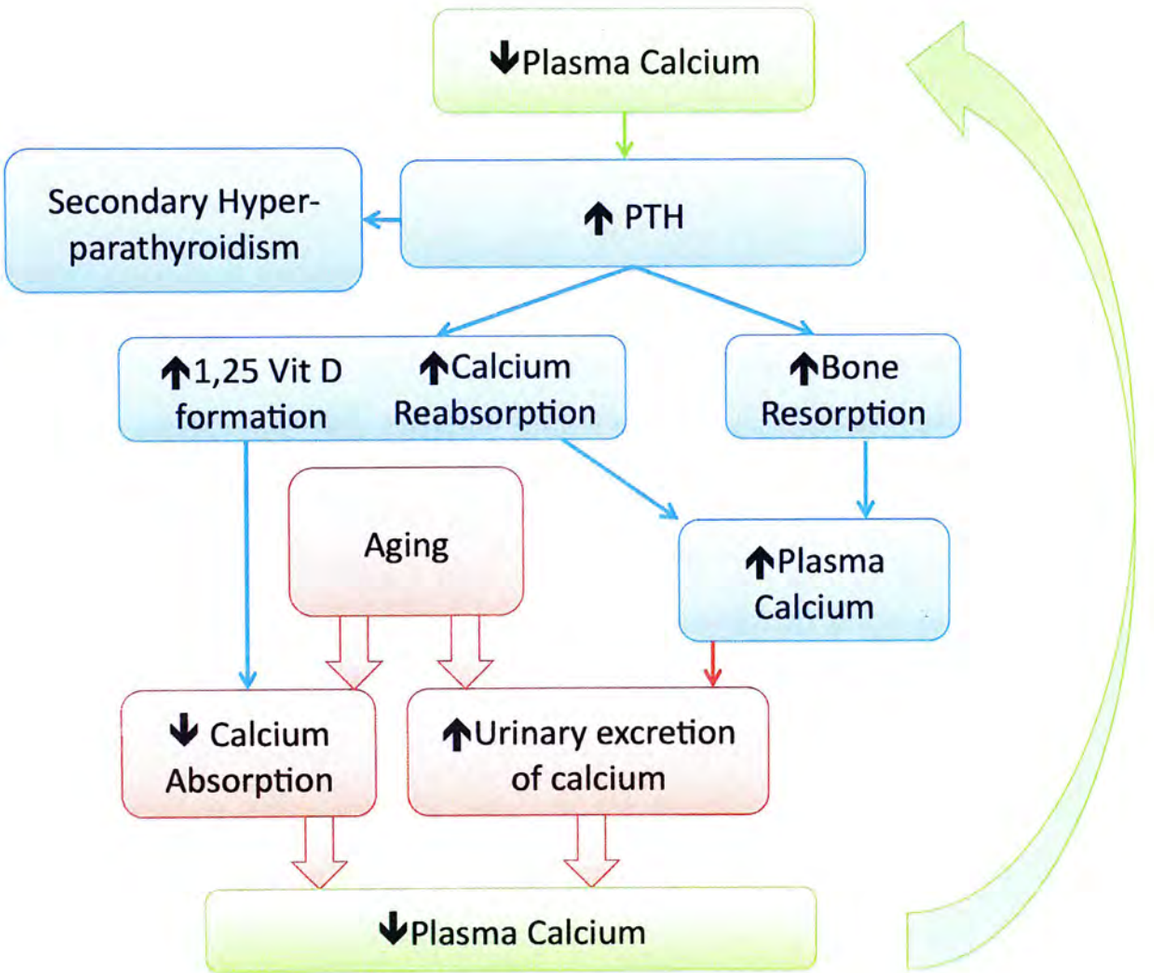

Figure 1.9: Impaired calcium balance in postmenopausal osteoporosis. The body increases secretion of PTH and production of 1,25-dihydroxycholecalciferol to compensate the lost of calcium. However, aging lead to impaired kidney function and cause excess urinary excretion of calcium.(Modified from Ganong *et al.* 2009[48])

1.4.3 Osteoporotic Fracture Healing

Under osteoporotic conditions, the fracture process of bone is delayed even though it goes through all the normal stages[50, 97]. Factors which may contribute to the

delay healing in osteoporotic patients are decreased bone mechanical stability[23], impaired angiogenesis[110], reduced osteoblastic activity to signaling molecules[96], and deficiencies of mesenchymal stem cells[16]. In our previous study, there is a reduction of callus area and width, and mechanical strength in the femoral fracture of osteoporotic rats compared to normal rats[129]. Clinically, increase in the rate of failure of implant fixation in osteoporotic patients was observed[6].

Management of Osteoporotic Fracture

For treating osteoporotic fractures, there are three factors that the surgeon would consider (Figure 1.10). The three factors are the quality of the soft tissue surrounding the fracture site, the fracture pattern, and the patient[50]. For soft tissue quality, the elderly might have thin skin due to atrophy or malnutrition would be susceptible to degloving injuries[50].Other soft tissue problems found in the elderly include arterial diseases such as venous hypertension, and ulcers[50]. The fracture pattern for the elderly are often complex because of the changes in mechanical properties of bone. The elderly often has medical comorbidities which would have a major impact on the patient factor for treatment options[50].

The operative treatment for osteoporotic fracture is a challenge for surgeons because the outcome is often unpredictable. Since there is endosteal diaphyseal resorption and medullary expansion in osteoporotic bone, the bending and torsional characteristics of the entire bone would be changed. In addition, the holding capacity of the screws might also be affected due to the decreased density in cortical bone[50].

Osteoporotic Fracture Model

Osteoporotic fracture model was used in order to study the effect of LMHFV on bone remodeling in fracture healing. Osteoporosis delays fracture healing even though healing goes through all the normal stages. The advantage of using this fracture model is that the prolonged fracture healing which would allow detailed observation of each healing stage. Therefore, the subtle changes within the fracture callus can

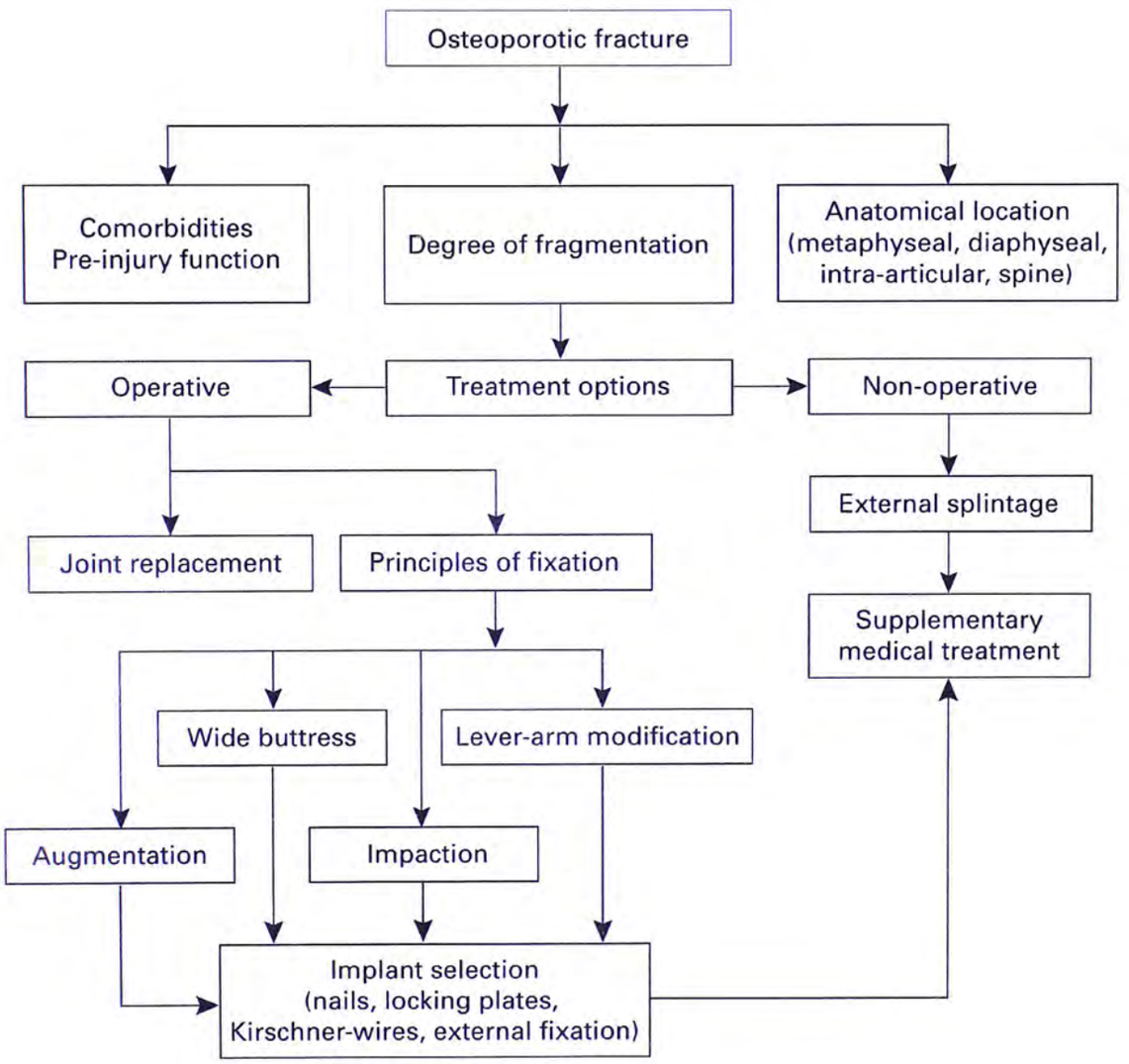

Figure 1.10: An algorithm for the management of osteoporotic fracture. (Reprinted from Giannoudis *et al.* 2006)[50].

be observed and studied.

1.5 Bisphosphonate

Bisphosphonate is a anti-catabolic agent which is used for osteoporosis. It is taken up by osteoclast during resorption at active remodeling sites. Uptake of bisphosphonate by osteoclasts causes osteoclast apoptosis and leads to inhibition of bone remodeling[103, 121, 130].

1.5.1 Background

Bisphosphonate is an effective inhibitor of bone resorption for the treatment and prevention of osteoporosis[112]. Depending on the specific bisphosphonate, the risk of hip and vertebral fractures was reduced by 40 – 60% (Table 1.1)[1, 112]. Bisphosphonates decrease rate of bone remodeling into premenopausal range, maintain trabecular and cortical microarchitecture, reduce cortical porosity, and improve bone mineralization[19, 38, 113].

Table 1.1: Reduction of vertebral fracture risk by alendronate, risedronate, and ibandronate with daily or intermittent regimen (Source: Adami 2007)[1].

Bisphoshonate	Fracture Risk Reduction	
	Vertebral Fracture	Non-vertebral Fracture
Alendronate [10 mg/day]	47%	36%
Risedronate [5 mg/day]	49%	39%
Ibandronate [2.5 mg/day]	62%	69%

Bisphosphonates are analogs of pyrophosphate which has a high affinity for calcium crystals[103]. Bisphosphonates have a backbone structure of (P–C–P), which is similar to the backbone structure of pyrophosphate (P–O–P)[112]. This backbone structure makes bisphosphonates resistant to biological degradation[102, 103]. Therefore bisphosphonate are excreted unmetabolized in urine[102, 103].

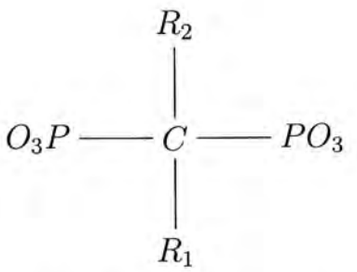

This P–C–P structure allows bisphosphonate to bind to the divalent metal ions, such as Ca^{2+}, on bone surfaces[27]. This high affinity to bone surface allow bisphosphonate to have a highly selective effect on osteoclast.

Bisphosphonate is different from pyrophosphates that it has two extra side chains, R_1 and $_2$, attached to the central carbon atom. Most of the common bisphosphonates, except clodronate, have a hydroxyl group (–OH) at R_1. This enhances the affinity of bisphosphonate to calcium crystals on the bone surface. However, different bisphosphonate have significantly different kinetic binding affinities for hydroxylapatite[94]. These differences in kinetic of binding are attributed to differences in the R_2 side chain[94]. R_2 side chain can influence the bone affinity as a result of the ability of nitrogen moiety to bind to the bone surface. The N-BP that has a larger R_2 side chain is more potent[94].

1.5.2 Mechanism of Action

Bisphosphonate is preferentially deposited at sites, such as fracture callus and active remodeling sites, where minerals are exposed by osteoclast[77, 103, 112]. There are two groups of bisphosphonates: nitrogen-containing (N-BP) and non-nitrogen-containing[121]. These are referred to whether the R_2 side chain contains a nitrogen atom[103].

The N-BP, such as alendronate, risedronate, ibandronate, and zoledronate, interfere other metabolic reactions in osteoclasts[121]. This group of bisphosphonate interferes the mevalonate biosynthetic pathway and affects cellular activity, cell survival, and protein prenylation. The mevalonate pathway is responsible for

the production of cholesterol, other sterols, and isoprenoid lips such as isopentenyl diphosphate, farnesyl diphosphonate (FPP) and geranylgeranyl diphosphoate (GGPP)[121]. FPP and GGPP are important for posttranslational modification and prenylation of small GTPases (Figure 1.11). N-BP has a mechanism of action is similar to statins, a drug known to target cholesterol pathway[41]. Both statin and N-BP inhibit osteoclast formation and osteoclastic bone resorption through inhibition of mevalonate pathway[112].

The non N-BP closely resemble pyrophosphate[121]. These non N-BP includes clodronate and etidronate. This group of bisphosphonate seem to act as prodrugs and converted to active metabolites after intracellular uptake by osteoclast[121]. These bisphosphonates are incorporated into nonhydrolzable analogues of adenosine triphosphate (ATP) by reversing the reactions of aminoacyltransfer RNA synthetases. This would create nonhydrolyzable metabolites that contain the P-C-P moiety in place of the β,γ-phosphate group of ATP (Figure 1.11). These metabolites would accumulate within osteoclasts and inhibits their function. This may also cause osteoclast apoptosis[121].

1.5.3 Usage of Bisphosphonate

As mentioned in section 1.5.1, bisphosphonate can decrease bone resorption. This effect of bisphosphonate allow it to be used in the management of conditions with excessive bone resorption which includes Paget's disease of bone and malignancy-associated hypercalcemia[103]. Furthermore, bisphosphonate administrated systematically or to be coat on the screw. These administration of bisphosphonate would increase the screw removal resistance and integration[4, 72]. Another usage of bisphosphonate is on cancer patients. Many cancers are associated with bone destruction and hypercalcemia due to increase of PTH[119]. Bisphosphonates may have direct effect on the tumor cells such as induction of tumor cell apoptosis[25].

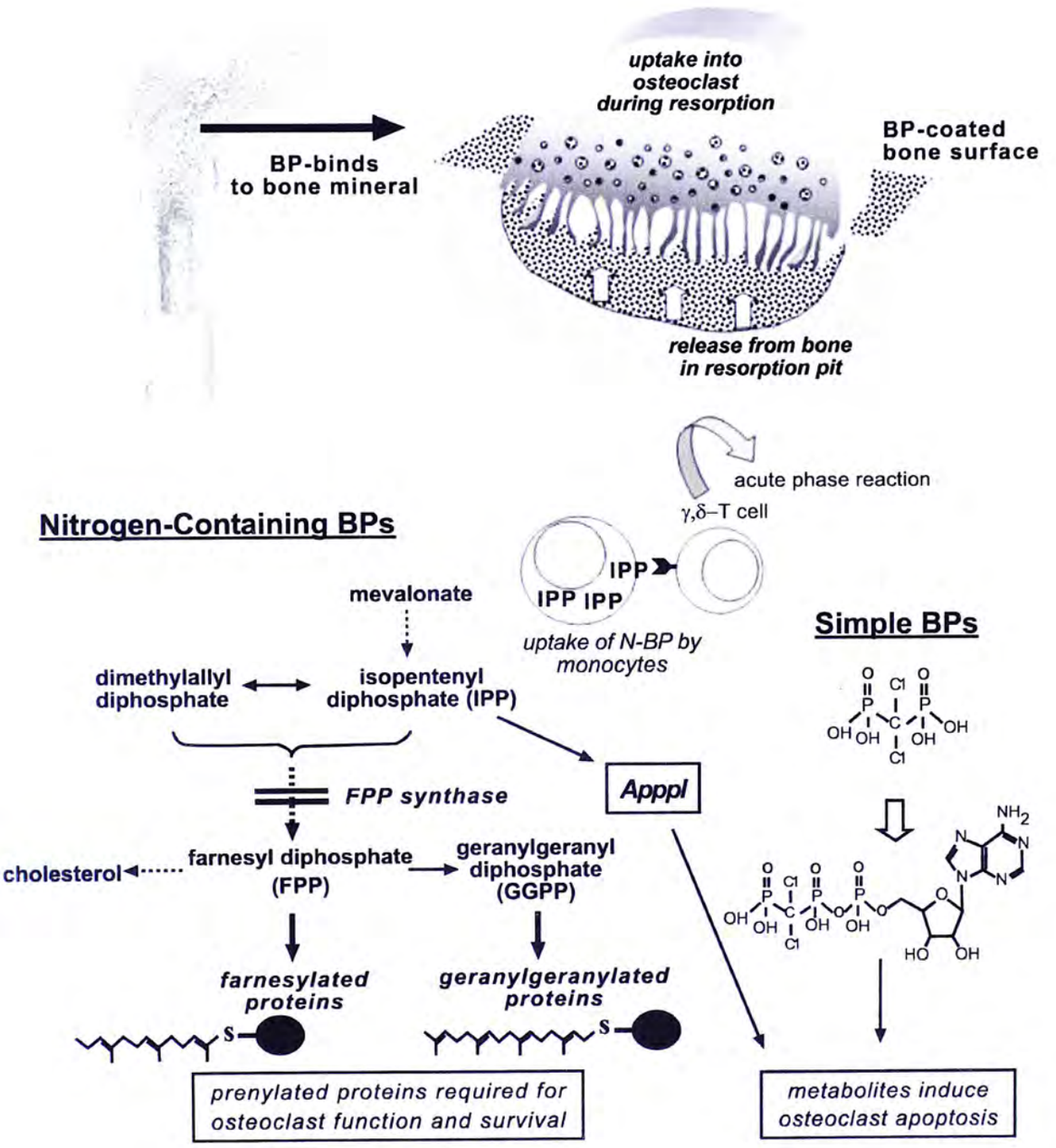

Figure 1.11: Mechanism of action of non-nitrogen-containing and nitrogen-containing bisphosphonate on osteoclast[121, 122]. Non-nitrogen-containing bisphosphonate incorporates into ATP and form non-hydrolyzable metabolite. Nitrogen-containing bisphosphonate inhibits prenylation of GTPasse in the mevalonate pathway. (Reprinted from Russell *et al.* 2009)[122]

1.5.4 Bisphosphonate Effects on Fracture Healing

Even though bisphosphonates reduce fracture risks significantly, there are issues with the use of bisphosphonate. Bisphosphonate remains in the skeleton for very long time due to their long half life (200 days for alendronate)[80]. The physiological effect of these bisphosphonate is still unknown. Bone turnover markers remained suppressed after discontinuation of bisphosphonate[34]. Suppression of bone remodeling would impair the repair ability of bone and lead to accumlation of microdamages in bone[86]. A large amount of bisphosphonate with low inhibitory efficacy, such as etidronate, would produce a mechanically weaker fracture callus[74]. In addition, administration of bisphosphonate during fracture healing might delay bone remodeling[90, 100].Furthermore, long-term usage of high dosage bisphosphonate might lead to atypical fracture of the femoral shaft[3, 9, 10, 51, 40, 124].

1.6 Hypothesis

As mentioned in section 1.3.2, our previous studies showed LMHFV (35 Hz, 0.3g peak-to-peak acceleration) enhanced callus formation, mineralization and fracture healing in both adult rats[76] and aged osteoporotic rats[129]. The mechanical strength of the healed fracture at the end of treatment was also improved[76, 129]. Furthermore, an increased rate of disappearance of callus in terms of callus area and width was observed in these studies. This observation suggested that LMHFV enhanced bone remodeling in fracture healing. However, more information is needed to verify this enhancement of bone remodeling and the mechanism of action of LMHFV on fracture healing was still not well understood. **Our hypothesis was that LMHFV enhanced bone remodeling in fracture healing.**

1.7 Study Plan

To verify our hypothesis, nine month old female OVX-induced osteoporotic rats were undergone closed-fracture surgery. LMHFV stimulation was applied on these rats. In addition, LMHFV-stimulated bone remodeling was suppressed by the administration of ibandronate (Bis), a nitrogen-containing bisphosphonate[121, 120]. The changes in both remodeling by LMHFV in the presence and absence of ibandronate would be investigated.

1.7.1 Objectives

The objectives of this study are listed as follows:

1. To study the effect of LMHFV on bone remodeling in fracture healing in the presence or absence of bisphosphonate with respect to radiological, microarchitectural, histomorphometric, and biochemical analyses.

2. To study the effect of LMHFV on bone resorption during fracture healing with respect to biochemical analysis.

3. To study the effect of LMHFV on bone formation during fracture healing with respect to radiological, microarchitectural, histomorphometric, and biochemical analyses.

Chapter 2

Method

2.1 Ovariectomized Rat Femoral Fracture Model

In this study, osteoporotic rats were used in this study. The female retired breeders of Sprague-Dawley (SD) rats were obtained from the Laboratory Animal Services Center (LASEC) of the Chinese University of Hong Kong (CUHK). The rats were housed and acclimatized at the laboratory of research animals of the Prince of Wales Hospital. The rats were housed in a 12-hour light-night cycle room. The rats were allowed with free cage movements and had *ad libitum* access to standard rat diet and tap water. The Chinese University of Hong Kong Animal Experimental Ethics Committee approved the experimental protocols of this study (Ref. No. 08/024/MIS).

2.1.1 Ovariectomized Rat Model

Osteoporotic rat were developed according to our previously established protocol[129]. Bilateral ovariectomies (OVX) were performed on six-month old female SD rats. The rats were then allowed three months for the development of osteoporosis.

Six-month old female SD rats (≈250 grams, retired breeders) were obtained from LASEC of CUHK. General anaesthesia (Ketamine (75 mg/kg) and Xylazine (10 mg/kg) mixture, i.p.)[128] was given to the rat. After the rat was anaesthetized, the hair on both sides of the rat was shaved from the lower rib to the top of the

thigh. The dimension of the area that the hair of the rat was shaved was approximately 4×4 cm. The region that the hair was shaved on the rat was sterilized with 0.5% Hibitane in 70% ethanol. Then the rat was positioned laterally. The ovariectomy was performed with bilateral ovaries approached (Figure.2.1). An incision of 8 mm was made between the lowest rib and the top of the thigh. The abdominal wall was dissected using a pair of scissors and an incision of 1 cm was made. After dissection of the lateral abdominal wall, the ovaries were explored in the abdominal cavity and exposed (Figure 2.1b). Then the ovary, part of the oviduct, concomitant vessel and some visceral fat were ligated (3-0 sutures, Mersilk, Ethicon Ltd., Belgium) and resected. The abdominal wall and the skin were then sutured in layers by interrupted suture (3-0 sutures). After the removal of the ovary was completed on one side, the rat was turned to the other side and the surgical procedures were repeated. Buprenorphine (0.03 mg/kg, subcutaneous injection (sc), Temgesic, Schering-Plough, NJ, USA) was given for analgesia after both ovaries were removed.

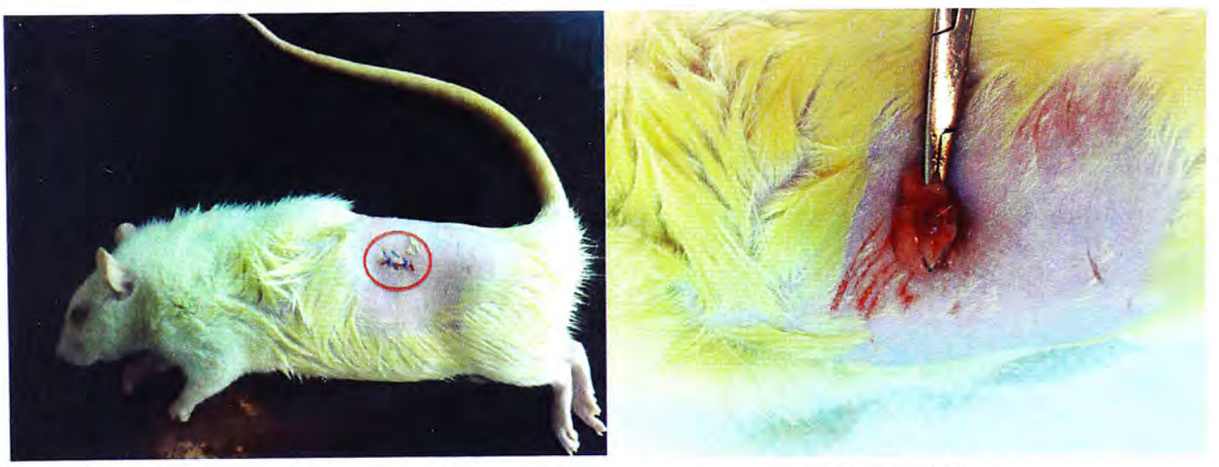

(a) Surgical Position and location of incision

(b) Exposed Ovary

Figure 2.1: The surgical procedure of bilateral ovariectomy. a: Lateral incision to approach bilateral ovaries. The red circle shows the location of incision. b: Exposed ovary surrounded by visceral fat.

2.1.2 Closed Femoral Fracture

After OVX was performed on the six month old rats, the rats were waited for three month to develop osteoporosis. When the osteoporotic rats were nine month old, closed femoral fracture was performed on the right femur of the rats according to our established protocol[76, 129]. This surgical procedure was modified from the closed femoral fracture surgery that was developed by Einhorn *et al.*[11]. All surgical equipments were autoclaved one day before the surgery. All surgical procedures were performed by a single experienced technician in order to keep the quality of the surgery consistent. After general anaesthesia was adminstrated to the rat, the rat was placed on the surgical table supinely. The hair on the right hinder limb was shaved and prepared with aseptic techniques (0.5% Hibitane in 70% ethanol). A 10 mm incision was made on the medial side of the limb and 2 mm medial to the patella (parapatellar incision). The femoral condyle was exposed by dissection of joint capsule of the knee. The patella was laterally dislocated and the intercondylar notch was exposed (Figure 2.2a). The intercondylar notch was used as an entry point for reaming. Reaming was performed with an 18G needle (Figure 2.2b and 2.2c). A sterilized Kirschner wire (K-wire, ⌀ 1.2 mm, Sanatmetal Ltd., Eger, Hungary) was inserted through the entry point into the medullary canal. The K-wire perforated at the proximal femur. The end of the K-wire at the proximal femur was bended into a hook to prevent distal movement. The K-wire at the femoral condyle was cut at the level of the articular surface at the distal femur to ensure smooth joint movements. The patella was relocated onto the articular surface with joint capsule. The skin was stitched discontinuously (3-0 sutures, Mersilk, Ethicon Ltd., Belgium).

After the intramedullary pin was inserted, the rat was positioned on a customized 3-point-bending apparatus (Figure 2.3a) which was used in our previous studies[76, 129]. A transverse fracture was created in the midshaft (diaphysis) of the right femur by dropping a metal blade ($\approx$ 500 g) from a height of 35 cm. The fracture was confirmed by anteroposterior and lateral radiographs (Radiological protocol in section 2.6.1). The rats with comminuted fracture were excluded from the

experiment. Buprenorphine (0.03 mg/kg sc. Temgesic, Schering-Plough, NJ, USA) was given 15 min pre-operation, and one day post-operation for analgesics.

2.2 Study Design

Eighty osteoporotic and femoral fractured rats were randomly divided into four groups: control (CG) , LMFHV group (VG) (See Section 2.3 for details), bisphosphonate group (BG) (See section 2.4 for details), and both LMFHV and bisphosphonate treated group (VBG) . In each treatment group, the rats underwent treatment for one of the four durations: 2, 4, 6, or 8 weeks. All treatments were started five days post-fracture to ensure full weight bearing on the fractured femur[76, 129]. Lateral x-rays (Faxitron X-ray system model 43855C, Wheeling, IL) were taken weekly (3 sec exposure time with a tube voltage of 60 kVp) in order to monitor the fracture healing status (See section 2.6.1 for details). At the end of treatment, the rats were anaesthetized and blood was collected by cardiac puncture. After blood collection, the rats were euthanized using overdose of sodium pentobarbital and the fractured femora were collected for μCT analysis.

2.3 LMHFV Treatment Protocol

In this study, the vertical LMHFV was created by a customized magnetic levitation vibration platform which was developed and used in our previous studies[76, 129] (US patent pending). Since the platform was initially designed for human subjects, modification of the vibration platform was made to allow to be used for animals. An aluminum platform, which was custom-made to the dimension of the vibration platform by the Mechanical Service Unit in CUHK, was placed on top of the vibration platform. Two pieces of plastic foam (2.5 cm thick for each) were placed between the aluminum platform and two 25 kg mass (Figure 2.4a). A plastic plate and a aluminum plate was placed between and on top of the plastic foam respectively. This setup would ensure the weight of the two 25kg mass was distributed

(a) Medial parapatellar incision

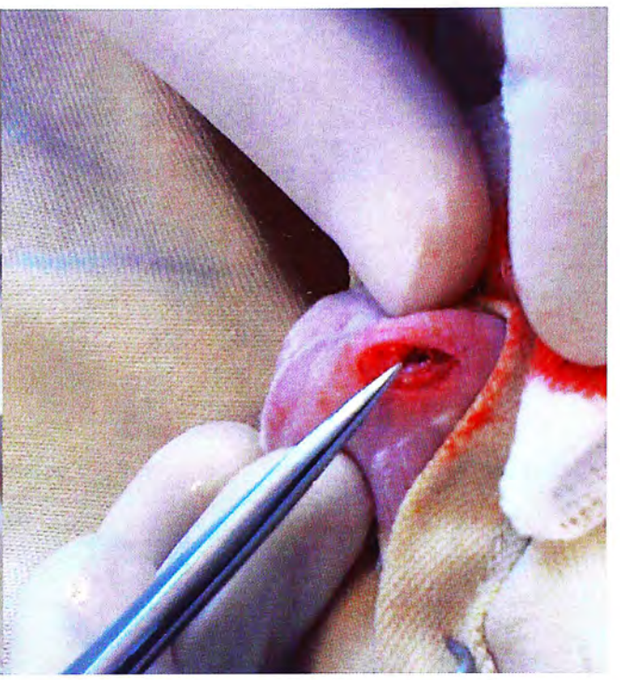

(b) Intercondylar notch

(c) Intramedullary drilling and reaming

(d) K-wire Insertion

Figure 2.2: Surgical procedures for intramedullary pinning. a: Medial parapatellar incision and articular surface of the femoral condyle. b: Intercondylar notch was exposed by lateral dislocation of the patella. c: Intramedullary drilling and reaming with an 18G needle. d: The tip of the K-wire was bended to prevent distal migration.

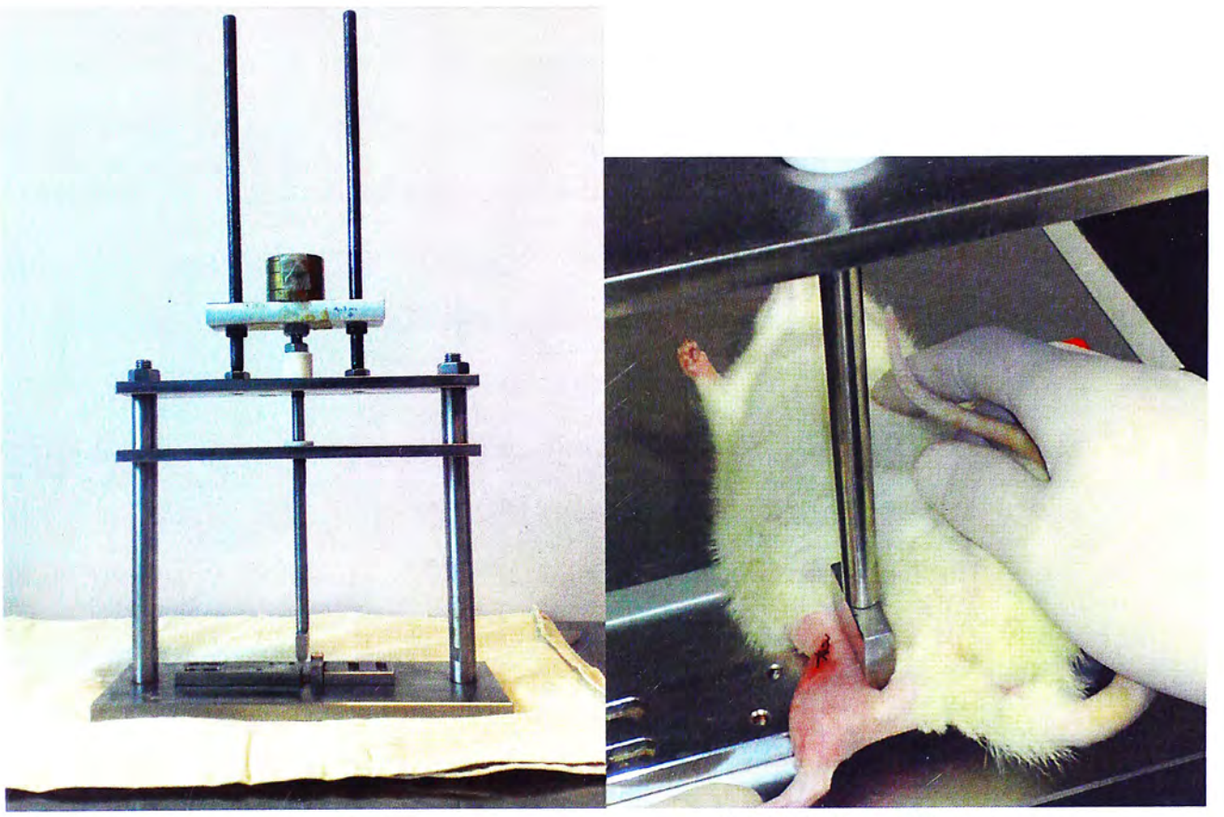

(a) Three-point-bending apparatus (b) Right femoral fracture on rat

Figure 2.3: Closed femoral fracture procedure and apparatus. a: Three-point-bending apparatus used to create closed femoral fracture. b: The blade was dropped onto the midshaft of the right femur after the intramedullary pin was inserted.

evenly over the vibration platform and eliminated the need to remove the weights after completion of each treatment. This would reduce the variation of wave form between treatments (Figure 2.4b).

A plastic sheet was placed under the bottomless and compartmented cage to transfer the rats onto the vibration platform (Figure 2.4a). The cage with the plastic sheet was slid into position on the vibration platform. The plastic sheet was slid out under the cage while keeping minimal disturbance to the rats. This allowed the rats to stand on top of the vibration platform and the vibration stimulation would transfer to the rat through their feet directly (Figure 2.4c). The duration of treatment was electronically controlled by a timer. After 20 min of treatment, the rats were transferred back to their cages.

The rats in VG and VBG stood separately in a bottomless, compartmented cage on the vibration platform for 20 min/day, 5 days/week[76, 129]. The black partitions were used to prevent the rats from disturbing each other. This was necessary to stablilize animal behaviors. The vibration platform provided vertical low-magnitude high-frequency vibrations at 35 Hz with a peak-to-peak acceleration of 0.3g (g = gravitational acceleration), which were the same parameters that were used in our previous studies[76, 129]. The rats in CG and BG stood on the unpowered vibration platform in order to receive sham treatment with same regime.

2.4 Bisphosphonate Treatment Protocol

2.4.1 Pharmacological Parameters

There are a few commonly used bisphosphonates available in the market including alendronate (Fosamax®), ibandronate (Boniva®), and risedronate (Actonel®)[91]. Ibandronate was chosen for bisphosphonate treatment due to its high efficacy compared to other available bisphosphonates. The pharmacokinetics of ibandronate are studied preclinically[93, 5].

The optimal ibandronate dosage to prevent bone lost was determined to be 1

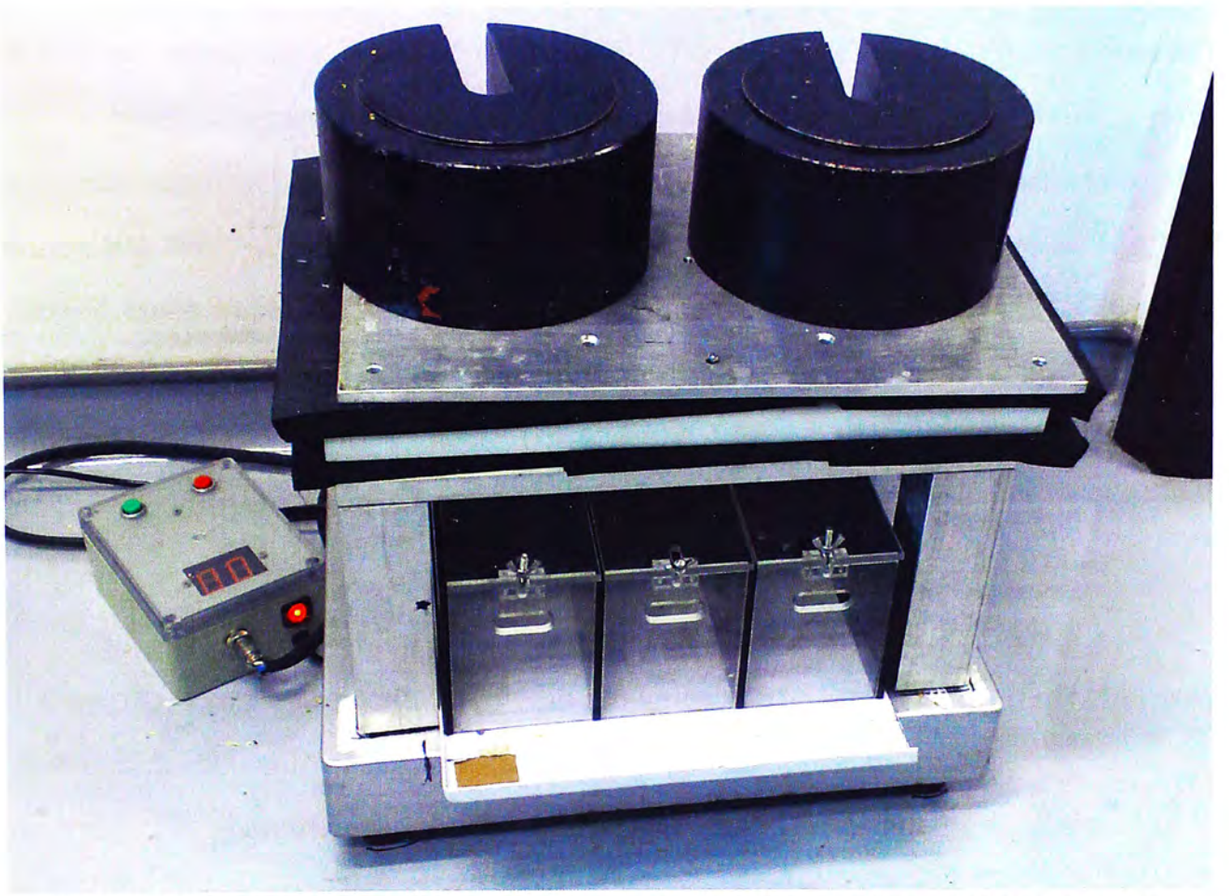

(a) LMHFV treatment setup: LMHFV platform, bottomless cage, aluminum platform, and timer

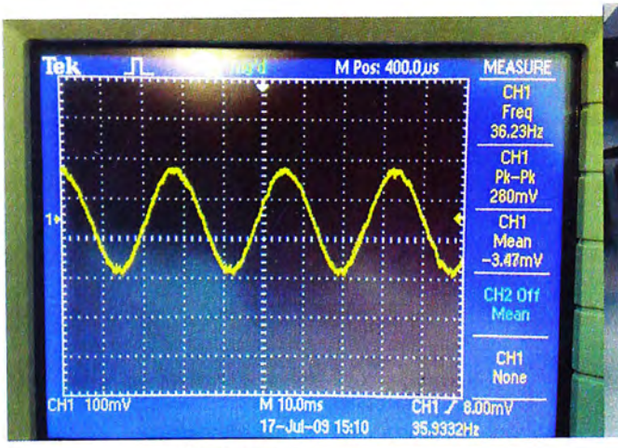

(b) LMHFV wave form

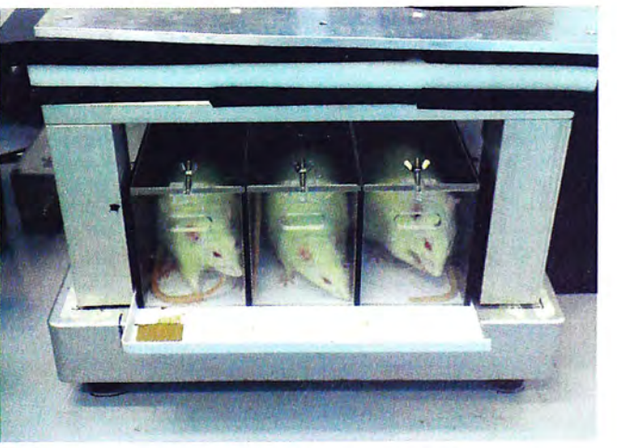

(c) Rats in bottomless cage

Figure 2.4: LMHFV procedure and setup. a: An aluminum platform is placed on top of the LMHFV platform. Two pieces of plastic foam are placed between the two 25 kg weights and the aluminum platform. A plastic plate and a aluminum plate was placed between and on top of the plastic foam respectively. The bottomless cage is placed under the aluminum platform. The piece of plastic is removed during treatment. b: The waveform of LMHFV measured by a oscilloscope. The waveform was sinusoidal. c: The rats stand inside the bottomless cage individually while the hind legs stand on the platform directly.

μg/kg/day in OVX rats[8, 120]. The frequency of administration for bisphosphonate would not affect the efficacy of the drug[8]. The effect of bisphosphonate depends on the total administered dose in a given period[8, 120]. The bioavailability does not vary significantly between different routes of administration other than oral, which has bioavailability of <1%[5, 39, 80]. In addition, subcutaneous injection showed comparable bone concentration to intravenous injections[80]. Therefore, weekly subcutaneous injection of ibandronate (1 μg/kg/day) was administered for the optimal anti-resorptive effect. For CG and VG, saline was injected weekly for sham ibandronate treatment.

2.4.2 Ibandronate Injection Solution Preparation

1.4 mg of ibandronate sodium (Sigma Chemical Ltd., St. Louis, MO, USA) was dissolved in 200 mL of 0.9% saline to make an ibandronate injection solution (7 μg/mL). The ibandronate solution was stored at 4°C until injection. Before injections, the ibandronate solution was equilibrated at room temperature.

2.4.3 Injection

General anesthesia (Ketamine (75 mg/kg) and Xylazine (10 mg/kg) mixture, i.p.) was given to the rats before ibandronate injection. The rat was weighted on a spring balance before each injection to ensure the injected dosage of ibandronate was accurate and consistent. The equation for calculating the dose and the corresponding volume of injection is

$$\text{Dosage [mg/kg]} \times \text{mass [kg]} = \text{Dose [mg]} = \text{Solution Concentration [mg/mL]} \times \text{Volume [mL]} \tag{2.1}$$

For subcutaneous injection, the rat was put into supine position. The back skin of the rat was gently raised. A 25G needle was inserted at a shallow angle and parallel to the back of the rat. Ibandronate solution (7 μg/mL) was injected subcutaneously on the dorsal side of the rat.

2.5 Fluorochrome Labeling

2.5.1 Fluorochrome Preparation

Calcein green (Sigma, Deisenhoren, Germany) and xylenol orange (Sigma, Deisenhoren, Germany) fluorochrome injection solutions were prepared according to our previous established protocol[75]. Calcein green and xylenol orange (0.5 g and 9 g respectively) were dissolved in 100 mL of distilled water to make up a concentration of 5 mg/mL and 90 mg/mL of calcein green and xylenol orange respectively. The pH of the solutions were adjusted to 7.2 with sodium hydroxide solution. The fluorochrome solutions were filtered and kept at room temperature and in dark.

2.5.2 Injection

General anesthesia (Ketamine (75 mg/kg) and Xylazine (10 mg/kg) mixture, i.p.) was given to the rats before fluorochrome injection. The fluorochromes were injected subcutaneously on the dorsal side of the rat. Calcein green and xylenol orange were injected at different time during treatment period. Calcein green (5 mg/kg) was injected two-weeks before euthanasia while xylenol orange (90 mg/kg) was injected one-week before. All the rats were weighted before each injection. The volume of injection was calculated by dividing the dosage of fluorochrome by mass of the rat. For fluorochrome injections, the value for dosage and concentration of solution were the same. From equation 2.1, the volume [mL] of injection is equal to mass [kg] of the rat. The fluorochrome was injected subcutaneously. A similar injection technique for administration of ibandronate was used for injection of fluorochrome (Section 2.4.3).

2.6 Assessments

2.6.1 Radiographic Analysis

Making of Radiographs

The radiographs were taken according to our established protocols[76, 129]. General anesthesia (Ketamine (75 mg/kg) and Xylazine (10 mg/kg) mixture, i.p.) was given to the rats before x-rays were taken. The radiographs were taken with an x-ray machine for small animals (Faxitron X-ray Corporation, Wheeling, IL. USA). The exposure time was set as three seconds with and tube voltage of 60kVp. For the lateral x-ray, the rat was placed in prone position with the hip joints in abduction and 135° of flexion (Figure 2.5a). The knee joints were flexed. For anterior-posterior (AP) radiographs, the rat was placed in supine position and the hip joints were fixed in adduction, extension, and 0° rotation. The distance between the x-ray source and the rat was kept at 40 cm. The X-ray films (18 × 24 cm X-Ray Film, Fujifilm Corporation, Tokyo, Japan) were developed by an automated developer (Optimax X-Ray Film Processor, Protec GmbH & Co. KG, Oberstenfeld, Ludwigsburg, Germany). The developed film was scanned (16 bit gray scale, 300 dpi, JPEG format) by a scanner (Epson Perfection 4990 Photo scanner, Epson Hong Kong Ltd., Wanchai, Hong Kong).

Radiographic Measurements

The radiographs were analyzed according to our established protocol[76, 129]. Two experienced orthopedic surgeons, who were blinded from the time point and groupings of the digital x-ray, graded the fracture healing status for each rat according to our previous protocols[76, 129]. Radiographic healing was defined as complete bridging of all four cortices of a mineralized callus[129]. Callus width (CW) is defined as the maximum width of callus minus the outer diameter of femur (Figure 2.5b). Callus area (CA) is equal to the size of radiopaque area of callus (Figure 2.5c). Both CW and CA were measured on lateral x-rays of each rat by using Meta-

morph Image Analysis System (Universal Imaging Corporation, Downingtown, PA, USA)[76, 129]. Each callus measurement was repeated three times and the average was recorded. The average for each group was plotted in a line graph.

2.6.2 μCT Analysis

The fracture femur was harvested after euthanasia and the K-wire was removed gently. Then the fracture femur was wrapped in gauze and fitted in the sample tube (⌀ 16 mm) (Figure 2.6a) and scanned with micro-CT (μCT40, Scanco Medical, Brttisellen, Switzerland) according to our established protocol[76, 129]. The scan range was set to be 7 mm (368 slides) and the fracture line was set in the middle of this range. The resolution was set to be 16 μm per voxel and 1024×1024 pixels. Region of interest (ROI) was selected from 2D images with a standardized threshold (>165) as mineralized tissue according to established protocol[76, 129]. Three dimensional (3D) reconstruction of mineralized tissue was performed according to our established protocol[76, 129]. A low pass Gaussian filter (Sigma = 1.2, Support = 2) was used for 3D reconstruction. Different thresholds were used in order to distinguish old cortical bone, and low and high density mineralized tissue in the callus[43]. The low density (150 – 350) and high density (> 350) analysis were performed in order to distinguish woven bone from old cortical bone or laminar bone.

Quantitative analysis used all 368 slides of the 2D images. Low and high density evaluations were performed separately. Morphometric parameters that were evaluated were total tissue volume (TV), total bone volume (BV) , high- and low-density bone volume (BV_h and BV_l respectively) (where BV_h + BV_l = BV), and their respective normalized BV with TV (BV/TV, BV_h/TV, and BV_l/TV) were performed. The average for each group was recorded.

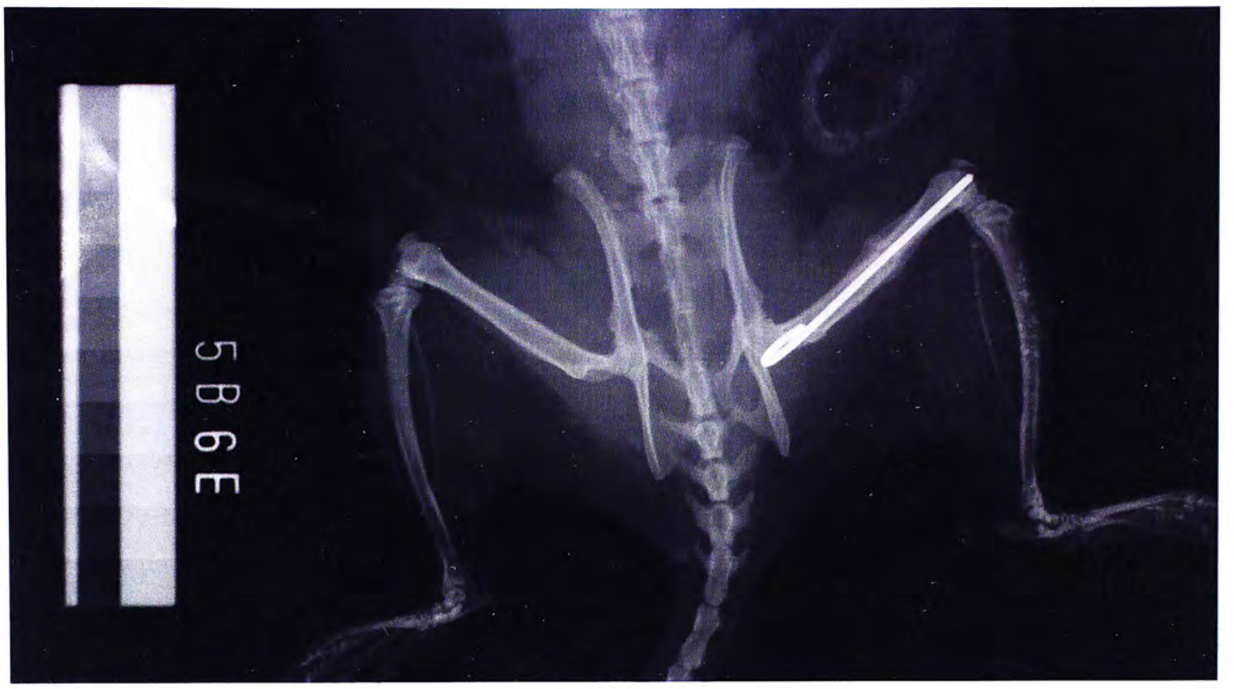

(a) Lateral X-Ray

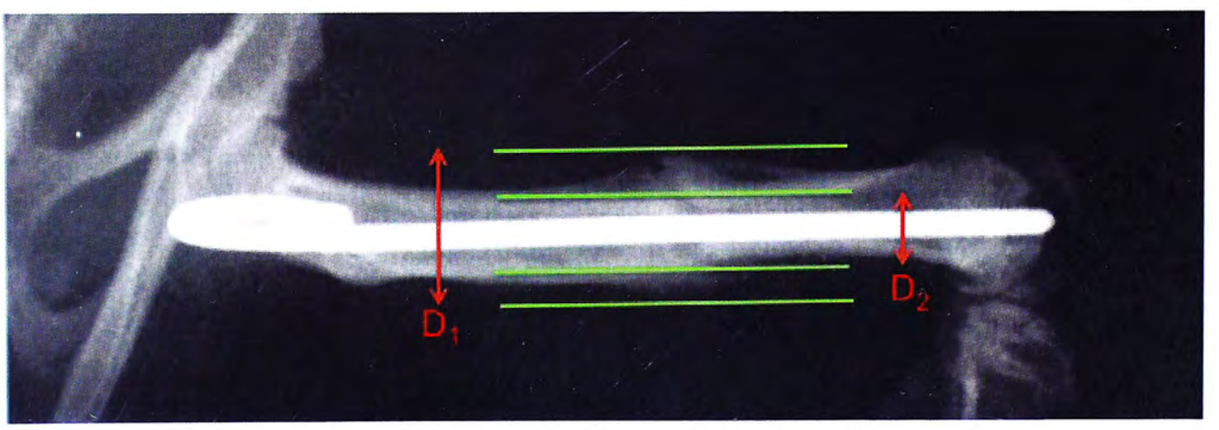

(b) Distance measurements for callus width analysis

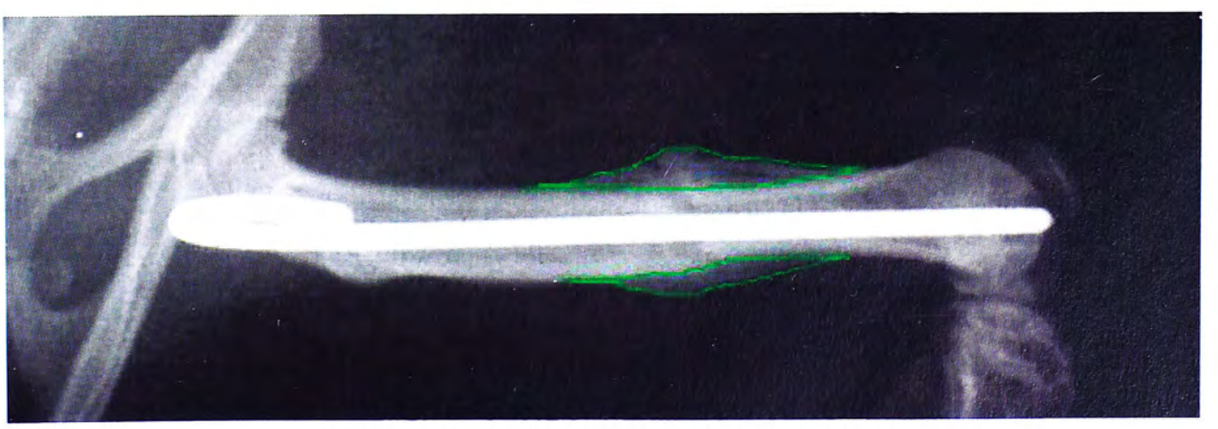

(c) Contouring of the callus for callus area analysis

Figure 2.5: X-Ray analysis. a: Lateral X-ray was taken weekly to evaluate fracture healing status. A calibrator was placed next to the rat as a length reference. b: Callus width measurement (D_1 – D_2) on latera x-ray. c: Region of interest (Highlighted in green) for the analysis of callus area on latera x-ray.

(a) μCT placement of sample

(b) μCT 2D Contouring

Figure 2.6: Micro-architecture analysis by μCT. a: Placement of the sample in sample tube and μCT. b: 2D contouring of the region of interest (ROI). The region enclosed by the green line is the ROI.

2.6.3 Undecalcified Histology

MMA Sample Preparation

Two weeks and one week before the euthanasia of the rats, calcein green (5 mg/kg) and xylenol orange (90 mg/kg) were injected respectively. The fluorochromes were purchased from Sigma (Deisenhoren, Germany). After scanning by μCT, the fracture femora were dehydrated and prepared for undecalcified histomorphometry according to established protocol[36, 75] . The excess muscle on the fractured bone was removed. The fracture femora were dehydrated serially in alcohol (70%, 95%, and 100%) and xylene, After dehydration was completed, the samples were embedded in methylmethacrylate (MMA) (Table 2.1). The MMA solutions were prepared according to our established protocol[75].

Table 2.1: Tissue dehydration and embedding in methylmethacrylate for undecalcified histology.

Reagent	Day Per Change	Sample inside Vacuum	Storage Temperature
Buffered Formalin	1 Day	No Vacuum	Room Temperature
70% Ethanol	2 Days	1 hour/day	Room Temperature
95% Ethanol	2 Days	1 hour/day	Room Temperature
100% Ethanol	2 Days	1 hour/day	Room Temperature
Xylene	2 Days	4 hour/day	Room Temperature
MMA I	2 Days	4 hour/day	4°C
MMA II	2 Days	4 hour/day	4°C
MMA III	2 Days	4 hour/day	4°C

Note: All solutions were refreshed everyday.

MMA solutions Preparation

Water-free Methylmethacrylate (MMA) was prepared first. Washing solution was prepared by adding 200 grams of sodium chloride and 50 grams of sodium hydroxide in 1 L of distilled water. Then, 550 mL MMA (Merck Schuchardt OHG, Hohenbrunn, Germany) and 300 mL washing solution were poured into the funnel. The funnel

with the MMA mixture was shook vigorously. Then, the funnel was placed on a stand and the mixture was allowed to separate. The lower layer was drained into a waste bottle. The upper layer was washed with washing solution for two more times and with distilled water for three times (For a total of six times). After the washing was completed, the upper layer was drained into a 1 L glass bottle with 60 g of calcium chloride pellet ($CaCl_2$) . The MMA was shook vigorously and stood for 15 min for dehydration by $CaCl_2$ pellets. After the dehydration was completed, the $CaCl_2$ pellets were filtered by paper filters. The filtrate was the water-free MMA solution. MMA I, II, and III were prepared using different proportion of water-free MMA solution, butylmethacrylate, methylbenzoate, and benzoyl peroxide (Table. 2.2). Benzoyl peroxide were dried by using desiccates for at least 3 days before addition to MMA.

Table 2.2: Preparation of MMA solution I, II, and III.

MMA I		MMA II	
Materials	Volume [mL]	Materials	Amount
Water-free MMA	500	MMA I	800 mL
Butylmethacrylate	292	Benzoyl Peroxide	3.2 g
Methylbenzoate	42		
Polyethylene glycol 400	10		

MMA III		PMMA	
Materials	Amount	Materials	Amount
MMA I	800 mL	MMA III	40 mL
Benzoyl Peroxide	6.4g	N,N-dimethyl-p-toluidine	160 μL

MMA Embedding and Sectioning

After dehydration by serial alcohol and xylene, the samples were submerged in MMA solutions (Table. 2.1). Then, the sample was transferred to a vacuum for 4

hours. Afterwards, the sample was stored at 4°C. The MMA solutions were refreshed everyday and changed every 2-days. For polymerization, the sample was transferred to a 100 mL specimen cup. 20 mL of MMA III was added to the specimen cup and polymerized at −20°C. Polymerization reaction of MMA was initialized by adding N,N-dimethyl-p-toluidine to MMA III and spraying nitrogen gas the PMMA solution for 3 min. The specimen cup was half-opened by covering the cup with the lid. After spraying of nitrogen gas, the cup was covered, sealed, and stored at −20°C. By polymerizing 20 mL of MMA III solution, this created a smooth surface for embedding the sample. 40 mL freshly prepared MMA III was added to the sample. The sample was put in the vacuum for 4 hours. Then 160 μL of N,N-dimethyl-p-toluidine was added to MMA III and nitrogen gas was sprayed on the surface of the PMMA solution for 3 min. The specimen cup was half-opened by covering the cup with the lid. After spraying of nitrogen gas, the cup was covered, sealed, and stored at −20°C.

After polymerization was completed, the fractured femur would be embedded in a yellow transparent solid MMA. The excess surrounding solid MMA were trimmed to make the base of sample parallel to the sagittal plane. The embedded sample was fixed on a custom-made holder using cyanoacrylate-based glue. The samples were sectioned sagittally (300 μm thick) by saw microtome (Leica SP1600, Leica, Germany) using a circular saw which was 300 μm thick. Excess water was used to minimize heating during sawing. Each section was polished and grinded to 100 μm with different grades of sand paper before analysis. The polished samples were mounted on a plastic slide and were ready for analysis.

MMA Analysis on Bone Mineralization Rate

After preparing and grinding each slide to 100 μm, the fluorochrome-label femur sections were observed under an ultraviolet fluorescent microscope (Leica DMRXA2, Leica, Germany). A digital picture was taken by the camera attachment on the microscope. The analysis was performed using Metamorph Image Analysis System

(a) MMA embedding bottom

(b) Bone embedded in MMA

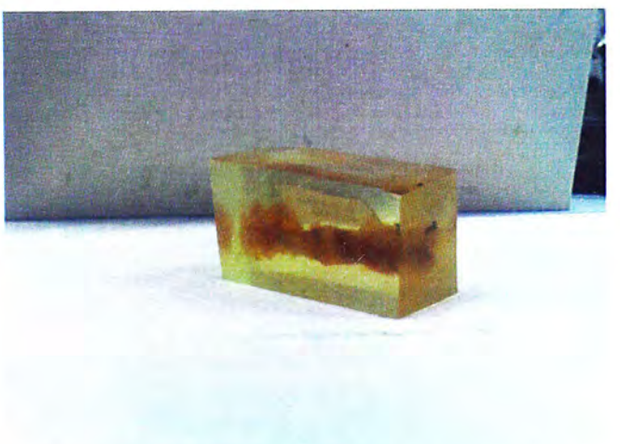

(c) MMA sample grinded to parallel to cutting surface

Figure 2.7: The procedure for embedding fracture femur in MMA. a: 20 mL of MMA was polymerized to provide a smooth surface for embedding of sample. b: Femur was embedded in polymerized MMA (total of 60 mL of MMA). c: Solid MMA was trimmed and grinded to be parallel to the cutting surface.

(Universal Imaging Corporation, Downingtown, PA, USA). Mineral apposition rate (MAR) was measured using standard histomorphometric procedure[109, 133]. MAR The region of interest for the MAR measurement was defined to be 2 mm to the proximal and distal to the fracture site. For each quarter of the callus that is within the region of interest, five points, which are 0.2 mm apart, on the distinct fluorochrome bands were chosen. If there were no distinct bands within the region of interest, the equal distance points were chosen at the lateral edge of the fluorochrome patch. The distance between the two fluorochromes was measured at these points. The average MAR was calculated to be the averages of the 20 measurements (5 points/quarter, 4 quarters in the region of interest). MAR was measured from week 4 – 8. The distance between the fluorochrome bands for 2 weeks treatment groups was not included because callus mineralization occurs during mid-second week post fracture (10 – 14 days post fracture)[33].

2.6.4 ELISA Analysis on Bone Markers

Blood Sampling Procedure

5 mL blood sample of the rat was collected via cardiac puncture under general anesthesia[28]. The rat was given general anesthesia and put in a dorsal position (Figure 2.8a). The heart was palpated by placing fingers on the side of the chest at the level of the rat's elbows. The needle is directed into the heart at the place with the maximal heart beat. A 5 mL syringe with a 21G needle was used to puncture the heart from the left side laterally. When a flow of blood into the tip of the needle was observed, the syringe plunger was pulled back slowly to avoid hemolysis. After 5 mL of blood was collected, the needle was removed from the syringe. The blood in the syringe was emptied into a 15 mL centrifuge tube. After collection of blood from the rat, overdose of sodium pentobarbital was administrated to make sure that the rat would be dead after exsanguination.

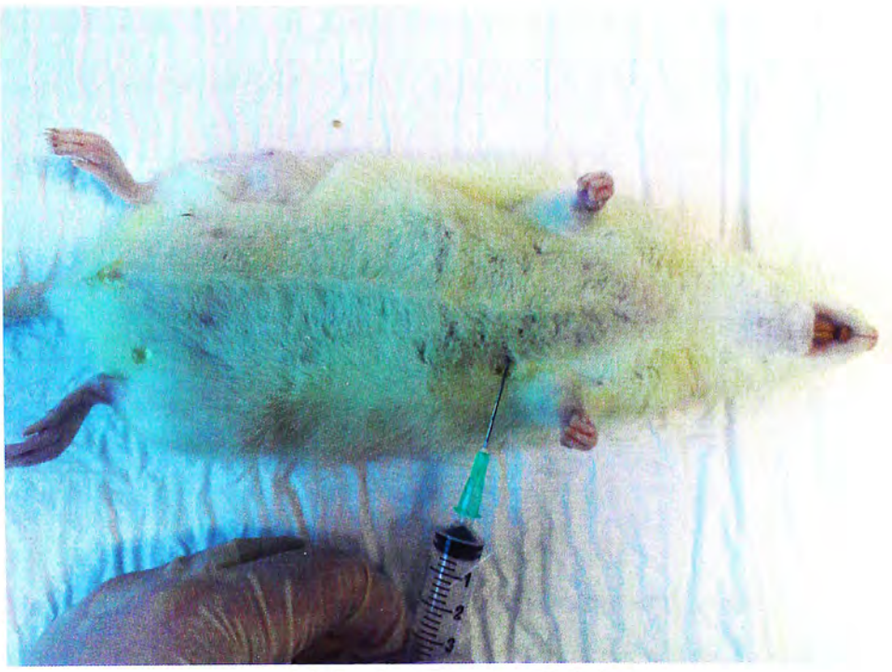

(a) Cardiac Punction Position

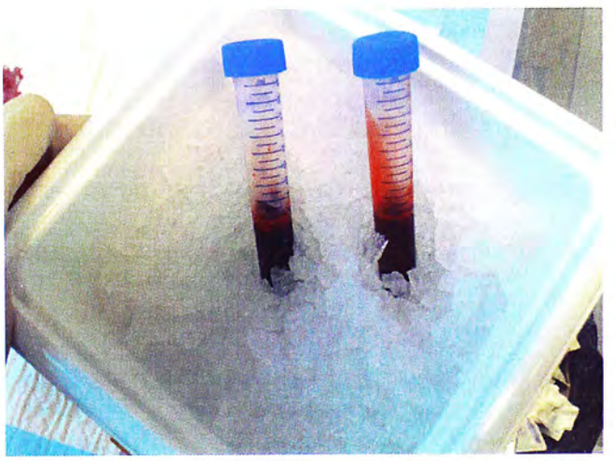

(b) Blood samples were stored in ice

Figure 2.8: The blood sampling procedure. a: Lateral incision to puncture the heart with a syringe needle. b: Collected blood was stored in ice before separation of blood by certrifugation

Blood Serum Preparation

The whole blood samples were kept in ice for one hour before separation by centrifugation. The blood samples were centrifuged at 3000 rpm (≈2000g) for 15 min. The blood serum was separated and aliquoted into 500 μL portions. After aliqoting the serum, the serum was stored at −80°C until analysis by ELISA. Commercially available ELISA kits were used to measure serum concentration of osteocalcin (Rat-Mid Osteocalcin, Nordic Bioscience Diagnostics A/S, Denmark) and tartrate-resistant acid phosphatase 5b (TRAP 5b) (RatTRAP, Immunodiagnostic System Limited, United Kingdom). Concentration of osteocalcin and TRAP5b in serum were measured to analyze bone formation[95] and resorption[141, 71] rate respectively.

Osteocalcin and TRAP5b ELISA Procedure

The osteocalcin ELISA (Enzyme-Linked Immunosorbent Assay) kit (Rat-Mid Osteocalcin, Nordic Bioscience Diagnostics A/S) and TRAP5b ELISA kit (RatTRAP, Immunodiagnostic System Limited) were used to measure the serum concentration of osteocalcin and TRAP5b enzyme respectively. The osteocalcin ELISA uses monoclonal antibody to competitively bind to soluble or immobilized osteocalcin. The monoclonal antibody in this kit recognized the mid-molecular part (amino acid 21 – 29) of the rat osteocalcin protein[115]. The TRAP5b ELISA is a solid phase immunofixed enzyme activity assay.

The kits were stored in a 4°C cold room until analysis. All solutions and samples were equilibrated to room temperature before use. The assay was performed at room temperature. All samples were performed in duplicate. The thawed sample would not be stored and used for another measurement. This would prevent the degeneration of osteocalcin and TRAP5b by freeze-and-thaw[14, 141]. The instructions from the manufacturers were followed strictly without modification. The absorbance for osteocalcin was measured immediately at 450 nm with a reference at 650 nm[127] while absorbance for TRAP5b was measured at 405 nm[141]. Calibration curves for osteocalcin and TRAP5b were plotted. The concentration of osteocalcin and

TRAP5b was calculated from their respective calibration curve.

TRAP5b ELISA Kit Validations

The validation of the TRAP5b ELISA kit was performed by Wu *et al*[141]. The method validation experiments were conducted for inter- and intra-assay accuracy and precision, establishment of sample control, range findings of different population groups, selectivity tests, parallelism and stability. The analytical range was 1.00 – 10.0 U/L and the total errors of lower limit of quantification and upper limit of quantification validation samples were 8% and 21%, respectively. Selectivity results showed accurate spike recovery among the majority of test samples from target populations. Samples were demonstrated to be stable for up to four freeze/thaw cycles and for 24 months at $-70 \pm 10°C$.

2.7 Statistical Analysis

All quantitative data were expressed as mean ± standard deviation (SD). All analyses were performed with SPSS version 16.0 software (SPSS Inc, Chicago, IL, USA) in Microsoft Windows XP. One-way Analysis Of Variance (ANOVA) with Bonferroni Post Hoc test and two-way ANOVA were performed to analyze difference among groups and interaction of Bis and Vib respectively. Statistical significance was set at a probability level of 95% ($p<0.05$).

Chapter 3

Results

In this experiment, bilateral ovariectomy (OVX) and closed femoral fracture were performed on 80 SD rats. There was no significant bleeding occurred during the two procedures. However, two rats died from the OVX procedure and four were either died after the fracture surgery or excluded due to non-transverse fracture. The overall rate of success for the creation of transverse fracture was 92.5% (74/80) (Table 3.1). One rat died unexpectedly during the study for unknown reason. Therefore, there was 73 rats left, out of a total of 80 rats, for analysis. The rats with a successful surgical procedure showed no surgical complications such as wound infections. All rats recovered full weight-bearing walking before commencing treatment (Day 5 post-fracture). This was comparable to the results in our previous studies which also found that the rats regained full weight-bearing before Day 5 post-fracture[76, 129]. No panic behaviors and weight loss for all groups were observed during the treatment period. Subcutaneous injection of ibandronate, saline, or fluorochromes did not cause any complications or death to the rats.

Table 3.1: Sample size for four groups (CG, BG, VG, and VBG) at different time points (2, 4, 6, and 8 weeks post-treatment).

Group	Week 2	Week 4	Week 6	Week 8
CG	4	4	4	5
BG	5	4	5	5
VG	5	5	5	4
VBG	5	5	5	4

3.1 Radiographic Analysis

3.1.1 Callus Bridging Rate

From the weekly lateral and AP radiographs, radio-opaque external callus was observed around the fracture site from week 1 to week 8 in all groups. A callus gap at the fracture line was located between the calluses from the proximal and distal bone fragments. The size of the callus gap decreased over the treatment period. VG showed the earliest bridging of cortical bone at week 6. Also, CG and VBG bridged at week 8 on the serial radiographs respectively (Figure 3.1). BG showed incomplete bridging of the callus up to week 8. In addition, VG showed the highest bridging rate of cortical bone (100%) and BG had the lowest (20%) (Table 3.2).

3.1.2 Callus Width and Area

In quantitative assessment, both CA and CW showed that VG and CG peaked at around week 3 and week 4 (Figure 3.2). From week 1 to week 4, the callus measurements were increasing for all the groups. However, the trend was different for different treatment group from week 4 to week 8.

Week 1 – 4

From week 1 to week 4, all callus measurement showed an increasing trend (Figure 3.2). From week 1 to week 2, VG and VBG showed a comparable increase in CW

(from 1.85 to 2.26 mm) and CA (from 13.23 to 17.69 mm^2). At week 3 and week 4, the radiological callus measurements for all the groups peaked. The peak values for CG were lower than the rest of the groups (CW: 86% of VG, and CA: 86% of VG). CG was significantly lower than the other treatment groups in CW (Week 1, 2, 3, and 4 with $p < 0.01$) and CA (Week 2, 3, and 4 with $p < 0.05$). From week 1 to week 4, the average CW and CA for BG, VG, and VBG were comparable among each other. Therefore, there was no significant difference between these three groups.

Week 4 – 8

From week 4 to week 8, BG maintained a plateau trend while VBG showed a dropping trend. At week 8, BG had the largest callus measurements among different treatment groups. BG was 30.05% ($p < 0.0005$) and 50.11% ($p = 0.002$) greater than CG in CW and CA respectively. VBG had the second highest CW and CA in the four treatment groups. VG and CG had the smallest callus. At week 8, there was no significant difference between CG and VG in terms of CW and CA. VG was significantly different from BG in CW ($p < 0.0005$) and CA ($p = 0.003$) while VG found statistical difference with VBG in CA ($p = 0.005$) at week 8. Two-way ANOVA showed that there were significant interactions between the LMHFV and ibandronate for CA at week 6 ($p = 0.045$), week 7 ($p = 0.005$), and week 8 ($p = 0.004$).

When analyzing the rate of callus disappearance, from week 4 to week 8, VG had the largest drop in CA while CG and VBG had comparable reduction (Table 3.3). BG showed increasing CA from week 4 to week 8. Similar observations were also found in CW (Decreased CW in CG, VG and VBG; Increased CW in BG).

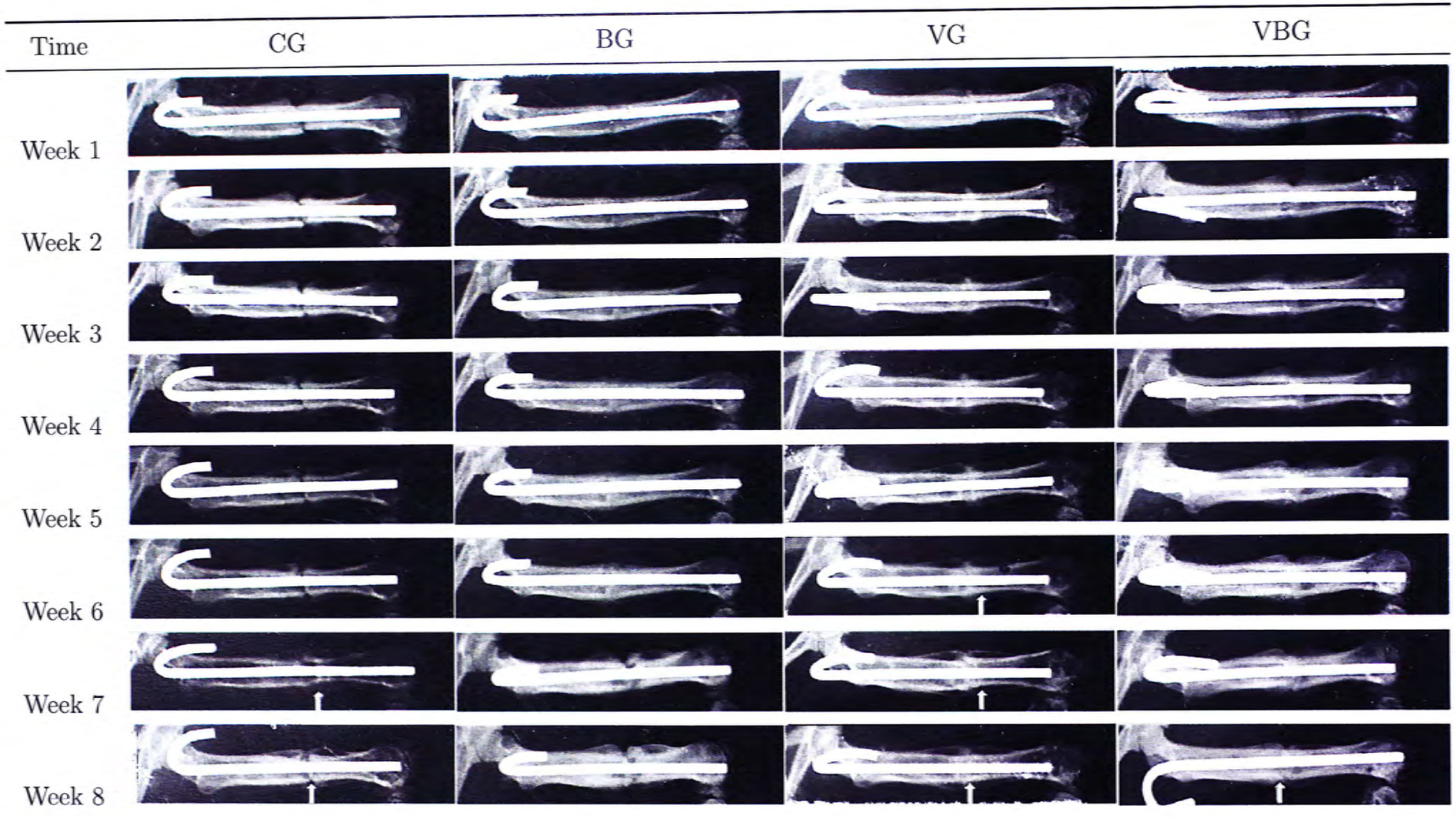

Figure 3.1: Representative serial lateral radiographs from week 1 to week 8 shows the fracture healing status in all groups (CG, BG, VG, and VBG). The white arrows represent bridged callus and no fracture gap. Faster healing was found in VG while CG and VBG showed similar healing.

Table 3.2: Callus bridging rate of the four groups (CG, BG, VG, and VBG) at different time points (4, 6, and 8 weeks post-treatment).

Group	Week 4	Week 6	Week 8
CG	30.77%	44.44%	80.00%
BG	28.57%	30.00%	20.00%
VG	35.71%	47.22%	100.00%
VBG	28.57%	44.44%	75.00%

Table 3.3: Callus area and width percentage changed from week 4 to week 8 for all treatment groups.

Group	CA	CW
CG	−16.09%	−5.04%
BG	5.39%	2.53%
VG	−24.42%	−18.44%
VBG	−12.17%	−12.09%

3.2 μCT Analysis

Microarchitecture analysis using μCT was completed. A trend was observed in the bone density (BV density) of the callus from week 2 to week 8. When comparing Bis-treated groups with non-Bis-treated groups, Bis-treated groups (BG and VBG) showed higher BV, BV_l, and BV_l/TV values but lower BV density from week 2 to week 8 (Table. 3.4).

Week 2 – 4

Mineralization of callus at the peri-fracture regions was observed on the μCT images at week 2 (Figure 3.3). At week 2, the 3D image of the fracture callus showed mineralized calluses in the peri-fracture regions. The quantitative measurements of BV/TV showed that all groups showed an increasing trend in BV/TV from week 2

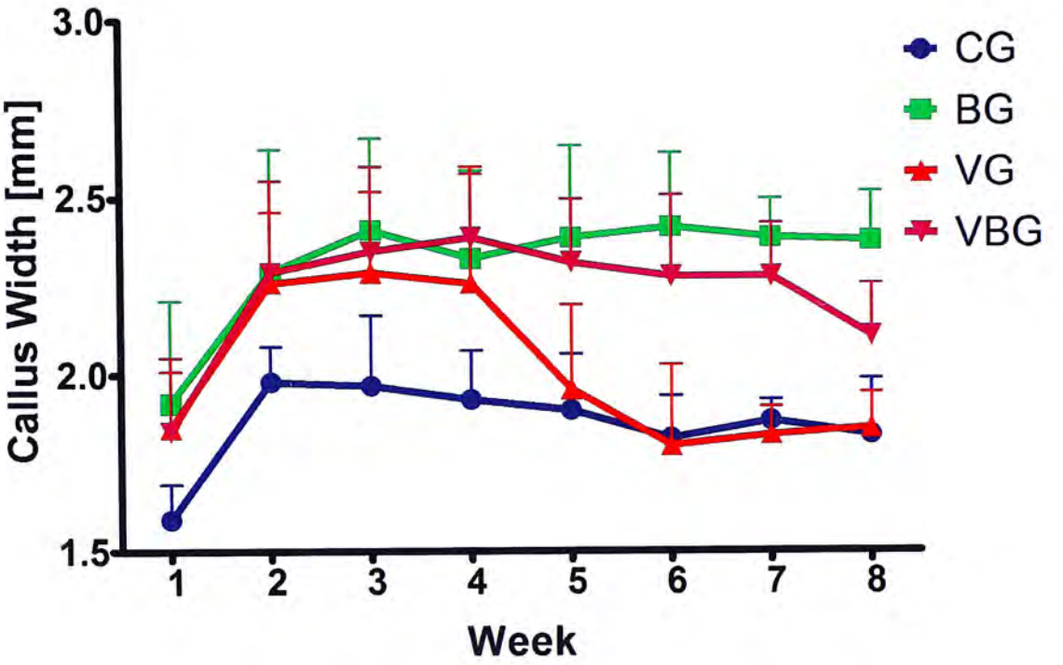

(a) Average callus width measured over 8 weeks radiologically

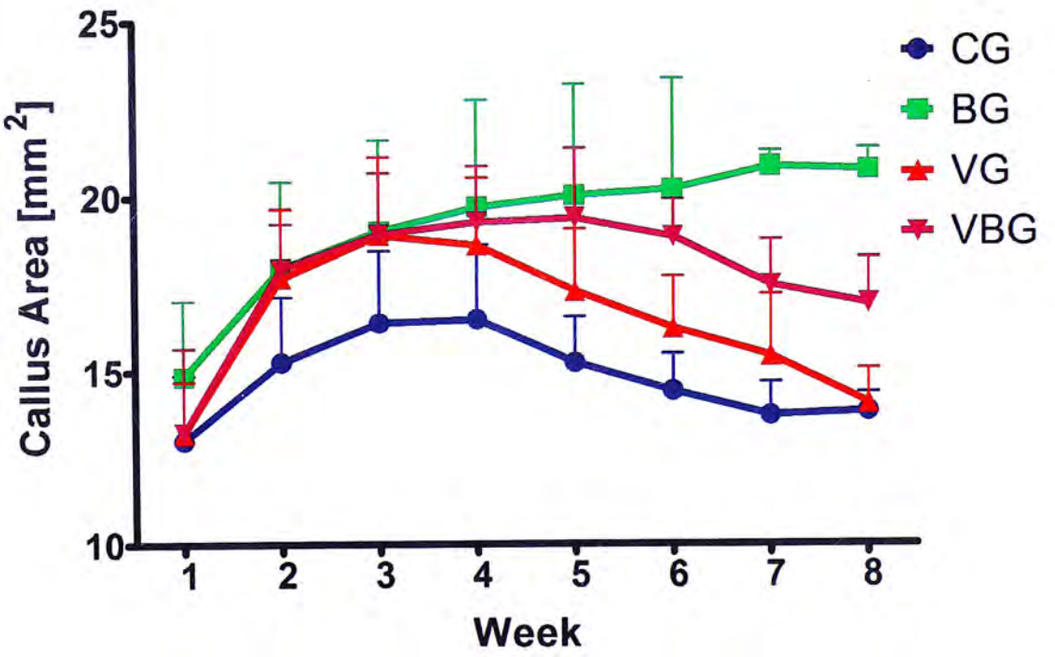

(b) Average callus area measured over 8 weeks radiologically

Figure 3.2: Changes of callus area and width over 8 weeks period in all groups (CG, BG, VG, and VBG) (Error bar represents 1SD). a: Callus width. b: Callus area. BG maintained a plateau trend while VBG showed a dropping trend. At week 8, BG had the largest callus (greater than CG in CW (30.05%, $p = 0.002$) and CA (50.11%, $p < 0.0005$) respectively), followed by VBG. VG and CG had the smallest callus and there was no significant difference among them. Significant interactions for CA at week 6 ($p = 0.045$), week 7 ($p = 0.005$), and week 8 ($p = 0.004$).

to week 4. At week 4, CG and VG reached their peaks (Figure 5.1). In addition, BV/TV for VG was 19.23% higher than CG ($p = 0.003$) at week 4.

Week 4 – 8

At week 6, BG and VBG reached the peak at week 6. VBG had the largest BV/TV . When compared to CG, VBG showed a 43.64% higher than CG ($p < 0.0005$). In addition, a decreasing trend of BV/TV in VBG was observed from week 6 to week 8 while BG showed a plateau trend (Figure 5.1). This decreasing trend of BV/TV observed in VBG was comparable to CG the drop drop in BV/TV in CG at week 6 to week 8. These two groups showed a 5% decrease of BV/TV from week 6 to week 8. At week 8, BV/TV for VG dropped from 19% higher than CG to a comparable level to CG at week 8. In addition, from the serial 3D images of the callus, VG showed smaller callus gap than the other three groups. CG and VBG showed comparable callus gap while BG showed the largest (Figure 3.3).

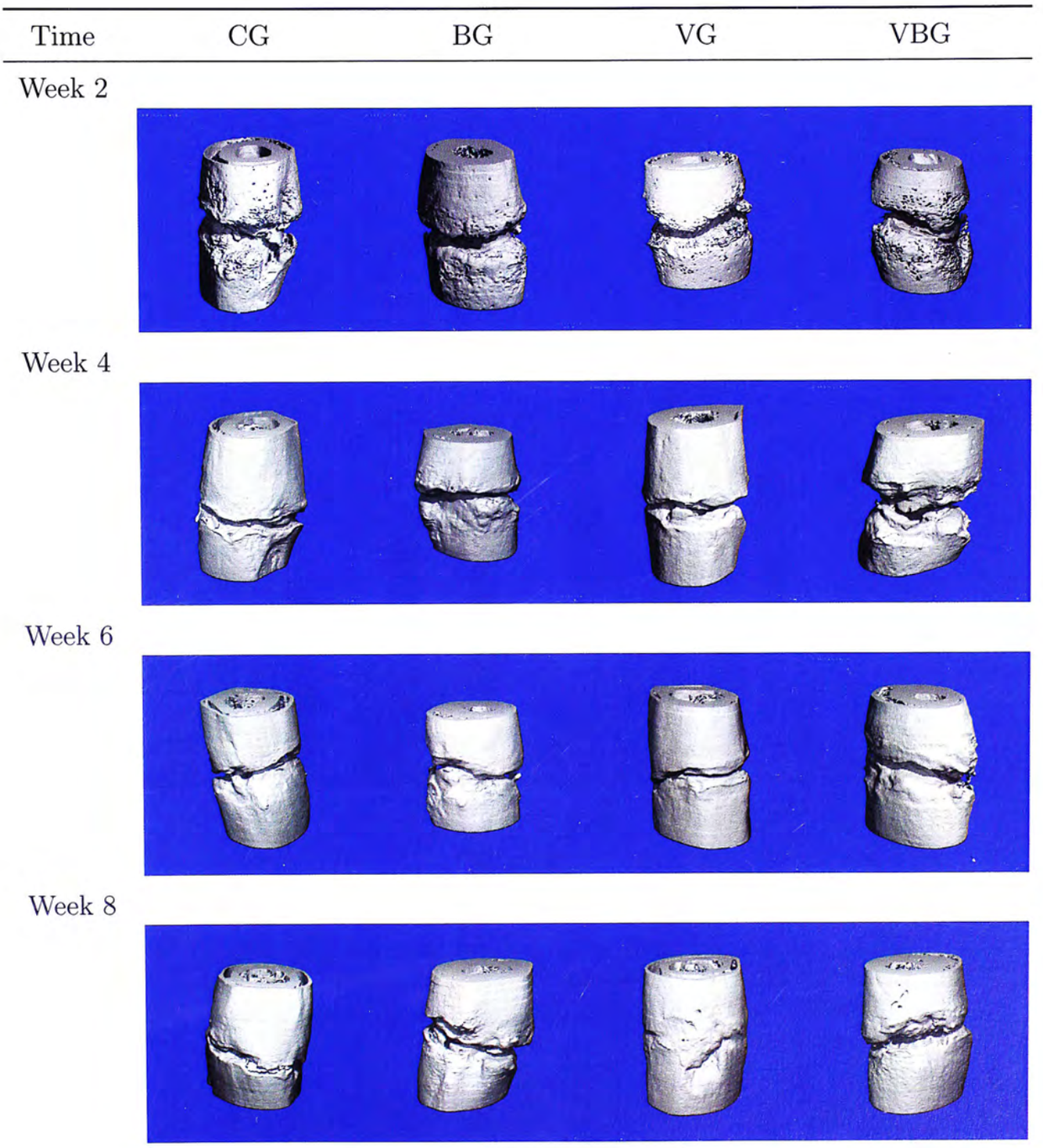

Figure 3.3: Serial μCT 3D images for different groups (CG, BG, VG, and VBG) from week 2 to week 8.

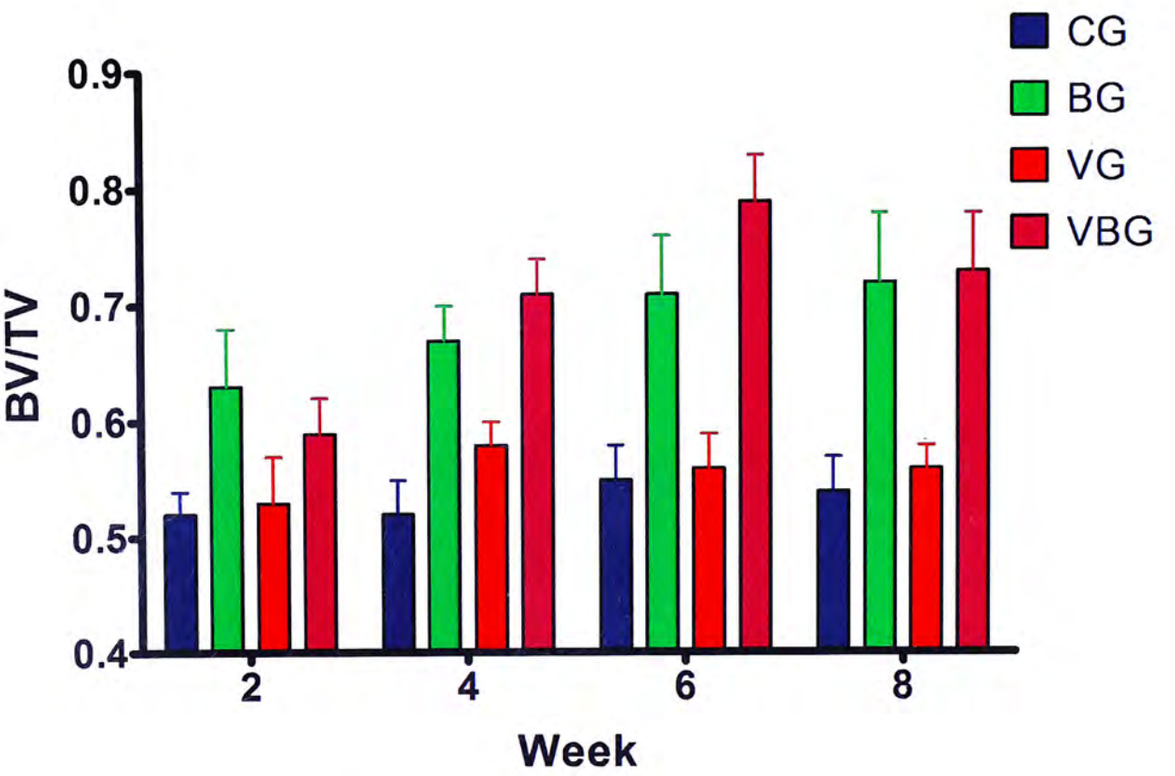

Figure 3.4: BV/TV bar graph showed that the normalized bone volume for CG and VG peaked at week 4 while BG remained the same level throughout the eight weeks period. VBG peaked at week six and dropped afterwards. (Error Bar represents 1SD)

Table 3.4: μCT data on femoral microarchitecture of the four groups (CG, BG, VG, and VBG) at different time points.

	Week 2				Week 4			
	CG	BG	VG	VBG	CG	BG	VG	VBG
TV [mm^3]	175.09 ± 8.76	163.00 ± 22.27	162.32 ± 27.16	162.45±17.26	167.94 ± 7.34	184.04 ± 27.19	157.23 ± 5.21	163.76±10.67^a
BV [mm^3]	90.51 ± 5.78	102.75 ± 9.55	85.59 ± 13.48	95.19 ± 7.47	86.80 ± 3.09^b	123.95 ± 16.00^a	90.78 ± 4.61^b	115.73 ± 7.92
BV/TV	0.52 ± 0.02^b	0.63 ± 0.05^a	0.53 ± 0.04^b	0.59 ± 0.03^a	0.52 ± 0.03	0.67 ± 0.03	0.58 ± 0.02^{ab}	0.71 ± 0.03^a
BV$_l$ [mm^3]	44.60 ± 2.95	59.40 ± 8.01	42.21 ± 11.31	50.42 ± 4.97	42.26 ± 1.42^b	73.62 ± 9.21^a	42.93 ± 4.42^b	70.57 ± 6.32^a
BV$_l$/TV	0.25 ± 0.01	0.37 ± 0.03	0.26 ± 0.03	0.31 ± 0.01^{ab}	0.25 ± 0.01	0.40 ± 0.03	0.28 ± 0.03	0.44 ± 0.04
BV$_h$ [mm^3]	*45.91±3.25*	*43.35±1.79*	*43.38±2.83*	*44.77±2.87*	*44.54±3.46*	*50.33±7.41*	*46.85±3.78*	*42.58±1.08*
BV$_h$/TV	0.26 ± 0.01	0.27 ± 0.03	0.27 ± 0.04	0.28 ± 0.02	*0.27±0.03*	*0.27±0.01*	*0.30±0.02*	*0.27±0.01*
BV Density	929.61 ± 4.47	858.33 ± 22.76	938.91 ± 38.96	892.48 ± 12.45	953.69 ± 9.32	851.69 ± 9.32	937.88 ± 36.20	810.23 ± 13.01
	Week 6				Week 8			
	CG	BG	VG	VBG	CG	BG	VG	VBG
TV [mm^3]	161.52 ± 8.19	174.34 ± 22.01	156.69 ± 23.33	165.83 ± 14.62	*176.28±20.26*	*166.86±31.08*	*161.31±22.92*	*179.53±11.23*
BV [mm^3]	89.42 ± 7.78^b	124.40 ± 19.19^a	87.63 ± 8.54	130.93±10.21^a	*94.55±8.07*	*118.18±13.02*	*90.41±11.78*	*131.30±1.97*
BV/TV	0.55±0.03	0.71 ± 0.05	0.56 ± 0.03	0.79 ± 0.04	0.54 ± 0.03^b	0.72 ± 0.06^a	0.56 ± 0.02^b	0.73 ± 0.05^a
BV$_l$ [mm^3]	40.53 ± 6.15^b	70.06 ± 22.13^a	41.03 ± 8.31	81.38 ± 11.46^a	*41.75±6.61*^{b}	*57.25±6.13*^{a}	*39.28±7.58*^{b}	*70.73±5.32*^{b}
BV$_l$/TV	0.27 ± 0.06^b	0.40 ± 0.07	0.27 ± 0.01^b	0.49 ± 0.04	0.24 ± 0.01^b	0.35 ± 0.04^a	0.24 ± 0.03^b	0.04 ± 0.05^b
BV$_h$ [mm^3]	48.89 ± 3.15	54.34 ± 7.32	44.36 ± 0.59^b	49.55 ± 2.58	52.80 ± 3.35	60.93 ± 8.71	51.13 ± 5.01	60.58 ± 4.83
BV$_h$/TV	0.30 ± 0.01	0.32 ± 0.07	0.29 ± 0.05	0.30 ± 0.04	0.30 ± 0.04^b	0.37 ± 0.04^a	0.32 ± 0.02	0.34 ± 0.02
BV Density	949.52 ± 38.59	857.58 ± 59.24	942.96 ± 25.12	819.60 ± 27.23	956.89 ± 24.89	891.86 ± 21.48	942.74 ± 13.27	871.17 ± 26.05

Note: Mean ± 1SD, n = 5. 1-way ANOVA: a represents significance with CG ($p < 0.05$); b represents significance with BG ($p < 0.05$); 2-way ANOVA: *Italic* represent significant interaction between LMHFV and Bis.

3.3 Histomorphometric Analysis

3.3.1 Bone Mineralization Rate

Week 2

As mentioned in section 2.6.3, MAR for 2 weeks treatment groups was not included because callus mineralization occurs during mid-second week post fracture (10 – 14 days post fracture)[33]. Calcein green (the green fluorochrome band) labelled the old femoral cortical bone while xylenol orange (the orange fluorochrome band) labelled the newly mineralized callus (Figure 3.5).

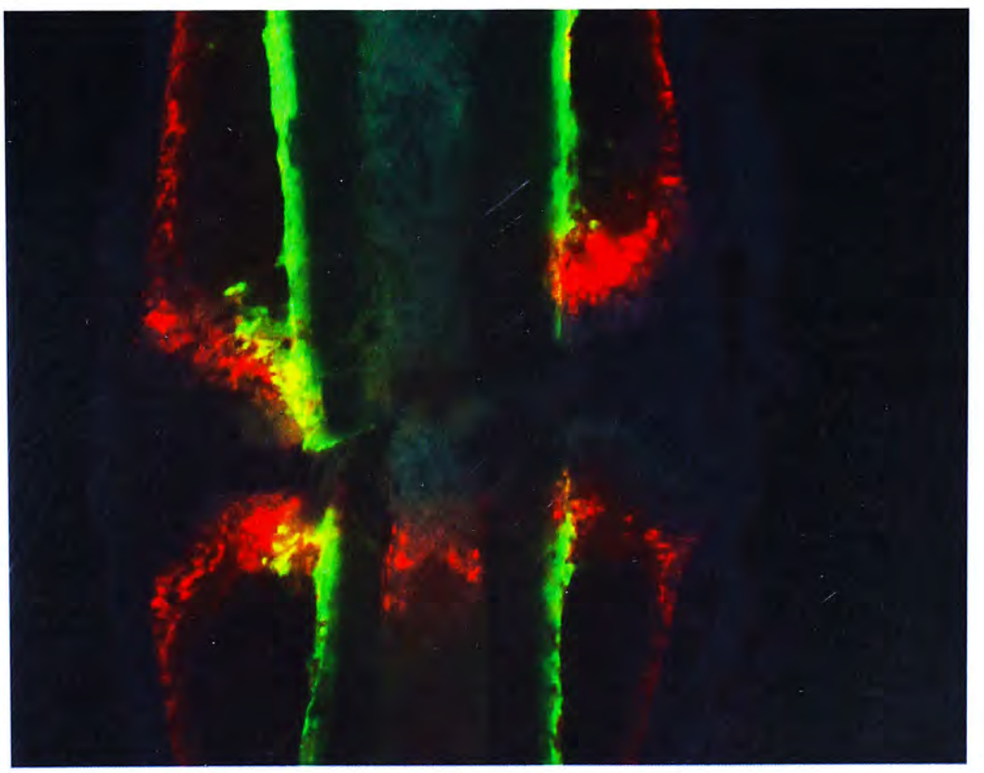

Figure 3.5: Undecalcified histology image of a callus at week 2. The fluorochrome bands labelled the old cortical bone (green band) and the newly mineralized callus (orange band).

Week 4 – 8

The two fluorochromes labeled the fracture callus on all samples from week 4 to week 8. Fluorochrome labeled entire region of interest in all groups from week 4 to week 8. Distinct bands of fluorochrome were also found in all groups (Figure 3.7). Both qualitative (Figure 3.7) and quantitative analysis (Figure 3.6) showed

that VG had the highest MAR (9.07 ± 0.75 $\mu m/day$, $p < 0.01$ compared to all other groups) at week 6. CG and VBG showed lower MAR than VG (CG: 65.05% of VG (p = 0.009), VBG: 56.89% of VG (p = 0.0004)). Moreover, there was no significant difference between CG and VBG. BG had the lowest MAR at week 4 and week 6. At week 6, BG was 45% of VG ($p < 0.0005$). Two-way ANOVA showed that there was interaction that was marginal significance between LMHFV and Bis at week 6 (p = 0.072). At week 8, the MAR dropped and there was no significant difference among groups.

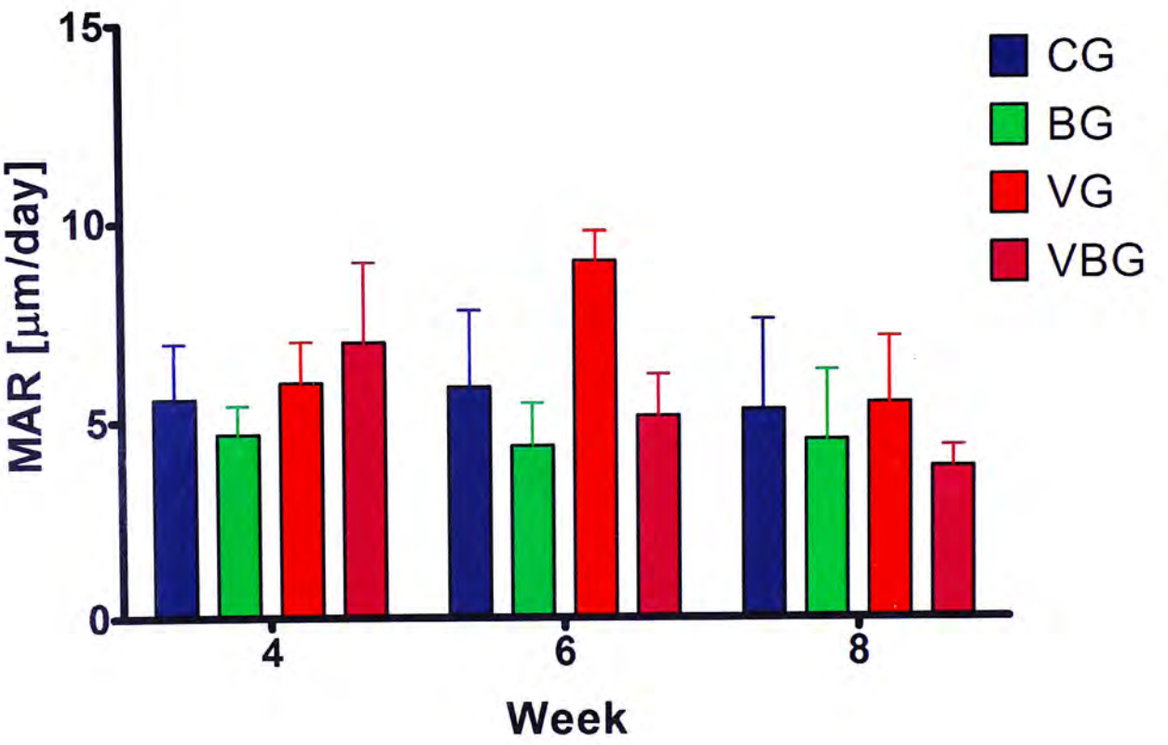

Figure 3.6: Average mineral apposition rate (MAR) of all treatment groups from week 4 to week 8 post-treatment. VG showed the highest MAR at week 6. There was no significant difference between groups at week 8. (Error Bar represents 1SD)

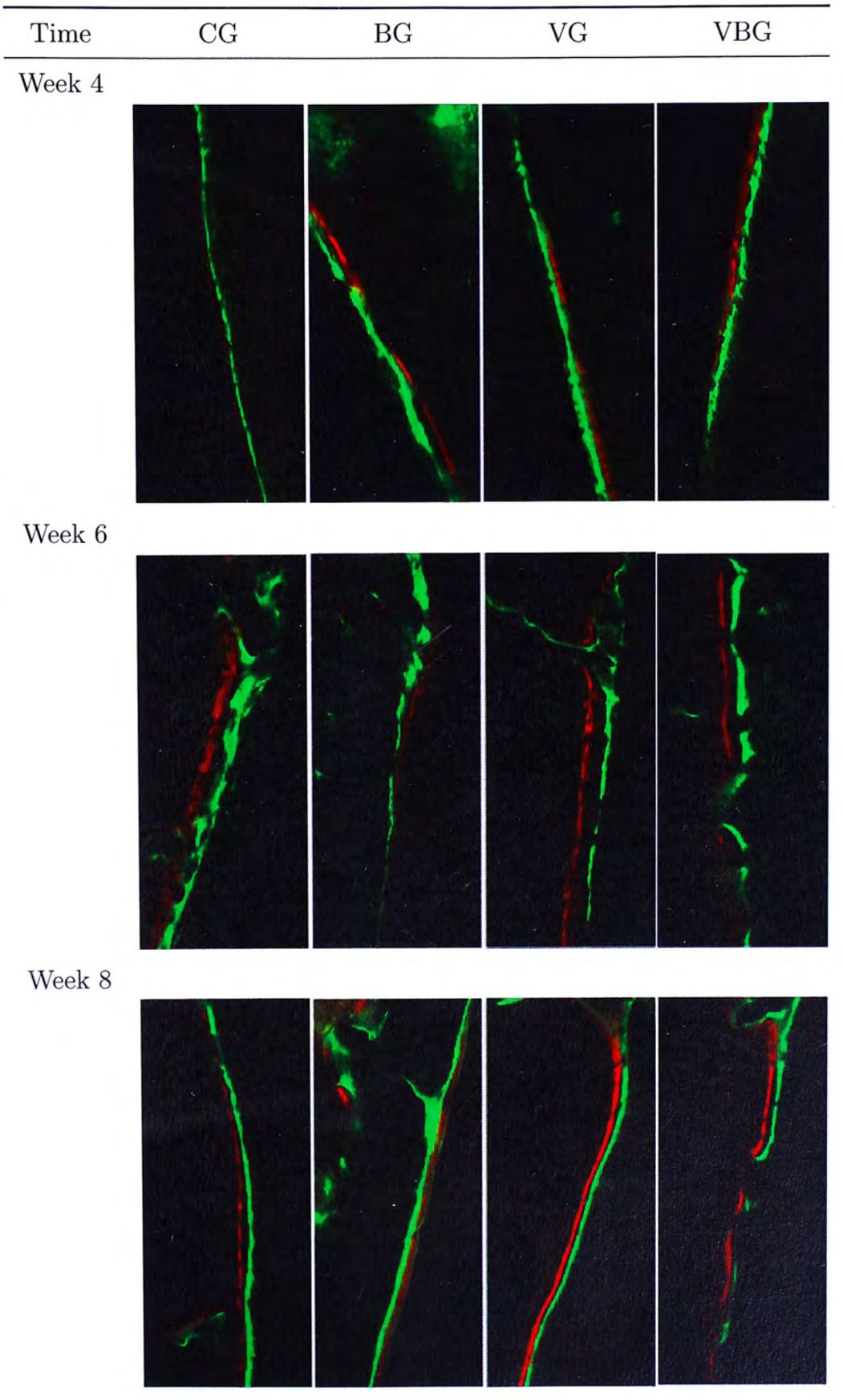

Figure 3.7: Undecalcified histology for different groups (CG, BG, VG, and VBG) from week 4 to week 8. All groups at all time points showed distinct bands of fluorochromes. There was no observable difference between groups at week 4 and week 8. At week 6, VG showed the longest distance between the two fluorochrome bands while VBG was the second longest.

3.4 Bone Markers Analysis

3.4.1 Osteocalcin

A calibration curve was obtained and the line of best fit had a R^2 value of 0.99041. Serum concentration of osteocalcin showed a decreasing trend for VG from week 2 (128.31 ± 40.80 ng/mL) to week 8 (42.95 ± 25.99 ng/mL). In addition, CG and VBG showed peaks at week 4 and week 6 respectively (Figure 3.8). VG showed significantly higher osteocalcin concentration than CG in week 2 (4.79 times of CG, $p < 0.0005$), week 6 (2.56 times of CG, $p = 0.046$) while showed no significant difference at week 4 ($p = 0.599$)and week 8 ($p = 0.444$). Osteocalcin concentration for BG peaked at week 4 (52.93 ± 14.16 ng/mL) and dropped to minimal level at week 6 to week 8.

3.4.2 TRAP5b

A calibration curve was obtained and the line of best fit had a R^2 value of 0.9908. Serum concentration of TRAP5b for VG peaked at week 2 and week 8 while a decreasing trend was observed for CG (Figure 3.9). From week 2 to week 8, CG had significantly higher serum concentration of TRAP5b than BG ($p < 0.0005$ from week 2 to week 8). At week 2, TRAP5b serum concentration for VG was significantly lower than CG ($p = 0.001$). In addition, there was no significant difference between VG and BG ($p = 0.140$) while VBG had the lowest level. CG showed the highest TRAP5b concentration in week 2 (3.60±0.84 U/L, $p < 0.0005$ for comparison to other groups). At week 8, VG shown significantly higher TRAP5b serum concentration than CG ($p = 0.006$). Two-way ANOVA showed that there was interaction that was marginal significance between LMHFV and Bis at week 8 ($p = 0.066$). The serum concentrations of TRAP5b for BG and VBG were almost not detectable from week 4 to week 8.

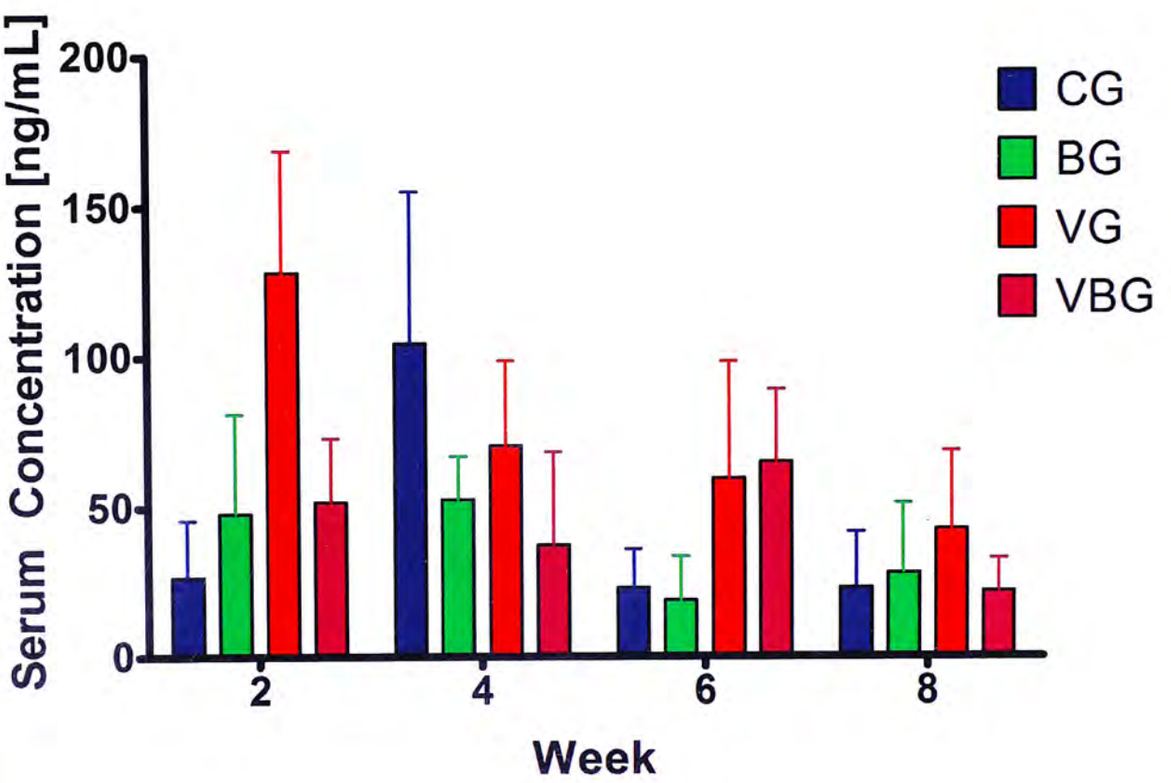

Figure 3.8: Serum concentration of osteocalcin over 8 weeks treatment. Serum concentration of osteocalcin for VG was the highest at week 2 while concentration for CG peaked at week 4. After the peaks, both group showed a decreasing trend. At week 8, the serum concentration for VG was significantly higher than CG ($p = 0.444$). (Error Bar represents 1SD)

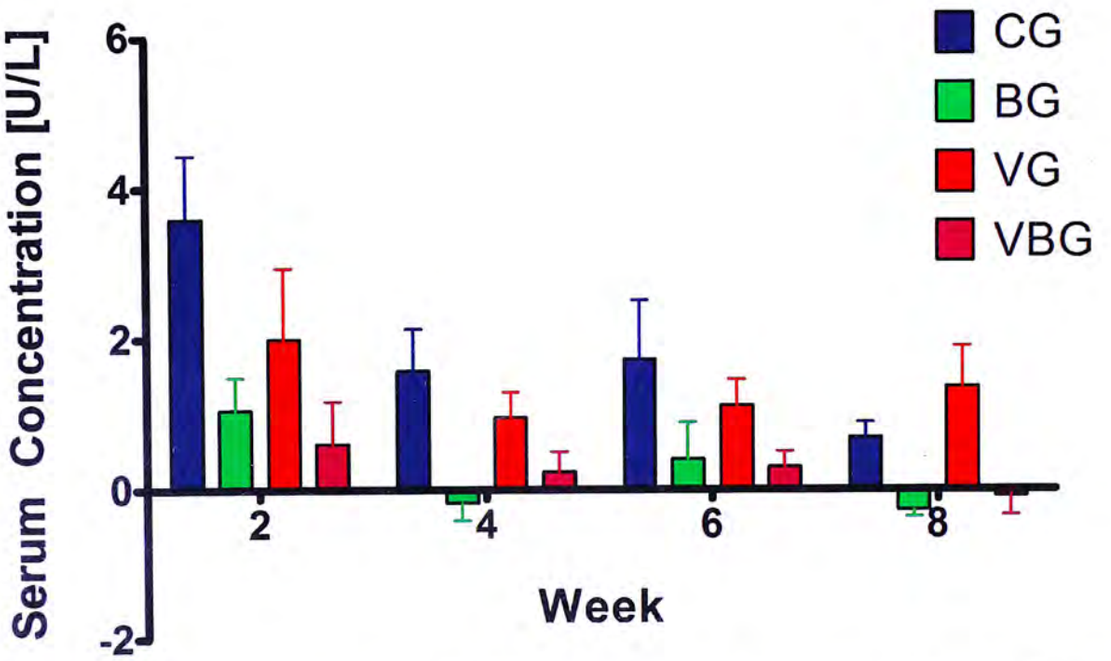

Figure 3.9: Serum concentration of TRAP5b over 8 weeks treatment. At week 2, TRAP5b serum concentration for VG was significantly lower than CG (p = 0.001). There was no significant difference between VG and BG (p = 0.140). The serum concentrations of TRAP5b for BG and VBG were almost not detectable from week 4 to week 8. At week 8, VG showed significant difference in TRAP5b serum concentration ($p < 0.0005$). (Error Bar represents 1SD)

3.4.3 Summary

To summarize, LMHFV treated group had the fastest decrease in callus measurements with respect to radiological and microarchitectural assessments. VG had the fastest drop in CA and CW, and BV/TV; whereas, a plateaued trend in BG and VBG was observed. With respect to callus mineralization, VG had the highest MAR at week 6. Biochemical analyses of bone markers found that the serum concentration of osteocalcin and TRAP5b were higher compared to other groups at week 8. A summary of all the statistical significant results is presented in table 3.5.

Table 3.5: Summary of all the statistical significant results ($p < 0.05$) from radiological, microarchitectural, histomorphometric, and biochemical analyses.

Assessment	Week 2	Week 4	Week 6	Week 8
Callus Width and Area	VG>CG BG>CG VBG>CG	VG>CG BG>CG VBG>CG	BG>VG BG>CG VBG>VG VBG>CG *$L \times B$	BG>VG BG>CG *VBG>VG *$L \times B$
BV/TV	BG>VG BG>CG VBG>CG	VG>CG BG>VG BG>CG VBG>VG VBG>CG	BG>VG BG>CG VBG>VG VBG>BG VBG>CG	BG>VG BG>CG VBG>VG VBG>CG
Mineral Apposition Rate	N/A		VG>BG VG>VBG VG>CG	
Serum Osteocalcin	VG>BG VG>VBG VG>CG $L \times B$	CG>BG CG>VBG	VG>BG VG>CG VBG>BG VBG>CG	
Serum TRAP5b	VG>VBG CG>VG CG>BG CG>VBG $L \times B$	VG>BG CG>BG CG>VBG $L \times B$	VG>BG VG>VBG CG>BG CG>VBG	VG>BG VG>VBG VG>CG CG>BG CG>VBG

Note: N/A represents that no such measurement was taken; $L \times B$ represents that 2-way ANOVA showed interactions between LMHFV and Bis; * represent significance only in callus area.

Chapter 4

Discussion

This is a factorial design study *in vivo*, looking into the effect of a treatment in the presence or absence of a known antagonist. It was performed to study the effect of LMHFV on bone remodeling. The presence of a known antagonist which has the same or opposite effect of the unknown treatment would change the effect of the treatment. The effect of LMHFV on bone remodeling in fracture healing was investigated directly by comparing difference in fracture healing between VG and CG, and indirectly by comparing how bone remodeling under LMHFV stimulation changes in the presence of Bis. LMHFV enhanced early phase of fracture healing through enhanced callus formation and faster mineralization which echoed our previous studies[129, 76]. The findings suggested that LMHFV hastened the disappearance of callus and partially reversed the delay of bone remodeling by ibandronate. These findings implied that LMHFV enhanced bone remodeling.

4.1 LMHFV Enhanced Bone Remodeling

As mentioned previously (Section 1.2), the traditional model of fracture healing is divided in four stages: inflammation, soft callus (fibrocartilage) formation, hard callus formation, and bone remodeling[126]. However, there is significant overlap between different stages and callus is not a homogeneous structure. Therefore, it would be difficult to determine the stage of fracture healing for a callus. Since all

radiological and micro-architecture measurements of callus for CG and VG peaked at week 3 to week 4 (Figure 3.2), bone remodeling for osteoporotic bone fracture should start around this period because bone remodeling occurs after callus reaches its maximal size when catabolism dominates over anabolism[81]. This finding echoed with our previous study in osteoporotic rats which bone remodeling was observed around week 3 to week 4[129]. In addition, in our previous study using young SD rats, bone remodeling started around week 2[76]. Since fracture healing of osteoporotic bone would be delayed, bone remodeling for normal rat began at week 2 would further confirmed that bone remodeling for OVX rat would commence around week 3 to week 4[89]. Therefore, fractures in OVX rats would start bone remodeling around week 4.

LMHFV enhanced bone remodeling in fracture healing. VG showed a faster drop than CG in CW (Figure 3.2a) and CA (Figure 3.2b) in radiographic analysis, and BV/TV in micro-architecture analysis (Figure 5.1) from week 4 to week 8. As mentioned previously (Section 1.3.2), our study in normal[76] and aged SD rat[129] also observed enhanced rate of disappearance of callus. VG also demonstrated an increased serum concentration of osteocalcin (Figure 3.8, on week 6 and week 8) and TRAP5b (Figure 3.9, on week 8), and a higher MAR than CG (Figure 3.6). These results suggested enhanced bone remodeling as a result of LMHFV treatment.

4.1.1 LMHFV Reversed Bis Inhibition on Bone Remodeling

Ibandronate is one of the nitrogen-containing bisphosphonates available on the market. Ibandronate was more potent than etidronate, clodronate, pamidronate, and alendronate[29] (Refer to section 4.4.2 for details). In this study, ibandronate was the bisphosphonate that was used to inhibit bone remodeling. LMHFV partially reversed the inhibitory effect by Bis in bone remodeling. This suggested that LMHFV had an opposite effect on bone remodeling than Bis. After callus in BG reached its maximal size in week 4, a plateau trend in radiographic analysis of CW (Figure 3.2a) and CA (Figure 3.2b), and BV/TV in μCT (Figure 5.1) was observed. This

suggested that weekly injection of Bis can cause delay in bone remodeling due to its anti-catabolic effect and this was observed in other fracture healing studies with an anti-catabolic intervention[81, 90, 104]. However, with the presence of LMHFV, VBG showed higher bridging rate, faster decrease in CA and CW at week 6 to week 8, and higher MAR at week 6 (Figure 3.6 and 3.7) than BG. In addition, two-way ANOVA analysis in CA and CW showed significant interaction between LMHFV and Bis, which also suggested that inhibition of bone remodeling by Bis was diminished by the presences of LMHFV. Therefore, LMHFV might have an opposite effect to Bis which might enhance bone remodeling.

4.1.2 LMHFV Effect on Osteoclastic Resorption During Bone Remodeling

Bone remodeling is the final stage of the classical fracture healing model which replaces woven bone in hard callus with laminar bone (Section 1.2). The remodeling process is coupled between bone resorption followed by bone formation[126, 130]. Osteoclast is the key cell type which is responsible for the resorption of mineralized bone[126, 130]. LMHFV might have stimulated osteoclastic resorption in bone remodeling which led to the increase in bone remodeling. The highest MAR at week 6 (Figure 3.6) and increased osteocalcin serum concentration in VG (Figure 3.8) suggested that LMHFV enhanced mineralization and osteoblastic activity respectively. Since the activity of osteoblast and osteoclast are coupled[130], this suggested that osteoclast activity might also be enhanced by LMHFV. Enhanced osteoclastic resorption by LMHFV was further supported by the increased TRAP5b serum concentration at week 8 (Figure 3.9). Higher serum concentration of TRAP5b was found in VBG than BG during bone remodeling. Since TRAP5b is a bone marker for resorption and found specifically in osteoclast[130, 141] increased concentration of TRAP5b also suggested higher resorption in VBG. Therefore, osteoclasts activity might also be enhanced by LMHFV.

4.2 Enhanced Fracture Healing by LMHFV

LMHFV enhanced early phase of fracture healing in osteoporotic bone. VG showed higher callus measurement from radiographs (Figure 3.2) and μCT (Table 3.4), and higher bridging rate than CG (Table 3.2) which implied that LMHFV improved fracture healing. VG also showed higher bone density than CG and increased mineralization rate which suggested that LMHFV enhanced mineralization of fracture callus. Similar results were found in our previous study[129]. In the current study and our previous study using aged OVX rats, LMHFV showed 10–20% increase in fracture healing, which were observed between VG and CG, while 25–30% was observed in young normal rats[76, 129]. In addition to the radiological and microarchitectural enhancement, VG showed higher osteocalcin concentration in serum than CG from week 2 to week 4 (Figure 3.8). This biochemical analysis of bone formation marker was a new finding in addition to our previous results. The results from the biochemical analysis were comparable to results from our previous experiments. This further supported that LMHFV enhanced callus formation.

4.2.1 Acceleration of Fracture Healing by LMHFV

Our previous study on aged OVX rat showed morphology of the callus at week 2, 4, and 8 while study in young rat showed data on week 1, 2, and 4[76, 129]. There was a lower ratio of cartilage area to callus area (Cg.Ar/Cl.Ar) in groups treated with LMHFV than control groups at week 4 and week 8 for young and aged rats respectively. The lowering of the Cg.Ar/Cl.Ar suggested that more woven bone was formed in the callus. Woven bone is mineralized tissue and stiffness (hardness) of the fracture callus closely correlates with its calcium content[33]. This also implied that in the later stage of fracture healing, callus with lower Cg.Ar/Cl.Ar would be more stable. However, no significant difference was detected in this ratio for these two studies[76, 129]. Therefore, weekly histological assessment on the callus morphology might be required in order to detect the acceleration of fracture healing progression

significantly. However, the accelerated trend was still observed.

The earlier peak of osteocalcin in VG than CG suggested faster progression of fracture healing by the effect of LMHFV. Osteocalcin is a noncollagenous protein found in bone (Please refer to Section 1.1.1 and 4.4.3 for details). Osteocalcin expression was initiated in Day 9 to Day 11 post-fracture and peak expression was observed around post-fracture Day 15 in non-osteoporotic rats[31, 68]. The peak expression of osteocalcin in the current study was found at week 4 post-treatment which was post-fracture Day 26 in CG. Therefore, by taking into account the delay of fracture healing caused by osteoporotic bone, this matched the peak expression found in other fracture healing studies. In addition, the peak expression of osteocalcin for VG was observed at week 2 post-treatment, which is equivalent to post-fracture Day 19. As mentioned previously (Section 1.2), fracture healing was classified into four overlapping stages: Hematoma formation, soft callus formation, hard callus formation, and bone remodeling. Since bone remodeling was the last stage of fracture healing and it occurred around week 4, therefore hard callus formation must have initiated before week 4. Osteocalcin gene expression was detected in the hard callus during endochondral ossification and remodeling[68]. However, during intramembranous bone formation or at any time in the soft callus, osteocalcin expression was not found[68]. Since the peak of osteocalcin concentration for VG was at week 2 while the peak for CG was at week 4, this might suggest that endochondral ossification, the process that modifies soft callus into hard callus, in VG might have started earlier than CG. This imply that not only LMHFV enhanced fracture healing, it also accelerated fracture healing progression so the callus underwent remodeling earlier than those that were not treated with LMHFV.

4.2.2 LMHFV Inhibits Osteoclast Activity in the Early Phase of Healing

LMHFV appeared to suppress osteoclast activity in early fracture healing when the bone was undergoing endochondral ossification. Serum concentration of TRAP5b was suppressed to the level comparable to BG under LMHFV treatment and lower

than the concentration in CG (Figure 3.9). Daily LMHFV inhibited bone resorption in growing skeleton which is also undergoing endochondral ossification[81, 142]. LMHFV might have a similar effect on fracture bone which is undergoing a similar process[81]. Therefore, as the fracture repair process convert from endochrondral ossification to intramembranous ossification, the suppression of LMHFV on the bone resorption decreased as it was observed in the increased expression of TRAP5b in VG to a level comparable to CG in week 4 to week 8. Inhibition of osteoclast activity in early phase of fracture healing was reported by other mechanical stimulation studies *in vitro*. LMHFV stimulation (0.3 g with 30, 60, or 90 Hz) on osteocytes-like cells decreased RANKL, an osteoclast differentiation protein[73]. The conditioned medium collected from vibrated osteocytes inhibited the formation of large osteoclast. Another biophysical stimulation study using low-intensity ultrasound stimulation (LIPUS) *in vitro* on alveolar mononuclear cell and osteoblast cells coculture found an increase in osteoblast count and a decrease in osteoclast count[132]. These findings substantiate to our study that mechanical stimulation might decrease osteoclast differentiation and survival in the early stage of fracture healing.

4.2.3 LMHFV Stimulates Osteoblast Activity in the Early Phase of Healing

From previous sections (Section 4.2.1 and 4.2.2), LMHFV inhibited the activity of osteoclast during the early phase of fracture healing while the progression of fracture healing was accelerated. This suggested that the effect by LMHFV during the early phase of fracture healing might depended on osteoblast. As mentioned, biomechanical stimulation by LIPUS on alveolar mononuclear cell and osteoblast cells coculture found an increase in osteoblast count and a decrease in osteoclast count[132]. Therefore, LMHFV might enhance the proliferation and differentiation of osteoblast. The increased osteocalcin concentration might imply that bone formation by osteoblast was enhanced because osteocalcin is a protein produced by osteoblast for bone formation[95]. Therefore, the enhanced of fracture healing by

LMHFV might be due to LMHFV stimulation on osteoblast.

4.3 Bis Delays Fracture Healing

Bis seems have no effect on the early phase of fracture healing. Ibandronate was injected weekly throughout the eight weeks treatment period. Initially, there was no significant difference between BG and other groups in CW, CA, or BV/TV analysis (Figure 3.2a, 3.2b, and 5.1 respectively). This suggested that Bis did not affect the early endochondral fracture repair[90]. However, Bis dosage was effective in suppressing resorption. As mentioned previously, BG showed delayed bone remodeling with respect to radiological, micro-architectural, and biochemical analysis. This phenomenon was expected and observed in other fracture healing studies that used bisphosphonate[90, 18, 87]. Cao *et al.* administrated alendronate ($10\mu g/kg/day$) for 6 weeks and 16 weeks in OVX femoral fractured SD rat and found that rats administrated alendronate had largest callus. Furthermore, at week 16, the original cortical shell remained but became porous in alendronate group while a new cortical shell and marrow cavity were forming in OVX control group. Also, Cao *et al* found that callus of alendronate group was made up of woven bone and the original fracture line was still observable[18]. This phenomenon was also found in this study since the bridging rate for BG group at week 8 was only 20% while it was 80% for CG (Table 3.2). Therefore, this result suggested that the large callus in bisphosphonate group appeared to be an adaption to provide better stability at fracture.

Inhibition of bone remodeling might be due to inhibition of angiogenesis during fracture healing. Other than bone resorption, osteoclasts may also involved in the stimulation of angiogenesis[17]. In addition to inhibition on osteoclasts, bisphosphonate might also inhibit endothelial progenitor cells, which are important for angiogenesis[144]. Since angiogenesis plays an important role during intramembranous bone formation and endochondral ossification[56], inhibition of angiogenesis would also delay bone remodeling. This delay in bone remodeling might have a neg-

ative effect on fracture strength since bone strength is determined by bone volume, micro-architecture of bone, and bone mineralization[135]. Even though bisphosphonate increases the callus volume and increased or unchanged of mechanical strength of the callus[78], delay in bone remodeling caused a disorganized matrix structure in the callus which would decrease the quality of tissue[90, 18]. Therefore, bisphosphonate might have a negative effect on fracture healing even though there is no significant difference in mechanical strength at the fracture site.

Different effects between LMHFV and Bis on callus size and morphology

Fracture healing results in a gradual decrease in micromotion between fractured bones[33, 140]. In the early phase of fracture healing, the fracture causes instability of the bone and micromotions[32]. The micromotion between the fragments is believed to govern the type of tissue formed between fracture fragments[33]. Hypertrophic non-union of the fracture would occur if the mechanical stability is insufficient[24].

Hematoma, soft callus, hard callus are stabilizing structure that is made of different tissues to stabilize the fracture site. LMHFV provides more micromotions and mechanical loading at the fracture site than sham. This would induce the formation of larger soft callus at the beginning of the healing (Before week 2)[24, 53]. On the other hand, BG and CG should receive the same amount of loading and micromotions so they should have the same size callus (Before Week 2). For the formation of hard callus, LMHFV accelerates the endochondral bone repair which enhances the formation of hard callus[53].

The mechanical strength of callus depends on the callus material and the geometry of the callus[135]. After week 2, hard callus, which was made of woven bone, was formed and bone remodeling started. As mentioned in section 1.2, in bone remodeling, woven bone would be replaced with lamellar bone. During bone remodeling, this study have shown that LMHFV stimulates the activities of osteoblasts and osteoclasts which would enhance bone remodeling (Refer to section

4.1 for details). In addition, LMHFV might increase the micromotions and mechanical loading at the fracture site which would induce osteogenesis through the process of mechanotransduction[136]. Therefore, bone remodeling in VG was enhanced and replaced mechanically inferior woven bone with mechanically superior lamellar bone. As a result, callus in VG would be made of both woven bone and lamellar bone.

Bis inhibited osteoclast activity and caused inhibition of remodeling throughout fracture healing. Bone can be directed osteogenesis to where it is most needed to improve bone strength[135]. One way that bone adapts to mechanical stress and enhance stability with a mechanically inferior material is by increasing the periosteal radius of bone. As explained by Turner[135], the second moment of area (I), important for the callus to resist bending[33], can be calculated from the periosteal radius (r_p) and the endosteal radius (r_e)

$$I = \frac{\pi}{4}(r_p^4 - r_e^4)$$

The r_p is about 1.8 tims r_e in mammalian long bones[135]. Therefore, the equation can be modified to

$$I = 0.71 r_p^4 \tag{4.1}$$

Equation 4.1 shows that periosteal radius is an important factor for bone structure rigidity[135]. Therefore, increase the periosteal radius by increasing the callus size would improve the stability of fracture in BG . Consequently, with bone remodeling inhibited, callus in BG would be made of woven bone and larger compared to CG.

For VBG, the remodeling should be delayed by Bis (LMHFV enhances remodeling while Bis inhibits remodeling). Callus of VBG would have a large amount of mechanical loading and micromotions which would increase the callus size. In addition, the callus of VBG would be made of woven bone at the beginning of bone remodeling due to inhibition of remodeling by Bis. However, as the inhibition on remodeling is reversed, the callus size should drop as the callus remodels into lamellar bone.

At week 8, the callus of VG should be mainly made up of lamellar bone while CG should be made up of woven bone and lamellar bone. VG has a higher ratio of lamellar bone to woven bone as compared to CG because there is higher mechanical loading in VG and callus size of VG is comparable to CG (Section 4.1). Since Bis inhibited remodeling, callus in BG should be mainly made up of woven bone. Lamellar bone should be found in the callus of VBG because LMHFV partially reversed the inhibition of remodeling by Bis (Section 4.1.1).

4.4 Experimental Design

4.4.1 Inhibition Study

In order to investigate in the effect of LMHFV on bone remodeling, an factorial design study, a classic research methodology for investigation on the effect of a new drug[137], would be sufficient. The magnitude of effect of the unknown drug would change if it has same or opposite effect of the known antagonist. By studying how the effect of unknown drug changes in the presence of a known antagonist, the effect of the unknown drug can be verified. Therefore, interference to a key component in bone remodeling should have an effect on bone remodeling.

Osteoblast is responsible for bone formation while osteoclast is responsible for resorption and removal of old bone. During fracture healing, bone resorption is coupled with bone formation to resorption[88, 85, 125]. Osteoclast removes dead bone during early phase of fracture healing and replaces the less mechanical support woven bone with high mechanical strength laminar bone in bone remodeling[125]. Therefore, to study the effect in bone remodeling by LMHFV, a known antagonist would be used to inhibit osteoclast activity.

Bisphosphonate can be used in an inhibition study and act as a known antagonist that inhibits bone remodeling. As mentioned previously, an inhibition study is a traditional approach to study the effect of an unknown treatment. Bisphosphonate inhibits osteoclast activity and causes inhibition of bone remodeling. Bisphospho-

nate binds to the calcium hydroxyapatite crystal selectively[103, 121]. Bisphosphonate is released and taken up by osteoclast during resorption and causes osteoclast apoptosis[103, 121]. This would lead to decoupling of the osteoblast-osteoclast activity and inhibit bone remodeling[103, 121, 130]. Therefore, administration of LMHFV in the presence or absence of bisphosphonate allowed investigation on the effect of LMHFV on bone remodeling in fracture healing.

4.4.2 Bisphosphonate Injection Protocol

Choice of Bisphosphonate

As mentioned previously (Section 4.4.1), bisphosphonate was used as a tool to inhibition bone remodeling in order to study the effect of LMHFV on bone remodeling. Alendronate, ibandronate, and risedronate[91] are the bisphosphonate that are commonly available on the market. Ibandronate was chosen for bisphosphonate treatment. The pharmacokinetics of ibandronate are studied preclinically[93, 5]. The efficacy of ibandronate was higher than other available bisphosphonates (Figure 4.1). In addition to a lower ED_{50}, the effective dose that creates 50% response, than alendronate *in vivo*, EC_{50}, the effective concentration that produces a 50% of response, for ibandronate (3.5×10^{-10} mol/L) is lower than alendronate (2×10^{-9} mol/L) *in vitro*[80]. In addition, ibandronate has the second highest relatively higher affinity and potency (Table 4.1). Therefore, ibandronate is a better bisphosphonate of choice since less amount of drug is required to achieve the same level of bone resorption inhibition.

Route of Administration

The bioavailability are low for most of the bisphosphonate that are administrated orally because they are poorly absorbed from the gastrointestinal tract (GI tract)[5]. The oral bioavailability of ibandronate was estimated to be less than 1%[5, 39]. In addition, oral absorption of bisphosphonate in rats is higher in the fasted state

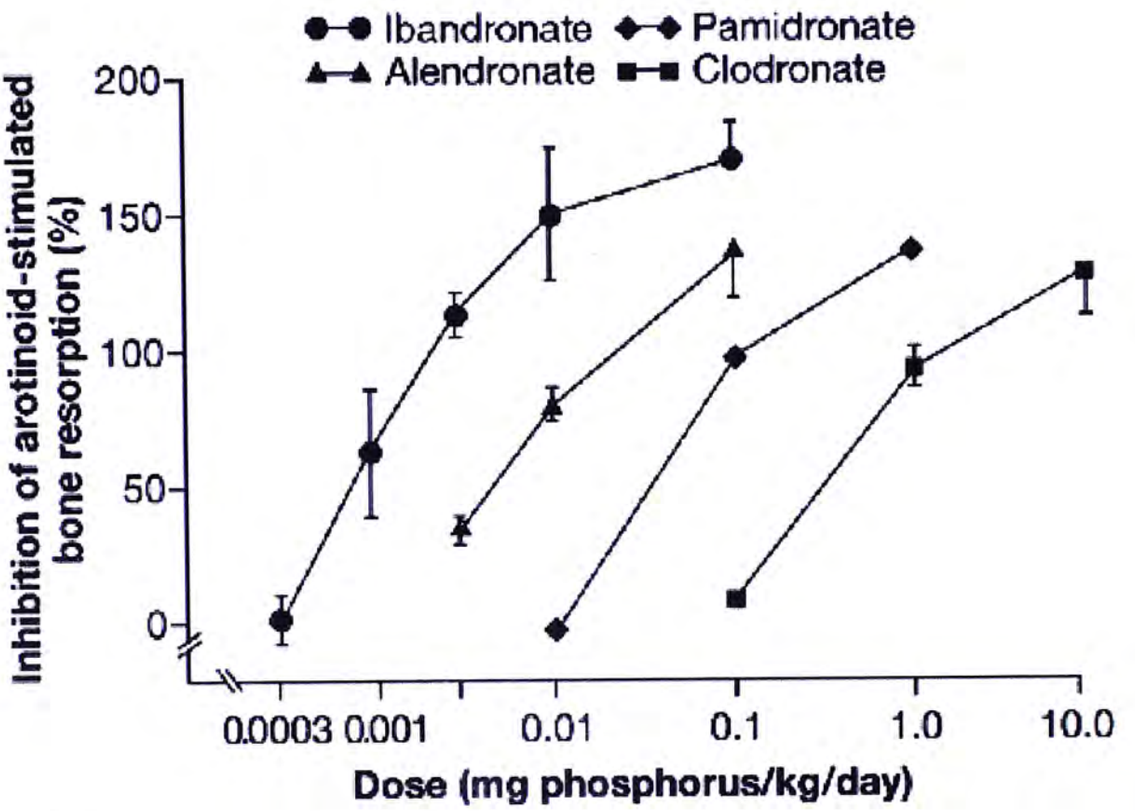

Figure 4.1: Dose-response curve of different bisphosphonates (Ibandronate, Pamidronate, Aldendronate, Clodronate) for inhibition of bone resorption in rats[35, 92]. Ibandronate has the highest efficacy ($ED_{50} \approx 0.001$ mg phosphorus/kg/day). (Reprinted from Epstein *et al.* 2005)[35]

Table 4.1: Affinity and potency of different commonly available bisphosphonates (Etidronate, Alednronate, Risedronate, Ibandronate, and Zoledronate). Zoledronate and Ibandronate have the highest and second highest potency and affinity out of the five bisphosphonates compared. (Source: Russell *et al.* 2006)[120].

Bisphosphonate	R^1	R^2	Potency	Affinity*
Etidronate	OH	CH_3	1	1.19
Alendronate	OH	$CH_2CH_2CH_2NH_2$	100 – 1000	2.94
Risedronate	OH	CH_2-3-pyridine	1000 –10000	2.19
Ibandronate	OH	$CH_2CH_2N(CH_3)(C_5H_{11})$	1000 – 10000	2.36
Zoledronate	OH	CH_2–imidazole	>10000	3.47

Note: **In vitro* HAP avidity [$K_L/10^6$ $Lmol^{-1}$]

than in the fed state[80]. The plasma concentration of ibandronate is reduced when ibandronate is administrated after meal[5].

There is no significant difference in efficacy when bisphosphonate is given by intraperitoneal, intramuscular, or subsutaneous administration. However, the sodium salt or calcium salt from bisphosphonate might cause pain and tissue necrosis at the site of injection after long term injection[80]. Therefore, lowering the dosage of bisphosphonate used might decrease the chance of tissue necrosis and pain. Since the efficacy of ibandronate is the highest of the available bisphosphonate (Section 4.4.2), the tissue damage and pain might be minimized.

Frequency of Injection

The effects of bisphosphonate depends on the total dose administrated than the dosing frequency[8, 120]. The dosing regimens of ibandronate were studied in OVX rats. Daily ibandronate and three intermittent dosing regimens (injection every two week, four weeks, or six weeks) with the total administrated dose showed equivalent effect on bone mass after one year of treatment (Figure 4.2)[8, 120]. Therefore, the dosing regimen would not affect the efficacy of ibandronate as long as the same dosage ($1\mu g/kg/day$) is administrated.

4.4.3 Individual Analysis of Bone Formation and Resorption

As mentioned previously (Section 1.2), fracture healing is a coupled process of bone formation and bone resorption. In order to confirm the effect of LMHFV on bone formation and investigate the effect of LMHFV on bone resorption, measurements which allows assessment on the anabolic and catabolic activity separately are required. However, radiological assessments do not allow measurements on bone formation or bone resorption separately.

Bone markers concentration analysis provides a noninvasive tool to assess change in bone metabolism. They are useful when monitor bone formation and bone resorption specifically. They can be used to detect both short- and long-term changes

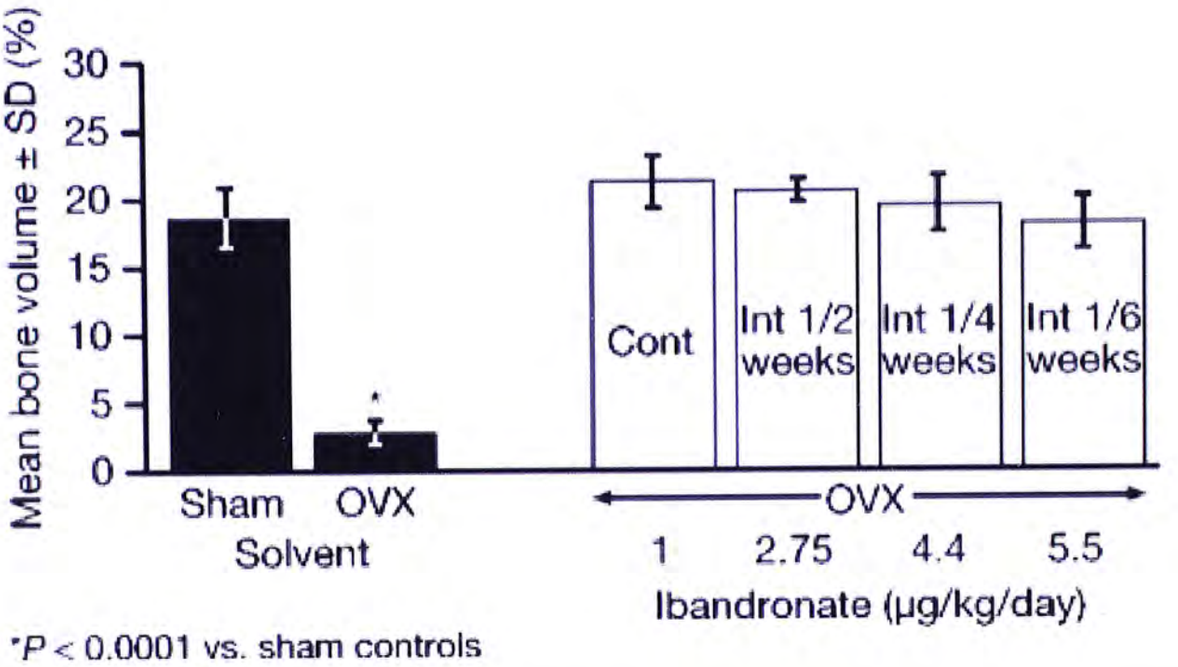

Figure 4.2: Effect of daily and different intermittent dosage regimens on bone resorption in aged OVX rats[120]. The same total amount of ibandronate was given in daily injection and intermittent injections.There was no significant difference between the different injection regimen. (Reprinted from Russell *et al.* 2006)[120]

in bone turnover[95]. An ideal marker should be tissue specific, only reflect only one process, and easily measured by specific and sensitive techniques[71].

Bone Formation Marker – Osteocalcin

Bone formation markers are proteins that are secreted by osteoblasts. Osteocalcin is an established marker of bone formation[95]. It is a noncollagenous protein found in bone[95]. The function of osteocalcin is unknown but it has a high affinity to bone minerals because the negatively charged osteocalcin is attracted to the positively charged ions in bone mineral. Serum osteocalcin has been shown to correlate with bone formation rate and calcium accretion and no correlation with bone resorption[95]. Osteocalcin concentration showed rapid response to glucocorticoid therapy and estrogen. In addition, osteocalcin in serum increased after fracture for at least 3 months post-fracture[95]. Therefore, osteocalcin serum concentration would correctly reflect changes in bone formation during fracture healing.

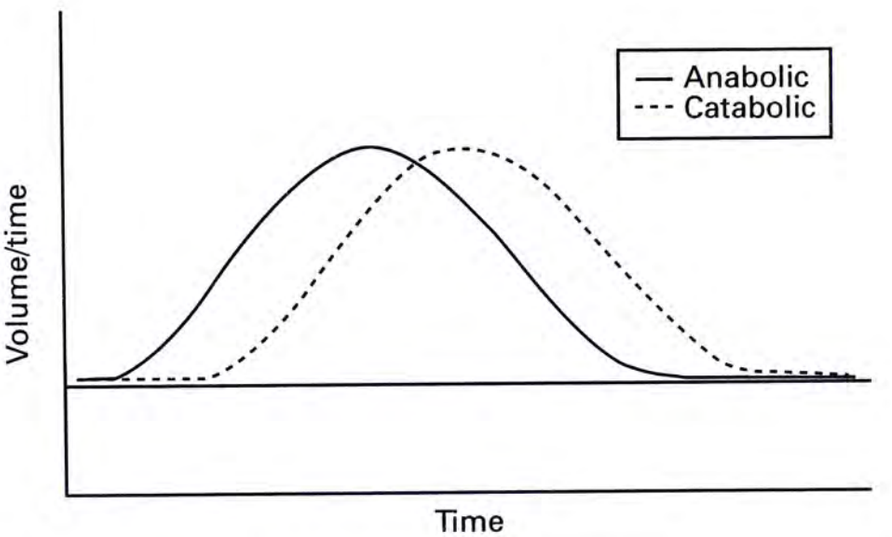

(a) Anabolic and catabolic response

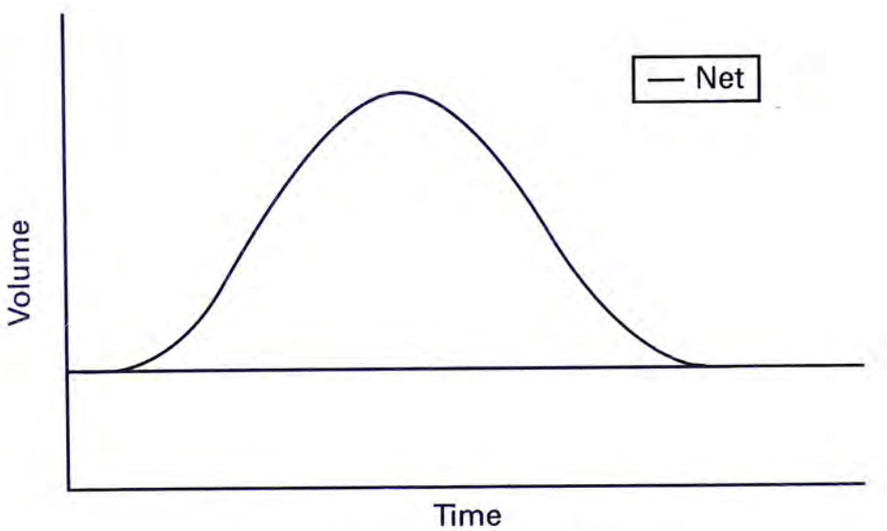

(b) Fracture healing progression observed

Figure 4.3: The anabolic and catabolic response during normal fracture healing. Figure 4.3a shows that fracture healing is a coupled process of bone formation (anabolic) and bone resorption (catabolic). Figure 4.3b shows the trend observed on x-rays and μCT are the net result of bone formation and resorption. When anabolism dominates over catabolism, bone accumulates. On the other hand, resorption of callus in bone remodeling occurs when catabolism dominates over anabolism[81]. (Reprinted from Little *et al.* 2007)[81]

Bone Resorption Marker – TRAP5b

Bone resorption may be assessed by measuring collagen degradation products, non-collagenous proteins of the bone matrix, or the enzymes expressed and secreted by osteoclast during bone resorption[71]. TRAP consists of two isoforms, 5a and 5b[71, 141]. TRAP5a are found in macrophages and dendritic cells while TRAP5b is the predominant form found in osteoclast[71, 141]. Serum concentration of TRAP5b was measured by ELISA in order to measure osteoclast activity accurately. Serum samples of TRAP5b were stable for up to four freeze/thaw cycles and 24 months at $-70 \pm 10°C$[141]. The bone resorptive effect in human was reflected by the serum concentration of TRAP5b[141]. Furthermore, the antibody that was used in ELISA would specifically bind to the active TRAP5b but not the inactive fragments[55, 141]. TRAP5b concentration correlates well with histological analysis of bone resorption[21]. TRAP5b concentration in serum was measured in patients with renal osteodystrophy disease. These patients often presented with secondary hyperparathyroidism (increased serum PTH concentration) and increase osteoclast activity[21]. Serum TRAP5b level correlated with serum interact PTH concentration and bone histological assessment of bone resorption such as number of osteoclast per bone area and osteoclast area per bone surface[21]. TRAP5b showed response to antiresorptive therapy with a lower biological variability. Since TRAP5b is stable and correlates with histological bone resorption assessments, measuring TRAP5b serum concentration would correctly reflect the bone resorption activity.

4.5 Clinical Implications

4.5.1 LMHFV Enhanced Remodeling

LMHFV showed anabolic effect on fracture healing in this study and previous studies[53, 76, 129, 69]. As mentioned previously, LMHFV showed anabolic effects on fracture healing by accelerated callus formation and mineralization, and enhanced mechanical strength at the fractured site in both normal adult and aged

osteoporotic rats[129, 69]. LMHFV also enhanced the endochondral ossification in bone repair[53]. Moreover, the current study showed that LMHFV enhance bone remodeling. This suggested that LMHFV might be beneficial to patient and administrated throughout the process of fracture healing. The healing stage of the fracture would not affect the effect of LMHFV. Therefore, the enhancement of LMHFV is prolonged and may benefit patients in different stage of healing.

4.5.2 Bisphosphonate Delayed Remodeling

The administration of Bis might have a negative effect on the healing of fracture. As mentioned in Section 4.3, Bis delays bone remodeling in fracture healing. In addition, the microarchitecture of the bone is weakened. The cortical shell of the bone became porous and the original fracture line was still observable. Even though large callus measurements were the result of bisphosphonate treatment, but this increase in callus appeared to be only an adaption to provide better stability at the fracture. Therefore, this suggested that Bis delays fracture healing and this might be a negative effect. This suggested that it might be necessary to discontinue administration of Bis to patients who have fracture and were taking Bis.

4.6 Limitations

4.6.1 Measurement of Bone Resorption

Bone remodeling during fracture healing is a coupled process of both bone formation and bone resorption. The limitation of this study was that there was no direct measurement of bone resorption. A commonly use method to measure resorption directly is by counting the number of osteoclasts. However, the addition of bisphosphonate in this study would cause osteoclast apoptosis. It would be difficult to differentiate osteoclasts that are undergoing apoptosis and functional osteoclasts[67, 52, 139]. Bone biopsy of the patients who took three years of oral alendronate were examined and showed an increase in the number of normal osteoclast by 2.6 times[139]. In

addition, 27% of these osteoclasts were hypernucleated with 20 to 40 nuclei and 20% to 37% of these were apoptotic[139]. In addition, the morphology of normal osteoclasts are similar to these apoptotic hypernucleated osteoclast. Normal osteoclasts are also large and multinucleated with up to 50 nuclei[49]. Therefore, this method may over-estimate the number of osteoclast and under-estimate the effect of bisphosphonate. As mentioned previously (Section 4.4.3), serum concentration of TRAP5b was measured by ELISA in order to measure osteoclast activity accurately. This is because serum TRAP5b level correlated with serum concentration of interact PTH and bone histological assessment of bone resorption.

4.6.2 Osteoporotic Fracture Model

Osteoporotic fracture model was used in order to study the effect of LMHFV on bone remodeling in fracture healing. As mentioned previously (Section 1.4.3), osteoporosis delays fracture healing even though healing goes through all the normal stages. One of the advantages of using this fracture model is that the prolonged fracture healing allowed detailed observation of each healing stage. If normal adult rats were used, the healing process would be shorten to just four to five weeks[101]. This might not allow accurate investigation on bone remodeling with the current methods such as the mineral apposition rate. Therefore, it would be difficult to observe difference in MAR between different groups. The second advantage of using OVX-induced osteoporosis model is that it is an appropriate representation of elder human subjects. According to the FDA guidelines for the animal models for osteoporosis, OVX rat model mimics postmenopausal cancellous bone loss and it is a suitable model for evaluation of potential therapeutic agents for the prevention of osteoporosis[134]. Therefore, the results obtained from the current study in rat would be the best representations of the effect on humans.

Closed femoral fracture model in rats were used to study the effect of LMHFV on bone remodeling. Rat is a commonly used model to study fracture healing[101]. The rat model is typically more predictable and practical when performing both

surgery and analyses than mouse. The closed femoral fracture model was also used in our previous studies[76, 129]. The standard closed fracture was superior to an open osteotomy because this model eliminates the added variable of local wound healing[11]. The closed femoral fracture model resulted in a highly reproducible fracture site and configuration with minimal soft tissue trauma[11]. Moreover, the animal costs are still reasonable for larger group studies[99].

4.6.3 Inhibition of Bone Remodeling

As mentioned previously (Section 4.4.1), this inhibition study using ibandronate was undertaken in order to study the effect of LMHFV on bone remodeling. Ibandronate was administrated weekly on five days post-fracture. As mentioned previously (Section 4.1), bone remodeling did not start until three to four weeks after the fracture surgery. Therefore, ibandronate might have an effect on both the early fracture healing process in addition to bone remodeling during the later phase of fracture healing since osteoclast activity begins early in the fracture healing process[125]. As mentioned previously (Section Introduction), it is well-studied that bisphosphonate inhibits osteoclast activity. However, some studies found that osteoblasts might be inhibited by bisphosphonate[63, 66, 123]. Therefore, administration of ibandronate five days after fracture surgery might have a negative impact on bone formation during the early phase of fracture healing. However, this negative effect was not observed in the current *in vivo* study because there was no significant difference in osteocalcin concentration between BG and CG at week 2. Therefore, administration of ibandronate at the same time as LMHFV treatment would be the optimal method. There was no way to determine accurately the stage of fracture healing because of the significant overlapping between the four stages of fracture healing[130]. Also, there might be variation on the initiation of bone remodeling between LMHFV and control. Therefore, administration of ibandronate at the same time as LMHFV treatment would be the optimal method to ensure inhibition of any enhancement by LMHFV on bone remodeling when remodeling begins.

4.7 Future Studies

4.7.1 LMHFV Effect on Osteoclast *in vitro*

Our current study is an inhibition study *in vivo*, which studies the effect of LMHFV on bone remodeling. A future extension on this study could be repeating this experiment *in vitro* using osteoclast culture. The best way to obtain mature osteoclast is by mechanical isolation from neonatal (age: 2 – 3 days) rat long bone. Various osteoclastogenic culture can be obtained from bone marrow cells of young (age: 6 – 9 weeks) rat bone marrow. These cells are coculture with bone marrow stromal cells or cell lines under the stimulation of 1,25-dihydroxyvitamin D_3 or dexamethasone, or induced by M-CSF and RANKL only[75, 107]. In addition, small amount of concentrated HCl would be added to the osteoclast culture medium to produce a pH of 6.95 – 7.0, which is the optimal for resorption pit formation[2].

As mentioned previously, LMHFV might inhibit osteoclast activity in the early phase of fracture healing (Section 4.2.2), the level of inhibition and apoptosis on osteoclast during the early phase of healing would be studied instead of the stimulation on osteoclast activity during the later phase of fracture healing. By plotting a dose-response curve by changing one of the parameters of LMHFV treatment, such as frequency or acceleration, a better understanding on the effect of LMHFV on osteoclast and whether LMHFV stimulates osteoclast directly. To investigate the level of inhibition and apoptosis, the osteoclast cell culture will be covered with annexin-Propidium iodide solution in the dark. The apoptotic osteoclasts will be stained by annexin-PI and counted under a fluorescent microscope[75]. The effect on osteoclastic activity would be investigated by performing a pit-forming assay. Osteoclast culture would be transfered onto dentine slices and stained will 1% toluidien blue solution. The number of resorption pits on dentine slices would be counted under a light microscope[75]. The resorption lacunae would show a violet colour in bone slices after toluidine blue staining[75]. Therefore, the effect of LMHFV on bone remodeling and osteoclast would be investigated by using osteoclast cell culture

stained with annexin-PI solution and pit-forming assay.

4.7.2 Biomechanics of Fracture Callus

As mentioned previously (Section 1.4), osteoporosis is characterized by decreased bone mineral density (BMD) and deterioration in the bone microarchitecture[89]. In addition, bone strength is determined by bone volume, microarchitecture of bone, and bone mineralization[135]. Therefore, osteoporotic bone are fragile when compared to normal healthy bone. However, in our previous studies, LMHFV enhanced the mechanical properties of callus, such as energy to failure and ultimate load, in OVX rats to a level that show no significant difference with callus in normal LMHFV group[129]. The ultimate load reflects the general integrity of bone while energy to failure represents the amount of energy required to break the bone[135]. Since there was no significant difference in ultimate load and energy to failure found between OVX-LMHFV group and normal-LMHFV group, the mechanical properties between these two groups may be the same. The biomechanical investigation confirms the mechanical properties of the healed callus. Since bone remodeling was also enhanced in these studies, the mechanical properties of the fracture femur by LMHFV should also be confirmed to be improved. The mechanical properties of the callus can be assessed by a four-point bending test. After tested to failure using this test, the load-displacement curves of the fracture femora can be generated and ultimate load, stiffness, and energy to failure can be measured.

4.7.3 LMHFV Effect on Leptin-Adrenergic Pathway

The effect of LMHFV on the leptin-adrenergic pathway might affect fracture healing. LMHFV has potential effects on skeletal[64, 82, 106], muscular[42], endocrine[13], nervous[106], and vascular systems[83, 70] and also the interactions among systems[106]. Therefore, it might be necessary to investigate other signaling pathways which might play a role in those systems. Leptin, a peptide hormone synthesized by adipocytes that affects appetite and energy metabolism, and adrenergic system are believed to

play a role in the control of bone remodeling[12, 22, 114, 143]. The central effect of leptin seems to be antiosteogenic[22, 26]. LMHFV has shown to reduced serum concentration of leptin[84, 118]. Therefore, it would be necessary to investigate whether the LMHFV enhanced fracture healing and bone remodeling via reduction of leptin expression.

An *in vivo* inhibition study, similar to the current study, could be undertaken to study the effect of LMHFV on leptin expression. Polyunsaturated Fatty Acid (PUFA) was shown to have an effect on the expression of leptin[111, 62, 138, 105, 60]. PUFA includes two major compositions of fatty acids: n-3 and n-6 fatty acids which found in fish oil and vegetable oil respectively. n-3 fatty acid would decrease leptin expression while n-6 would increase leptin expression[111]. Therefore, treating osteoporotic fracture rats with LMHFV in the presence or absence of either n-3 or n-6, the effect of LMHFV on leptin expression can be investigated. The project might provide evidence that the enhanced fracture healing and remodeling by LMHFV might be a systematic effect in addition to the local bone effect. In addition, this project might provide insights on whether changing the dietary in-take of n-3 and n-6 fatty acid would have an effect on fracture healing.

Chapter 5

Conclusion

In conclusion, the question that "Does Low-Magnitude High-Frequency Vibration enhance bone remodeling?" is answered in this project. LMHFV enhances bone remodeling during fracture healing in osteoporotic rat. This was confirmed by investigating the changes in bone remodeling under LMHFV in the presence and absence of Bis, which was used as a tool to inhibit bone remodeling. LMHFV was able to partially reverse the inhibition effect of Bis on bone remodeling. The mechanism of the enhanced fracture healing by LMHFV seems to be

1. LMHFV enhanced bone remodeling by increasing osteoclastic resorption.
2. LMHFV enhanced bone remodeling by increasing osteoblastic formation.
3. LMHFV inhibiting osteoclast activity in the early phases of fracture healing (pre bone remodeling).
4. LMHFV accelerated fracture healing in the early phase of healing by enhancing callus mineralization and soft callus remodeling.
5. LMHFV enhanced early callus formation by enhancing osteoblast activity.

The finding of this study might provide evidence that LMHFV might be beneficial to patients throughout fracture healing. This study also provided better understanding on the effect of LMHFV on the elderly who is taking bisphosphonate for osteoporosis.

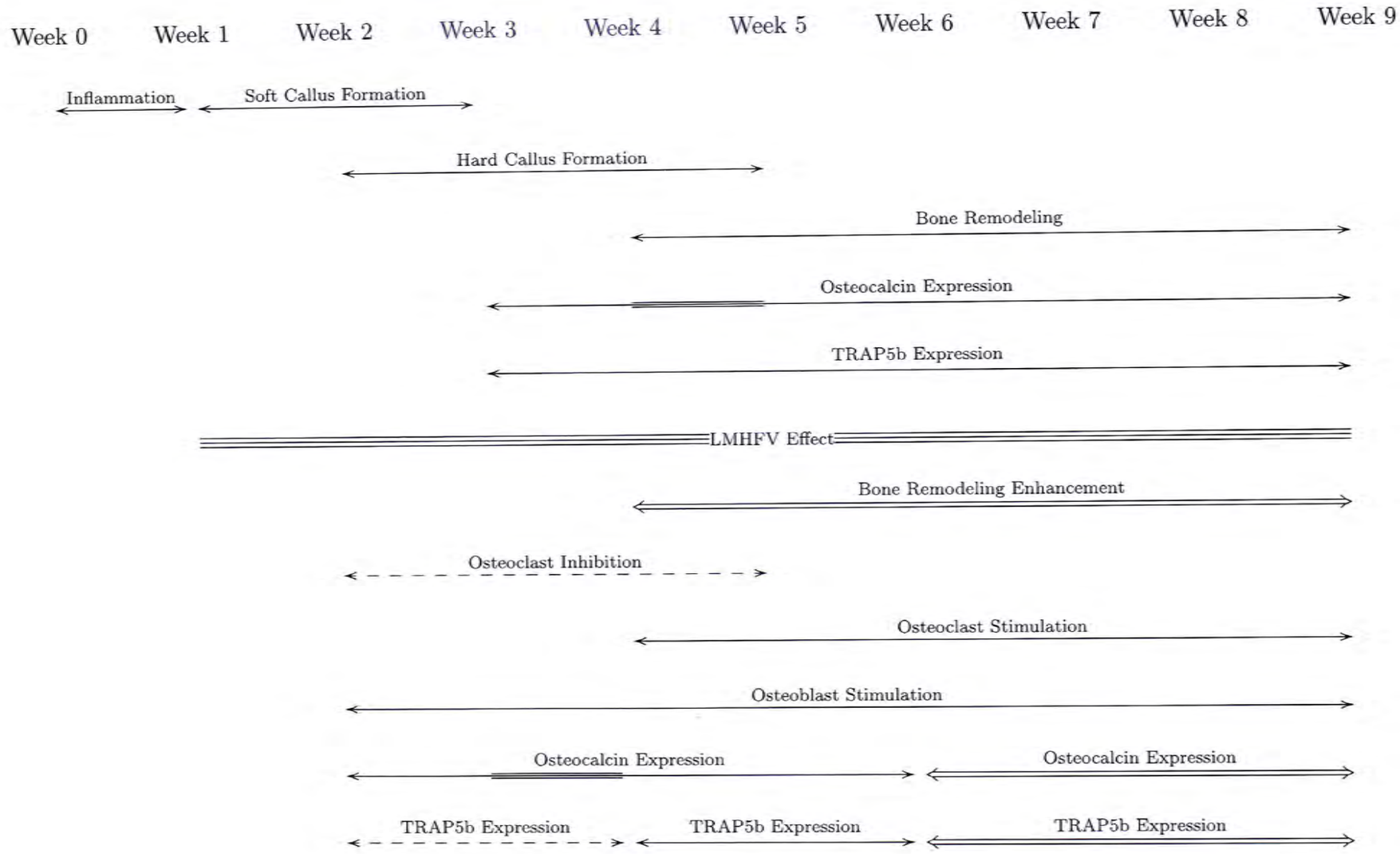

Figure 5.1: The effect of LMHFV at different stage of fracture healing. The time points are number of weeks post-fracture. <- - ->represents decrease expression; <=>represents increase expression; the thicken line represents peak expression.

Bibliography

[1] S. Adami. Bisphosphonate antifracture efficacy. *Bone*, 41(5, Supplement 1):S8–S15, Nov 2007.

[2] T. R. Arnett and M. Spowage. Modulation of the resorptive activity of rat osteoclasts by small changes in extracellular ph near the physiological range. *Bone*, 18(3):277–9, Mar 1996.

[3] P. Aspenberg. Bisphosphonate-induced fractures: nature strikes back? *Acta Orthop*, 79(4):459–60, Aug 2008.

[4] P. Aspenberg. Bisphosphonates and implants: an overview. *Acta Orthop*, 80(1):119–23, Feb 2009.

[5] J. Barrett, E. Worth, F. Bauss, and S. Epstein. Ibandronate: a clinical pharmacological and pharmacokinetic update. *J Clin Pharmacol*, 44(9):951–65, Sep 2004.

[6] C. Barrios, L. A. Broström, A. Stark, and G. Walheim. Healing complications after internal fixation of trochanteric hip fractures: the prognostic value of osteoporosis. *J Orthop Trauma*, 7(5):438–42, 1993.

[7] R. Bartl and B. Frisch. *Osteoporosis: diagnosis, prevention, therapy : a practical guide for all physicians–from pediatrics to geriatrics.* Springer, Berlin, 2004.

[8] F. Bauss and R. G. G. Russell. Ibandronate in osteoporosis: preclinical data and rationale for intermittent dosing. *Osteoporos Int*, 15(6):423–33, Jun 2004.

[9] Y. Bi, Y. Gao, D. Ehirchiou, C. Cao, T. Kikuiri, A. Le, S. Shi, and L. Zhang. Bisphosphonates cause osteonecrosis of the jaw-like disease in mice. *Am J Pathol*, May 2010.

[10] D. M. Black, M. P. Kelly, H. K. Genant, L. Palermo, R. Eastell, C. Bucci-Rechtweg, J. Cauley, P. C. Leung, S. Boonen, A. Santora, A. de Papp, D. C. Bauer, Fracture Intervention Trial Steering Committee, and HORIZON Pivotal Fracture Trial Steering Committee. Bisphosphonates and fractures of the subtrochanteric or diaphyseal femur. *N Engl J Med*, 362(19):1761–71, May 2010.

[11] F. Bonnarens and T. A. Einhorn. Production of a standard closed fracture in laboratory animal bone. *J Orthop Res*, 2(1):97–101, 1984.

[12] N. Bonnet, D. D. Pierroz, and S. L. Ferrari. Adrenergic control of bone remodeling and its implications for the treatment of osteoporosis. *J Musculoskelet Neuronal Interact*, 8(2):94–104, 2008.

[13] C. Bosco, M. Iacovelli, O. Tsarpela, M. Cardinale, M. Bonifazi, J. Tihanyi, M. Viru, A. De Lorenzo, and A. Viru. Hormonal responses to whole-body vibration in men. *Eur J Appl Physiol*, 81(6):449–54, Apr 2000.

[14] K. Brixen, E. F. Eriksen, M. J. Seibel, S. P. Robins, and J. P. Bilezikian. *Validation of Biochemical Markers of Bone Turnover*, pages 583–594. Academic Press, Burlington, 2006.

[15] F. Bronner, M. C. Farach-Carson, and J. Rubin. *Bone resorption*, volume v. 2. Springer, London, 2005.

[16] R. Burge, B. Dawson-Hughes, D. H. Solomon, J. B. Wong, A. King, and A. Tosteson. Incidence and economic burden of osteoporosis-related fractures in the united states, 2005-2025. *J Bone Miner Res*, 22(3):465–75, Mar 2007.

[17] F. C. Cackowski and G. D. Roodman. Perspective on the osteoclast: an angiogenic cell? *Ann N Y Acad Sci*, 1117:12–25, Nov 2007.

[18] Y. Cao, S. Mori, T. Mashiba, M. S. Westmore, L. Ma, M. Sato, T. Akiyama, L. Shi, S. Komatsubara, K. Miyamoto, and H. Norimatsu. Raloxifene, estrogen, and alendronate affect the processes of fracture repair differently in ovariectomized rats. *J Bone Miner Res*, 17(12):2237–46, Dec 2002.

[19] P. M. Chavassieux, M. E. Arlot, C. Reda, L. Wei, A. J. Yates, and P. J. Meunier. Histomorphometric assessment of the long-term effects of alendronate on bone quality and remodeling in patients with osteoporosis. *J Clin Invest*, 100(6):1475–80, Sep 1997.

[20] J.-H. Chen, C. Liu, L. You, and C. A. Simmons. Boning up on wolff's law: mechanical regulation of the cells that make and maintain bone. *J Biomech*, 43(1):108–18, Jan 2010.

[21] P. Chu, T.-Y. Chao, Y.-F. Lin, A. J. Janckila, and L. T. Yam. Correlation between histomorphometric parameters of bone resorption and serum type 5b tartrate-resistant acid phosphatase in uremic patients on maintenance hemodialysis. *Am J Kidney Dis*, 41(5):1052–9, May 2003.

[22] V. Cirmanová, M. Bayer, L. Stárka, and K. Zajícková. The effect of leptin on bone: an evolving concept of action. *Physiol Res*, 57 Suppl 1:S143–51, 2008.

[23] L. Claes, P. Augat, G. Suger, and H. J. Wilke. Influence of size and stability of the osteotomy gap on the success of fracture healing. *J Orthop Res*, 15(4):577–84, Jul 1997.

[24] L. Claes, K. Eckert-Hübner, and P. Augat. The effect of mechanical stability on local vascularization and tissue differentiation in callus healing. *J Orthop Res*, 20(5):1099–105, Sep 2002.

[25] P. Clézardin, F. H. Ebetino, and P. G. J. Fournier. Bisphosphonates and cancer-induced bone disease: beyond their antiresorptive activity. *Cancer Res*, 65(12):4971–4, Jun 2005.

[26] T.-A. Cock and J. Auwerx. Leptin: cutting the fat off the bone. *Lancet*, 362(9395):1572–4, Nov 2003.

[27] F. P. Coxon, K. Thompson, and M. J. Rogers. Recent advances in understanding the mechanism of action of bisphosphonates. *Curr Opin Pharmacol*, 6(3):307–12, Jun 2006.

[28] P. Cynthia and B. Vera. *Common Nonsurgical Techniques and Procedures.* CRC Press, Jan 2010.

[29] M. Dooley and J. A. Balfour. Ibandronate. *Drugs*, 57(1):101–8; discussion 109–10, Jan 1999.

[30] R. Eastell and H. Lambert. Strategies for skeletal health in the elderly. *Proc Nutr Soc*, 61(2):173–80, May 2002.

[31] T. A. Einhorn. The cell and molecular biology of fracture healing. *Clin Orthop Relat Res*, 355(Suppl):S7–21, Oct 1998.

[32] T. A. Einhorn. The science of fracture healing. *J Orthop Trauma*, 19(10 Suppl):S4–6, 2005.

[33] T. A. Einhorn and S. R. Simon. *Orthopaedic basic science: biology and biomechanics of the musculoskeletal system.* American Academy of Orthopaedic Surgeons, Rosemont, Ill., 2nd ed edition, 2000.

[34] K. E. Ensrud, E. L. Barrett-Connor, A. Schwartz, A. C. Santora, D. C. Bauer, S. Suryawanshi, A. Feldstein, W. L. Haskell, M. C. Hochberg, J. C. Torner, A. Lombardi, D. M. Black, and Fracture Intervention Trial Long-Term Extension Research Group. Randomized trial of effect of alendronate continuation versus discontinuation in women with low bmd: results from the fracture intervention trial long-term extension. *J Bone Miner Res*, 19(8):1259–69, Aug 2004.

[35] S. Epstein and M. Zaidi. Biological properties and mechanism of action of ibandronate: application to the treatment of osteoporosis. *Bone*, 37(4):433–40, Oct 2005.

[36] R. G. Erben. Embedding of bone samples in methylmethacrylate: an improved method suitable for bone histomorphometry, histochemistry, and immunohistochemistry. *J Histochem Cytochem*, 45(2):307–13, Feb 1997.

[37] E. F. Eriksen and B. L. Langdahl. The pathogenesis of osteoporosis. *Horm Res*, 48 Suppl 5:78–82, 1997.

[38] E. F. Eriksen, F. Melsen, E. Sod, I. Barton, and A. Chines. Effects of long-term risedronate on bone quality and bone turnover in women with postmenopausal osteoporosis. *Bone*, 31(5):620–5, Nov 2002.

[39] A. Ezra and G. Golomb. Administration routes and delivery systems of bisphosphonates for the treatment of bone resorption. *Adv Drug Deliv Rev*, 42(3):175–95, Aug 2000.

[40] O. Filleul, E. Crompot, and S. Saussez. Bisphosphonate-induced osteonecrosis of the jaw: a review of 2,400 patient cases. *J Cancer Res Clin Oncol*, May 2010.

[41] J. E. Fisher, M. J. Rogers, J. M. Halasy, S. P. Luckman, D. E. Hughes, P. J. Masarachia, G. Wesolowski, R. G. Russell, G. A. Rodan, and A. A. Reszka. Alendronate mechanism of action: geranylgeraniol, an intermediate in the mevalonate pathway, prevents inhibition of osteoclast formation, bone resorption, and kinase activation in vitro. *Proc Natl Acad Sci U S A*, 96(1):133–8, Jan 1999.

[42] A. Fratini, A. La Gatta, P. Bifulco, M. Romano, and M. Cesarelli. Muscle motion and emg activity in vibration treatment. *Med Eng Phys*, 31(9):1166–72, Nov 2009.

[43] T. A. Freeman, P. Patel, J. Parvizi, V. J. Antoci, and I. M. Shapiro. Micro-ct analysis with multiple thresholds allows detection of bone formation and resorption during ultrasound-treated fracture healing. *J Orthop Res*, 27(5):673–679, May 2009.

[44] S. P. Fritton, K. J. McLeod, and C. T. Rubin. Quantifying the strain history of bone: spatial uniformity and self-similarity of low-magnitude strains. *J Biomech*, 33(3):317–25, Mar 2000.

[45] H. M. Frost. Wolff's law and bone's structural adaptations to mechanical usage: an overview for clinicians. *Angle Orthod*, 64(3):175–88, 1994.

[46] H. M. Frost. Bone's mechanostat: a 2003 update. *Anat Rec A Discov Mol Cell Evol Biol*, 275(2):1081–101, Dec 2003.

[47] H. M. Frost. A 2003 update of bone physiology and wolff's law for clinicians. *Angle Orthod*, 74(1):3–15, Feb 2004.

[48] W. F. Ganong. *Review of medical physiology.* Appleton and Lange, Norwalk, Conn., 23th ed edition, 2009.

[49] L. P. Gartner and J. L. Hiatt. *Color textbook of histology.* Saunders/Elsevier, Philadelphia, PA, 3rd ed edition, 2007.

[50] P. V. Giannoudis and E. Schneider. Principles of fixation of osteoporotic fractures. *J Bone Joint Surg Br*, 88(10):1272–8, Oct 2006.

[51] C. M. Girgis, D. Sher, and M. J. Seibel. Atypical femoral fractures and bisphosphonate use. *N Engl J Med*, 362(19):1848–9, May 2010.

[52] J. Glowacki. The deceiving appearances of osteoclasts. *N Engl J Med*, 360(1):80–2, Jan 2009.

[53] A. E. Goodship, T. J. Lawes, and C. T. Rubin. Low-magnitude high-frequency mechanical signals accelerate and augment endochondral bone repair: preliminary evidence of efficacy. *J Orthop Res*, 27(7):922–30, Jul 2009.

[54] N. Gusi, A. Raimundo, and A. Leal. Low-frequency vibratory exercise reduces the risk of bone fracture more than walking: a randomized controlled trial. *BMC Musculoskelet Disord*, 7:92, 2006.

[55] J. M. Halleen, S. L. Alatalo, H. Suominen, S. Cheng, A. J. Janckila, and H. K. Väänänen. Tartrate-resistant acid phosphatase 5b: a novel serum marker of bone resorption. *J Bone Miner Res*, 15(7):1337–45, Jul 2000.

[56] J. Harper and M. Klagsbrun. Cartilage to bone–angiogenesis leads the way. *Nat Med*, 5(6):617–8, Jun 1999.

[57] N. Harvey, E. Dennison, and C. Cooper. Osteoporosis: impact on health and economics. *Nat Rev Rheumatol*, 6(2):99–105, Feb 2010.

[58] R. P. Heaney, R. R. Recker, and P. D. Saville. Menopausal changes in calcium balance performance. *J Lab Clin Med*, 92(6):953–63, Dec 1978.

[59] S. C. Ho, E. M. Lau, J. Woo, A. Sham, K. M. Chan, S. Lee, and P. C. Leung. The prevalence of osteoporosis in the hong kong chinese female population. *Maturitas*, 32(3):171–8, Aug 1999.

[60] L. A. Horrocks and Y. K. Yeo. Health benefits of docosahexaenoic acid (dha). *Pharmacol Res*, 40(3):211–25, Sep 1999.

[61] Y. Hui. Osteoporosis: should there be a screening programme in hong kong? *Hong Kong Med J*, 8(4):270–7, Aug 2002.

[62] G. R. Hynes and P. J. Jones. Leptin and its role in lipid metabolism. *Curr Opin Lipidol*, 12(3):321–7, Jun 2001.

[63] A. I. Idris, J. Rojas, I. R. Greig, R. J. Van't Hof, and S. H. Ralston. Aminobisphosphonates cause osteoblast apoptosis and inhibit bone nodule formation in vitro. *Calcif Tissue Int*, 82(3):191–201, Mar 2008.

[64] Y. Igarashi, M. Y. Lee, and S. Matsuzaki. Acid phosphatases as markers of bone metabolism. *J Chromatogr B Analyt Technol Biomed Life Sci*, 781(1-2):345–58, Dec 2002.

[65] J. Iqbal and M. Zaidi. Molecular regulation of mechanotransduction. *Biochem Biophys Res Commun*, 328(3):751–5, Mar 2005.

[66] K. Iwata, J. Li, H. Follet, R. J. Phipps, and D. B. Burr. Bisphosphonates suppress periosteal osteoblast activity independently of resorption in rat femur and tibia. *Bone*, 39(5):1053–8, Nov 2006.

[67] N. Jain and R. S. Weinstein. Giant osteoclasts after long-term bisphosphonate therapy: diagnostic challenges. *Nat Rev Rheumatol*, 5(6):341–6, Jun 2009.

[68] S. Jingushi, M. E. Joyce, and M. E. Bolander. Genetic expression of extracellular matrix proteins correlates with histologic changes during fracture repair. *J Bone Miner Res*, 7(9):1045–55, Sep 1992.

[69] S. Judex, X. Lei, D. Han, and C. Rubin. Low-magnitude mechanical signals that stimulate bone formation in the ovariectomized rat are dependent on the applied frequency but not on the strain magnitude. *J Biomech*, 40(6):1333–9, 2007.

[70] K. Kerschan-Schindl, S. Grampp, C. Henk, H. Resch, E. Preisinger, V. Fialka-Moser, and H. Imhof. Whole-body vibration exercise leads to alterations in muscle blood volume. *Clin Physiol*, 21(3):377–82, May 2001.

[71] M. E. Kraenzlin, M. J. Seibel, M. J. Seibel, S. P. Robins, and J. P. Bilezikian. *Measurement of Biochemical Markers of Bone Resorption*, pages 541–563. Academic Press, Burlington, 2006.

[72] A. H. A. Kurth, C. Eberhardt, S. Müller, M. Steinacker, M. Schwarz, and F. Bauss. The bisphosphonate ibandronate improves implant integration in osteopenic ovariectomized rats. *Bone*, 37(2):204–10, Aug 2005.

[73] E. Lau, S. Al-Dujaili, A. Guenther, D. Liu, L. Wang, and L. You. Effect of low-magnitude, high-frequency vibration on osteocytes in the regulation of osteoclasts. *Bone*, 46(6):1508–15, Jun 2010.

[74] T. M. Lenehan, M. Balligand, D. M. Nunamaker, and F. E. Wood, Jr. Effect of ehdp on fracture healing in dogs. *J Orthop Res*, 3(4):499–507, 1985.

[75] K. S. Leung. *A practical manual for musculoskeletal research.* World Scientific, Singapore, 2008.

[76] K. S. Leung, H. F. Shi, W. H. Cheung, L. Qin, W. K. Ng, K. F. Tam, and N. Tang. Low-magnitude high-frequency vibration accelerates callus formation, mineralization, and fracture healing in rats. *J Orthop Res*, 27(4):458–65, Apr 2009.

[77] J. Li, S. Mori, Y. Kaji, J. Kawanishi, T. Akiyama, and H. Norimatsu. Concentration of bisphosphonate (incadronate) in callus area and its effects on fracture healing in rats. *J Bone Miner Res*, 15(10):2042–51, Oct 2000.

[78] J. Li, S. Mori, Y. Kaji, T. Mashiba, J. Kawanishi, and H. Norimatsu. Effect of bisphosphonate (incadronate) on fracture healing of long bones in rats. *J Bone Miner Res*, 14(6):969–79, Jun 1999.

[79] J. R. Lieberman and G. E. Friedlaender. *Bone regeneration and repair: biology and clinical applications.* Humana Press, Totowa, N.J., 2005.

[80] J. H. Lin. Bisphosphonates: a review of their pharmacokinetic properties. *Bone*, 18(2):75–85, Feb 1996.

[81] D. G. Little, M. Ramachandran, and A. Schindeler. The anabolic and catabolic responses in bone repair. *J Bone Joint Surg Br*, 89(4):425–33, Apr 2007.

[82] M. A. Lynch, M. D. Brodt, and M. J. Silva. Skeletal effects of whole-body vibration in adult and aged mice. *J Orthop Res*, 28(2):241–7, Feb 2010.

[83] N. Lythgo, P. Eser, P. de Groot, and M. Galea. Whole-body vibration dosage alters leg blood flow. *Clin Physiol Funct Imaging*, 29(1):53–9, Jan 2009.

[84] G. F. Maddalozzo, U. T. Iwaniec, R. T. Turner, C. J. Rosen, and J. J. Widrick. Whole-body vibration slows the acquisition of fat in mature female rats. *Int J Obes (Lond)*, 32(9):1348–54, Sep 2008.

[85] T. Martin, J. H. Gooi, and N. A. Sims. Molecular mechanisms in coupling of bone formation to resorption. *Crit Rev Eukaryot Gene Expr*, 19(1):73–88, 2009.

[86] T. Mashiba, C. H. Turner, T. Hirano, M. R. Forwood, C. C. Johnston, and D. B. Burr. Effects of suppressed bone turnover by bisphosphonates on microdamage accumulation and biomechanical properties in clinically relevant skeletal sites in beagles. *Bone*, 28(5):524–31, May 2001.

[87] M. A. Matos, F. P. Araújo, and F. B. Paixão. The effect of zoledronate on bone remodeling during the healing process. *Acta Cir Bras*, 22(2):115–9, 2007.

[88] K. Matsuo and N. Irie. Osteoclast-osteoblast communication. *Arch Biochem Biophys*, 473(2):201–209, May 2008.

[89] R. M. McCann, G. Colleary, C. Geddis, S. A. Clarke, G. R. Jordan, G. R. Dickson, and D. Marsh. Effect of osteoporosis on bone mineral density and fracture repair in a rat femoral fracture model. *J Orthop Res*, 26(3):384–93, Mar 2008.

[90] M. M. McDonald, S. Dulai, C. Godfrey, N. Amanat, T. Sztynda, and D. G. Little. Bolus or weekly zoledronic acid administration does not delay endochondral fracture repair but weekly dosing enhances delays in hard callus remodeling. *Bone*, 43(4):653–62, Oct 2008.

[91] C. D. Morris and T. A. Einhorn. Bisphosphonates in orthopaedic surgery. *J Bone Joint Surg Am*, 87(7):1609–18, Jul 2005.

[92] R. C. Mühlbauer, F. Bauss, R. Schenk, M. Janner, E. Bosies, K. Strein, and H. Fleisch. Bm 21.0955, a potent new bisphosphonate to inhibit bone resorption. *J Bone Miner Res*, 6(9):1003–11, Sep 1991.

[93] R. Müller and R. R. Recker. Bisphosphonate action on bone structure and strength: Preclinical and clinical evidence for ibandronate. *Bone*, 41(5, Supplement 1):S16–S23, Nov 2007.

[94] G. H. Nancollas, R. Tang, R. J. Phipps, Z. Henneman, S. Gulde, W. Wu, A. Mangood, R. G. G. Russell, and F. H. Ebetino. Novel insights into actions of bisphosphonates on bone: differences in interactions with hydroxyapatite. *Bone*, 38(5):617–27, May 2006.

[95] K. E. Naylor, R. Eastell, M. J. Seibel, S. P. Robins, and J. P. Bilezikian. *Measurement of Biochemical Markers of Bone Formation*, pages 529–540. Academic Press, Burlington, 2006.

[96] C. Neidlinger-Wilke, I. Stalla, L. Claes, R. Brand, I. Hoellen, S. Rübenacker, M. Arand, and L. Kinzl. Human osteoblasts from younger normal and osteoporotic donors show differences in proliferation and tgf beta-release in response to cyclic strain. *J Biomech*, 28(12):1411–8, Dec 1995.

[97] V. S. Nikolaou, N. Efstathopoulos, G. Kontakis, N. K. Kanakaris, and P. V. Giannoudis. The influence of osteoporosis in femoral fracture healing time. *Injury*, 40(6):663–8, Jun 2009.

[98] B. E. Nordin. Calcium and osteoporosis. *Nutrition*, 13(7-8):664–86, 1997.

[99] D. M. Nunamaker. Experimental models of fracture repair. *Clin Orthop Relat Res*, 355(Suppl):S56–65, Oct 1998.

[100] C. V. Odvina, J. E. Zerwekh, D. S. Rao, N. Maalouf, F. A. Gottschalk, and C. Y. C. Pak. Severely suppressed bone turnover: a potential complication of alendronate therapy. *J Clin Endocrinol Metab*, 90(3):1294–301, Mar 2005.

[101] P. F. O'Loughlin, S. Morr, L. Bogunovic, A. D. Kim, B. Park, and J. M. Lane. Selection and development of preclinical models in fracture-healing research. *J Bone Joint Surg Am*, 90 Suppl 1:79–84, Feb 2008.

[102] S. E. Papapoulos. Bisphosphonate actions: physical chemistry revisited. *Bone*, 38(5):613–6, May 2006.

[103] S. E. Papapoulos. Bisphosphonates: how do they work? *Best Pract Res Clin Endocrinol Metab*, 22(5):831–47, Oct 2008.

[104] C. P. Peter, W. O. Cook, D. M. Nunamaker, M. T. Provost, J. G. Seedor, and G. A. Rodan. Effect of alendronate on fracture healing and bone remodeling in dogs. *J Orthop Res*, 14(1):74–9, Jan 1996.

[105] E. Peyron-Caso, M. Taverna, M. Guerre-Millo, A. Véronèse, N. Pacher, G. Slama, and S. W. Rizkalla. Dietary (n-3) polyunsaturated fatty acids up-regulate plasma leptin in insulin-resistant rats. *J Nutr*, 132(8):2235–40, Aug 2002.

[106] R. D. Prisby, M.-H. Lafage-Proust, L. Malaval, A. Belli, and L. Vico. Effects of whole body vibration on the skeleton and other organ systems in man and animal models: what we know and what we need to know. *Ageing Res Rev*, 7(4):319–29, Dec 2008.

[107] L. Qin. *Advanced bioimaging technologies in assessment of the quality of bone and scaffold materials: techniques and applications*. Springer, Berlin, 2007.

[108] Y. X. Qin, C. T. Rubin, and K. J. McLeod. Nonlinear dependence of loading intensity and cycle number in the maintenance of bone mass and morphology. *J Orthop Res*, 16(4):482–9, Jul 1998.

[109] R. R. Recker. *Bone histomorphometry: techniques and interpretation*. CRC Press, Boca Raton, Fla., 1983.

[110] M. J. Reed and J. M. Edelberg. Impaired angiogenesis in the aged. *Sci Aging Knowledge Environ*, 2004(7):pe7, Feb 2004.

[111] J. E. Reseland, F. Haugen, K. Hollung, K. Solvoll, B. Halvorsen, I. R. Brude, M. S. Nenseter, E. N. Christiansen, and C. A. Drevon. Reduction of leptin gene expression by dietary polyunsaturated fatty acids. *J Lipid Res*, 42(5):743–50, May 2001.

[112] G. A. Rodan and A. A. Reszka. Osteoporosis and bisphosphonates. *J Bone Joint Surg Am*, 85-A Suppl 3:8–12, 2003.

[113] P. Roschger, S. Rinnerthaler, J. Yates, G. A. Rodan, P. Fratzl, and K. Klaushofer. Alendronate increases degree and uniformity of mineralization in cancellous bone and decreases the porosity in cortical bone of osteoporotic women. *Bone*, 29(2):185–91, Aug 2001.

[114] C. J. Rosen. Bone: serotonin, leptin and the central control of bone remodeling. *Nat Rev Rheumatol*, 5(12):657–8, Dec 2009.

[115] C. Rosenquist, P. Qvist, N. Bjarnason, and C. Christiansen. Measurement of a more stable region of osteocalcin in serum by elisa with two monoclonal antibodies. *Clin Chem*, 41(10):1439–45, Oct 1995.

[116] P. D. Ross, J. W. Davis, R. S. Epstein, and R. D. Wasnich. Pre-existing fractures and bone mass predict vertebral fracture incidence in women. *Ann Intern Med*, 114(11):919–23, Jun 1991.

[117] C. Rubin, A. S. Turner, S. Bain, C. Mallinckrodt, and K. McLeod. Anabolism. low mechanical signals strengthen long bones. *Nature*, 412(6847):603–4, Aug 2001.

[118] C. T. Rubin, E. Capilla, Y. K. Luu, B. Busa, H. Crawford, D. J. Nolan, V. Mittal, C. J. Rosen, J. E. Pessin, and S. Judex. Adipogenesis is inhibited by brief, daily exposure to high-frequency, extremely low-magnitude mechanical signals. *Proc Natl Acad Sci U S A*, 104(45):17879–84, Nov 2007.

[119] R. G. G. Russell. Bisphosphonates: from bench to bedside. *Ann N Y Acad Sci*, 1068:367–401, Apr 2006.

[120] R. G. G. Russell. Ibandronate: pharmacology and preclinical studies. *Bone*, 38(4 Suppl 1):S7–12, Apr 2006.

[121] R. G. G. Russell. Bisphosphonates: mode of action and pharmacology. *Pediatrics*, 119 Suppl 2:S150–62, Mar 2007.

[122] R. G. G. Russell, N. B. Watts, F. H. Ebetino, and M. J. Rogers. Mechanisms of action of bisphosphonates: similarities and differences and their potential influence on clinical efficacy. *Osteoporos Int*, 19(6):733–59, Jun 2008.

[123] M. Sahni, H. L. Guenther, H. Fleisch, P. Collin, and T. J. Martin. Bisphosphonates act on rat bone resorption through the mediation of osteoblasts. *J Clin Invest*, 91(5):2004–2011, May 1993.

[124] P. Sambrook and C. Cooper. Osteoporosis. *Lancet*, 367(9527):2010–8, Jun 2006.

[125] H. Schell, J. Lienau, D. R. Epari, P. Seebeck, C. Exner, S. Muchow, H. Bragulla, N. P. Haas, and G. N. Duda. Osteoclastic activity begins early and increases over the course of bone healing. *Bone*, 38(4):547–54, Apr 2006.

[126] A. Schindeler, M. M. McDonald, P. Bokko, and D. G. Little. Bone remodeling during fracture repair: The cellular picture. *Semin Cell Dev Biol*, 19(5):459–66, Oct 2008.

[127] D. Seidlová-Wuttke, H. Jarry, T. Becker, V. Christoffel, and W. Wuttke. Pharmacology of cimicifuga racemosa extract bno 1055 in rats: bone, fat and uterus. *Maturitas*, 44 Suppl 1:S39–50, Mar 2003.

[128] P. E. Sharp, M. C. La Regina, and M. A. Suckow. *The laboratory rat.* CRC Press, Boca Raton, Fla., 1998.

[129] H. F. Shi, W. H. Cheung, L. Qin, A. H. C. Leung, and K. S. Leung. Low-magnitude high-frequency vibration treatment augments fracture healing in ovariectomy-induced osteoporotic bone. *Bone*, 46(5):1299–305, May 2010.

[130] N. A. Sims and J. H. Gooi. Bone remodeling: Multiple cellular interactions required for coupling of bone formation and resorption. *Semin Cell Dev Biol*, 19(5):444–51, Oct 2008.

[131] W. Sipos, P. Pietschmann, M. Rauner, K. Kerschan-Schindl, and J. Patsch. Pathophysiology of osteoporosis. *Wien Med Wochenschr*, 159(9-10):230–4, May 2009.

[132] J. S. Sun, R. C. Hong, W. H. Chang, L. T. Chen, F. H. Lin, and H. C. Liu. In vitro effects of low-intensity ultrasound stimulation on the bone cells. *J Biomed Mater Res*, 57(3):449–56, Dec 2001.

[133] K. F. Tam, W. H. Cheung, K. M. Lee, L. Qin, and K. S. Leung. Shockwave exerts osteogenic effect on osteoporotic bone in an ovariectomized goat model. *Ultrasound Med Biol*, 35(7):1109–18, Jul 2009.

[134] D. D. Thompson, H. A. Simmons, C. M. Pirie, and H. Z. Ke. Fda guidelines and animal models for osteoporosis. *Bone*, 17(4 Suppl):125S–133S, Oct 1995.

[135] C. H. Turner. Bone strength: current concepts. *Ann N Y Acad Sci*, 1068:429–46, Apr 2006.

[136] A. K. Ulstrup. Biomechanical concepts of fracture healing in weight-bearing long bones. *Acta Orthop Belg*, 74(3):291–302, Jun 2008.

[137] H. G. Vogel. *Drug discovery and evaluation: pharmacological assays*. Springer, Berlin, 3rd completely rev., updated, and enl. ed edition, 2008.

[138] H. Wang, L. H. Storlien, and X.-F. Huang. Effects of dietary fat types on body fatness, leptin, and arc leptin receptor, npy, and agrp mrna expression. *Am J Physiol Endocrinol Metab*, 282(6):E1352–9, Jun 2002.

[139] R. S. Weinstein, P. K. Roberson, and S. C. Manolagas. Giant osteoclast formation and long-term oral bisphosphonate therapy. *N Engl J Med*, 360(1):53–62, Jan 2009.

[140] P. J. Wraighte and B. E. Scammell. Principles of fracture healing. *Surgery (Oxford)*, 24(6):198–207, 2006.

[141] Y. Wu, J. W. Lee, L. Uy, B. Abosaleem, H. Gunn, M. Ma, and B. DeSilva. Tartrate-resistant acid phosphatase (tracp 5b): a biomarker of bone resorption rate in support of drug development: modification, validation and application of the bonetrap kit assay. *J Pharm Biomed Anal*, 49(5):1203–12, Jul 2009.

[142] L. Xie, J. M. Jacobson, E. S. Choi, B. Busa, L. R. Donahue, L. M. Miller, C. T. Rubin, and S. Judex. Low-level mechanical vibrations can influence bone resorption and bone formation in the growing skeleton. *Bone*, 39(5):1059–66, Nov 2006.

[143] V. K. Yadav, F. Oury, N. Suda, Z.-W. Liu, X.-B. Gao, C. Confavreux, K. C. Klemenhagen, K. F. Tanaka, J. A. Gingrich, X. E. Guo, L. H. Tecott, J. J. Mann,

R. Hen, T. L. Horvath, and G. Karsenty. A serotonin-dependent mechanism explains the leptin regulation of bone mass, appetite, and energy expenditure. *Cell*, 138(5):976–89, Sep 2009.

[144] T. Ziebart, A. Pabst, M. O. Klein, P. Kämmerer, L. Gauss, D. Brüllmann, B. Al-Nawas, and C. Walter. Bisphosphonates: restrictions for vasculogenesis and angiogenesis: inhibition of cell function of endothelial progenitor cells and mature endothelial cells in vitro. *Clin Oral Investig*, Dec 2009.